

Die approbierte Originalversion dieser Dissertation ist an der Hauptbibliothek der Technischen Universität Wien aufgestellt (<http://www.ub.tuwien.ac.at>).

The approved original version of this thesis is available at the main library of the Vienna University of Technology (<http://www.ub.tuwien.ac.at/englweb/>).



TECHNISCHE  
UNIVERSITÄT  
WIEN  
VIENNA  
UNIVERSITY OF  
TECHNOLOGY

DISSERTATION

# New Strategies for Time Resolved Infrared Spectroscopy of Chemical Reactions in Solution

ausgeführt zum Zwecke der Erlangung des akademischen Grades eines Doktors der  
technischen Wissenschaften

unter der Leitung von

Ao. Univ. Prof. Dr. Bernhard Lendl

Institut für Chemische Technologie und Analytik, E164-AC

eingereicht an der Technischen Universität Wien

Fakultät für Technische Naturwissenschaften und Informatik

von

**Dipl. Ing. Nina Kaun**

Matr.-Nr. 9626163

Preßgasse 9/7, 1040 Wien

Wien, Mai 2006

## **Deutsche Kurzfassung**

Ziel der vorliegenden Arbeit war die Durchführung von zeitaufgelöster Infrarot (IR) Spektroskopie an biochemischen Reaktionen im Millisekunden-Bereich. Zu diesem Zweck wurde eine Durchflusszelle im Mikromaßstab mit integriertem Mischer erdacht, die sowohl das rasche Mischen von Lösungen ermöglicht, wie auch das Beobachten der Mischung unter kontinuierlichem Fluß entlang des Auslaß-Kanals. Zwei spezielle Designs wurden dafür in Zusammenarbeit mit Peter Svasek vom Institut für Sensor- und Aktuatorssysteme der TU-Wien entwickelt. Es handelt sich dabei um Sandwichkonstruktionen aus zwei  $\text{CaF}_2$  Platten und einer Schicht Epoxidharz SU-8 in der Mitte, welche die Konstruktion des Mixers und des Kanals ausbildet. Durch die Konstruktion werden zwei Flüssigkeitsströme entweder durch Überschichten oder Verengung des Kanals so nah aneinander gebracht, dass Diffusion ausreicht, um die Lösungen in wenigen Millisekunden zu Mischen. In Zusammenarbeit mit Michael Harasek vom Institut für Verfahrenstechnik, Umwelttechnik und Technische Biowissenschaften der TU-Wien wurden numerische Fluidsimulationen durchgeführt, um die Funktion des Mikromixers zu überprüfen und besseres Verständnis über das Fluidverhalten zu erlangen. Sobald das Mischen stattgefunden hat, kann die Reaktionszeit aus dem Abstand vom Misch-Punkt und dem Ort der Messung ermittelt werden. Daraus folgt, dass die erzielbare Zeitauflösung von der Distanz zweier benachbarter Meßpunkte, wie auch von der einsetzbaren Flußgeschwindigkeit abhängig ist. Zwar ist das Erhöhen der Flußrate in der Praxis begrenzt zum Beispiel durch Undichtheit aufgrund zu hoher Drücke, jedoch kann der Meßfleck durch den Einsatz von IR Mikroskopen stark verkleinert werden. Ein konventionelles mit einem Globar ausgestattetes IR Mikroskop ermöglicht Meßfleckgrößen von ungefähr 50  $\mu\text{m}$  im Durchmesser für den Einsatz am wassergefüllten Kanal des Mikromixers. Wird der Globar durch Synchrotron IR Licht ersetzt, kann die Meßfleckgröße bis auf 15 x 15  $\mu\text{m}$  reduziert werden. Eine weitere instrumentelle Neuheit auf dem Gebiet der IR Mikroskopie stellt die Detektion mittels eines Focal Plane Array (FPA) Detektors dar, der die simultane Aufnahme von Tausenden Spektren ermöglicht. Dessen Anwendung für zeitaufgelöste Messungen an einem durchströmten Kanal werden gezeigt.

Experimentelle Ergebnisse von Testreaktionen und von einem biochemischen System - der Reaktion des Glykopeptid-Antibiotikums Vancomycin mit einem Zellwand-Vorstufenpeptid von gram-positiven Bakterien - werden diskutiert.

Ein weiteres Thema dieser Arbeit ist der Einsatz von neuen Instrumenten im sehr fernen Infrarot (FIR)- bzw. terahertz (THz)-Bereich von  $1 - 100 \text{ cm}^{-1}$  zur Untersuchung von wäßrigen Lösungen, die als Grundlage dienen für zukünftige Experimenten von Proteinen in Lösung. Dazu wurden Spektren von Wasser und von Salz- und Zuckerlösungen in einer Durchflußzelle in einem gepulsten THz-Instrument sowie einem IR Instrument mit eingekoppelter Synchrotron FIR Strahlung aufgenommen. Ein konzentrationsabhängiger Anstieg der Absorptionsintensität gegenüber Wasser im untersuchten THz-Bereich ist für Lösungen mit chaotropen Salzen festzustellen, sowie ein Sinken für Lösungen von Kosmotropen.

## **Abstract**

The aim of this work is the set-up of a tool for the investigation of biochemical reactions such as protein folding or reaction kinetics of drugs. For that purpose the concept of continuous-flow monitoring of chemical reactions by time resolved infrared (IR) spectroscopy is employed.

The key of this concept is the combination of a micro-machined infrared transparent chip for rapid mixing of two solutions and IR microspectroscopy along the outlet channel of the mixer, while the reagents are fed into the mixer chip at constant flow rate. Two dedicated chip designs therefore have been developed in cooperation with Peter Svasek from the Institute of Sensor and Actuator Systems (Vienna University of Technology). The designs are based on sandwich constructions made up by calcium fluoride and the epoxy resin SU-8 forming the structure of the mixer and the channel. Mixing is achieved by narrowing two liquid streams separated directly into the 10  $\mu\text{m}$  high channel. Although diffusion is known as a rather slow process it is fast enough to mix two solutions in a few milliseconds on this small scale. The function of the developed mixer designs is outlined by Computational Fluid Dynamics, performed in cooperation with Michael Harasek from the Department of Chemical Engineering (Vienna University of Technology).

Once the mixing has occurred the reaction time can be measured as the distance from the mixing point to the observation point. As a consequence, the achievable time resolution in the continuous-flow mode is determined by either the linear flow rate and by the distance between two adjacent measurement spots. Whereas the increase in flow rate is limited due to practical aspects such as leaking, the sample spot can be reduced by several means. A conventional IR microscope equipped with a globar as light source enables a spot size of 50  $\mu\text{m}$  in diameter on the water filled mixer channel with acceptable noise. Replacing the globar by synchrotron infrared radiation (SIR) allows for measuring down to the diffraction limit, in our case to a size of 15 x 15  $\mu\text{m}$ . Another instrumental development in IR spectroscopy, produced for IR imaging, is the use of a focal plane array (FPA) detector providing measurement of thousands of spectra simultaneously. In this work an FPA equipped IR microscope is applied for time resolved measurements on a flow channel.

Experimental results on test reactions and on a biochemical reaction, the binding process between vancomycin, an important antibiotic, to a tripeptide involved in the build up of cell walls of gram positive bacteria are discussed as well.

Furthermore, the aim of this work is the evaluation of the ability of new instruments in the very far infrared region (FIR) or so-called terahertz (THz) range from 1 – 100  $\text{cm}^{-1}$  for monitoring proteins in aqueous solution. Therefore, water and aqueous solutions of salts and sugars are measured with a THz-pulsed instrument and an FTIR instrument coupled to a synchrotron FIR radiation source. A concentration dependent increased absorption across the investigated THz spectral region is recorded for all studied chaotropic solutions, whereas the opposite is obtained for kosmotrope containing solutions.

## ACKNOWLEDGMENT

During the last three years I gained a lot of experiences being part of the CAVS-group as a PhD student. I met a lot of people, some of them showing me new ideas, some being great support, and some who became friends.

Therefore I would like to say

### *thank you ...*

... to my supervisor Bernhard Lendl for the guidance through the last three years. He taught me a lot on Vibrational Spectroscopy and was an endless source of knowledge on these very important little details that are nowhere written.

... to the cooperation partners:

- *Ulli Schade*, at whose Synchrotron beamline I spent several wonderful months and who relentlessly filled up my lack of knowledge on physics.
- *Edda and Peter Svaseks*, for producing IR transparent micromixing machines.
- *Michael Harasek*, who did the simulations on the mixer, which had a high impact on my understanding on microfluidics.

... to my dearest colleagues, *Josefa Rodriguez Baena, Ana Dominguez Vidál, Stephan Kulka, Stefan Schaden, Johannes Schnöller, Wolfgang Ritter, Mercedes Lopez Pastór, Guillermo Quintas Soria, Barbara Muik, Maria José Ayora-Cañada* and all further guest that joined the CAVS-group, for their support and the good atmosphere.

... to my “predecessors” in the CAVS group on whose work this thesis is based: *Peter Hinsmann, Josef Diewok* and *Michael Haberkorn*.

... to *Christoph Wagner*, who contributed in his laboratory short course to this thesis.

... to *Johannes Frank*, who created the perfect support for the microchip and gave me useful lessons on engineering.

... to *Markus Schaufler*, who not only assembled electronically devices, but our group together for the movie evenings and not to forget by the photo stories on the CAVS-homepage.

... to my colleagues in Berlin, *Michele Ortolani* and *Jong-Seok Lee*, who gave me an impression on a physicists life in Vibrational Spectroscopy and who are responsible for many good memories to my stay at BESSY.

... to my friends *Yasemin, Fischl, Michl, Marko* and *Christian*, who were there during last 10 years of ups and downs.

... to *Volker* for his patience especially in the last month.

... to my beloved *family* for their never ending support.

Furthermore, I gratefully acknowledge the financing by the Austrian Science Fund FWF15531.

## **Table of Contents**

<b>Deutsche Kurzfassung</b>	<b>II</b>
<b>Abstract</b>	<b>IV</b>
<b>Table of Contents</b>	<b>VII</b>
<b>List of Publications</b>	<b>IX</b>
<b>List of Abbreviations</b>	<b>X</b>
<b>1 INTRODUCTION</b>	<b>1</b>
1.1 Motivation	1
1.2 IR Spectroscopy	2
1.3 Water in IR spectroscopy	7
<b>2 TIME RESOLVED FTIR SPECTROSCOPY</b>	<b>9</b>
2.1 Mixing induced time resolved FTIR spectroscopy	10
2.1.1 The microfluidic mixing system	10
2.1.1.1 Monitoring mode	12
2.1.1.1.1 Stopped-flow mode	12
2.1.1.1.2 Continuous-flow mode	13
2.1.2 The continuous-flow set-up	14
2.1.2.1 The mixer design	14
2.1.2.2 Simulations	18
2.1.2.3 Operation of the set-up	23
2.2 IR Microspectroscopy	26
2.2.1 Single point detector	26
2.2.1.1 The conventional IR microscope using globar	26
2.2.1.1.1 IRscope II, Bruker	30
2.2.1.2 Synchrotron Infrared radiation (SIR)	31
2.2.1.2.1 Synchrotron radiation	31
2.2.1.2.2 Characteristics of SIR	34
2.2.1.2.3 Synchrotron IR microscopy	35
2.2.1.2.4 Determination of the resolution	36
2.2.1.2.5 Application of SIR microspectroscopy	41
2.2.2 Array detector	44
2.2.2.1 Chemometric data evaluation for time resolved FTIR spectroscopy	46
2.3 Investigation of a drug's reaction mechanism	47
2.3.1 Time resolved reaction of vancomycin using the modified A590	50
2.3.2 Time resolved reaction of vancomycin using the IRscope II	51
2.3.3 Time resolved reaction of vancomycin using SIR (Continuum)	54

<b>2.4</b>	<b>Outlook - the next generation of micromixers</b>	<b>54</b>
2.4.1	The continuous-flow mode of the future	55
2.4.2	Both concepts into one	56
<b>3</b>	<b>WATER IN THE VERY FAR INFRARED REGION</b>	<b>58</b>
<b>3.1</b>	<b>Measurements using Terahertz pulsed Spectroscopy (TPS)</b>	<b>58</b>
3.1.1	Instrument	58
3.1.2	Characteristics of the TPI™ 1000	59
3.1.3	Application for aqueous solutions	60
<b>3.2</b>	<b>Synchrotron far infrared radiation</b>	<b>61</b>
3.2.1	Instrumentation	62
3.2.2	Characteristics	63
3.2.3	Application	63
<b>3.3</b>	<b>Conclusion and Outlook for aqueous FIR measurements</b>	<b>69</b>
<b>4</b>	<b>REFERENCES</b>	<b>70</b>
<b>5</b>	<b>APPENDIX</b>	<b>74</b>
	<b>Publication I</b>	<b>74</b>
	<b>Publication II</b>	<b>81</b>
	<b>Publication III</b>	<b>88</b>
	<b>Publication IV</b>	<b>92</b>
	<b>Publication V</b>	<b>108</b>
	<b>Curriculum Vitae</b>	<b>115</b>



## List of Publications

- I** N. Kaun, S. Kulka, J. Frank, U. Schade, M. J. Vellekoop M. Harasek and B. Lendl  
*„Towards Biochemical reaction monitoring using FT-IR Synchrotron radiation”*  
Analyst, 131,( 2006) 489–494
- II** S. Kulka, N. Kaun, J. R. Baena, J. Frank, P. Svasek,D. Moss,M.J. Vellekoop and B. Lendl  
*„Mid-IR synchrotron radiation for molecular specific detection in micro-chip based analysis systems”*  
Analytical and Bioanalytical Chemistry (2004), 378(7), 1735-1740
- III** N. Kaun, S. Kulka, J.R. Baena, U. Schade, M. Vellekoop, E. De Lorenzi, B. Lendl  
*„Synchrotron radiation for on-chip detection at the diffraction limit“*  
Proceedings of MicroTAS-2004, Malmö, Sweden, Sept. 2004, proc. vol. 2, p. 530-532
- IV** N. Kaun, M. J. Vellekoop, E. Pachalis and B. Lendl  
*„Time Resolved Fourier Transform Infrared Spectroscopy of Chemical Reactions in Solution using a Focal Plane array (FPA) detector”*  
submitted publication
- V** N. Kaun, J.R. Baena, D.Newnham, B. Lendl  
*„THz-Spectroscopy as a new tool for measuring the structuring effect of solutes on water”*  
Appl. Spectrosc. 59 4 (2005) 505-510

## ***List of Abbreviations***

CCD	Charge Coupled Device
CSR	Coherent Synchrotron Radiation
EPXMA	electron probe x-ray microanalysis
FIR	Far Infrared Radiation
FTIR	Fourier Transformation Infrared
FPA	Focal Plan Array
IR	Infrared Radiation
MCR	Multivariate Curve Resolution
MCT	Mercury Cadmium Telluride
MTF	Modulation Transfer Function
NA	Numerical Aperture
NEP	Noise Equivalent Power
PCA	Principal Component Analysis
SR	Synchrotron Radiation
SIR	Synchrotron Infrared Radiation
S/N	Signal to Noise Ratio
TPS	Terahertz Pulsed Spectroscopy
UHV	Ultra High Vacuum
UV	Ultra-Violet

# **1 Introduction**

## **1.1 Motivation**

In the “Chemical Analysis and Vibrational Spectroscopy” group at the Institute of Chemical Technologies and Analytics, Vienna University of Technology, emphasis is placed on the development and application of new analysis strategies employing Fourier transform infrared (FTIR) spectroscopy. One part is made up by monitoring chemical reactions for research, while another other part poses the topic sensors for online or offline control of the chemical composition of substances. Considering these fields in FTIR spectroscopy water as a solvent in IR spectra is an always-present topic as well, on that has been focused in thesis of Josef Diewok<sup>1</sup>.

Recently<sup>2</sup>, time resolved FTIR spectroscopy was introduced enabling direct insight in molecular changes of reaction taking place and poses a highly wanted tool for e.g. biochemists for understanding (bio)chemical reactions including bioligand interactions. A mixing device with an integrated transmission cell for IR Spectroscopy has been developed enabling measurements at a time resolution of 60 ms. So far, one type of micromixing set-ups, the stopped-flow mode, has been employed. It turned out that the 60 ms limit excludes a variety of reaction of interest and that there is a need for extension to higher time resolutions. This brought up the aim of this work, to set up and evaluate the continuous-flow mode, which is complementary to the stopped flow approach. The use of state-of-the-art instruments in IR will allow an estimation of the possibilities this set-up possesses, using in addition to conventional light sources, the synchrotron radiation. The recently available array detectors for the mid-IR microscopes providing another interesting possibility of monitoring simultaneously fluid elements of different age.

Furthermore, the advent of new instrumentation in a very far IR region, the terahertz (THz)–range, raises the interest for studying biochemical systems in aqueous solution in this region. Within this work the potential of a THz pulsed instrument and an FTIR spectrometer employing synchrotron radiation in this region on studying aqueous solution will be evaluated.

## 1.2 IR Spectroscopy

Infrared spectroscopy is a molecular specific analysis method providing inherent information on functional groups of molecules including their interaction and orientation. The operation principle is based on the excitation of vibrational states of molecules by absorbance of energy in form of radiation in the infrared spectral region.

Electromagnetic radiation can be characterised in general by the wavelength ( $\mu\text{m}$ ) of the radiation, by its frequency (Hz), number of the oscillations per second, or a dimension direct proportional to Hz, which is commonly used for IR-Spectroscopy, the wavenumber ( $\text{cm}^{-1}$ ). Furthermore, the dimension electron volt (eV) is used denoting the energy of the photons. The context of these three is given by

$$E = h \cdot \nu \quad (\text{Eq 1})$$

$$\lambda = c / \nu \quad (\text{Eq 2})$$

$$\tilde{\nu} = 1 / \lambda \quad (\text{Eq 3})$$

with  $E$  the energy,  $h$  Planck's constant,  $\nu$  the frequency,  $\lambda$  the wavelength,  $c$  speed of light,  $\tilde{\nu}$  the wavenumber. The according values are presented in Table 1. The ranges of energy that are used for excitation of different modes split IR spectroscopy in three sections. The “mid-IR”, the most prominent of the three, ranges from  $4000 - 400 \text{ cm}^{-1}$ . Within this region the typical normal stretching and bending modes of intramolecular vibrations are observed. Employing higher energy, overtone vibrations and combinations of mid-IR vibrations are excited. This field using radiation between  $4000$  and  $10\,000 \text{ cm}^{-1}$  is called “near IR” spectroscopy. Consequently, in the region of wavenumbers lower than  $400$  to  $40 \text{ cm}^{-1}$  the method is called “far IR” spectroscopy<sup>3</sup>. Miscellaneous modes such as low frequency bonds, skeletal vibrations, crystalline phonon vibrations and intermolecular vibrations are induced<sup>4</sup>. Nowadays with the advent of new instrumentation operating in the very far IR a special term for the range between  $1$  and  $100 \text{ cm}^{-1}$  has emerged, the THz-spectroscopy. This term derives from the frequency conversion of  $33.3 \text{ cm}^{-1}$ , which equals a frequency of  $1 \text{ THz}$ .

A more detailed introduction to the type of vibrations and its generation in IR spectroscopy can be found in various books<sup>5,6</sup>.

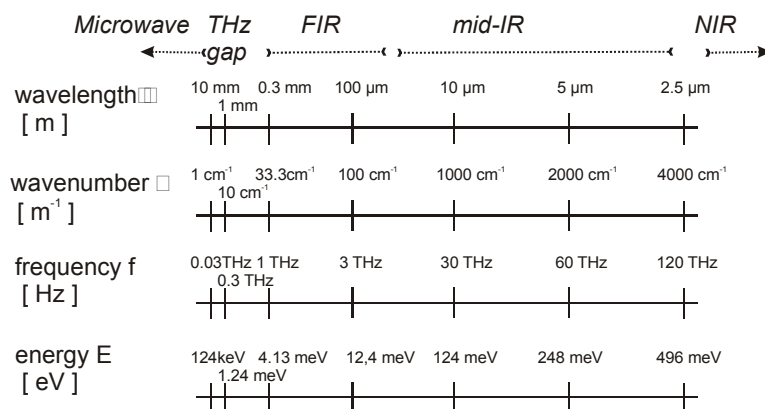


**Table 1 Conversion table for the electromagnetic spectrum in the employed region**

The required radiation for performing spectroscopy using polychromatic radiation enables measurements of a broad spectral region. The ideal polychromatic radiation source is a black body. Its energy distribution shows a maximum, whose position shifts with increasing temperature towards lower wavenumbers. Planck's law is characterising a blackbody<sup>7</sup> by giving the spectral energy density  $U$  as

$$U_{\tilde{\nu}}(T) = \frac{C_1 \tilde{\nu}^3}{e^{C_2 \tilde{\nu}/T} - 1} \quad (\text{Eq 4})$$

where  $C_1$  and  $C_2$  are the first and second radiation constants,  $C_1 = 1.191 \cdot 10^{-12} \text{ Wcm}^{-2}\text{sr}^{-1}(\text{cm}^{-1})$  and  $C_2 = 1.439 \text{ Kcm}$ . The most common light source for mid-IR spectroscopy a globar, a rod made out of silicon carbide, strongly resembles a blackbody. By electrical heating to temperatures of 1200 to 1500 K the emission spectrum can be adjusted to the frequency region of interest. For the near-IR a similar source, a Nernst glower is used. For measurements in the far-IR a mercury lamp, which makes the surrounding quartz emitting radiation, is employed. Types of alternative light sources will be discussed throughout this work.

### The Interferometer

Early mid-IR spectrometers were dispersive instruments with monochromators recording the spectral region sequentially by scanning the different wavenumbers stepwise. Introduction of the mathematical principle of Fourier-Transformation (FT) started a new era in IR spectroscopy, while dispersive instruments remained in use only for special applications. The best known experimental implementation of the FT-principle is the Michelson-Interferometer. Its working mechanism is shown in (Figure 1). The emitted light is hitting the beamsplitter, where one part is directed towards the mirror in fixed position and the other part is passing

through onto the movable mirror. Both radiation parts are reflected and merging at the beamsplitter, from where the light propagates through the sample and is then collected by the detector. The detector records the sum-intensity of the interfering radiation parts as a function of the retardation of the mirror resulting in the sinusoidal interferences. The principle is graphically explained for monochromatic radiation. Employing polychromatic light the interferogram appears more complex, but the transformation of the interferogram from the time domain back gives the familiar spectrum of wavenumbers.

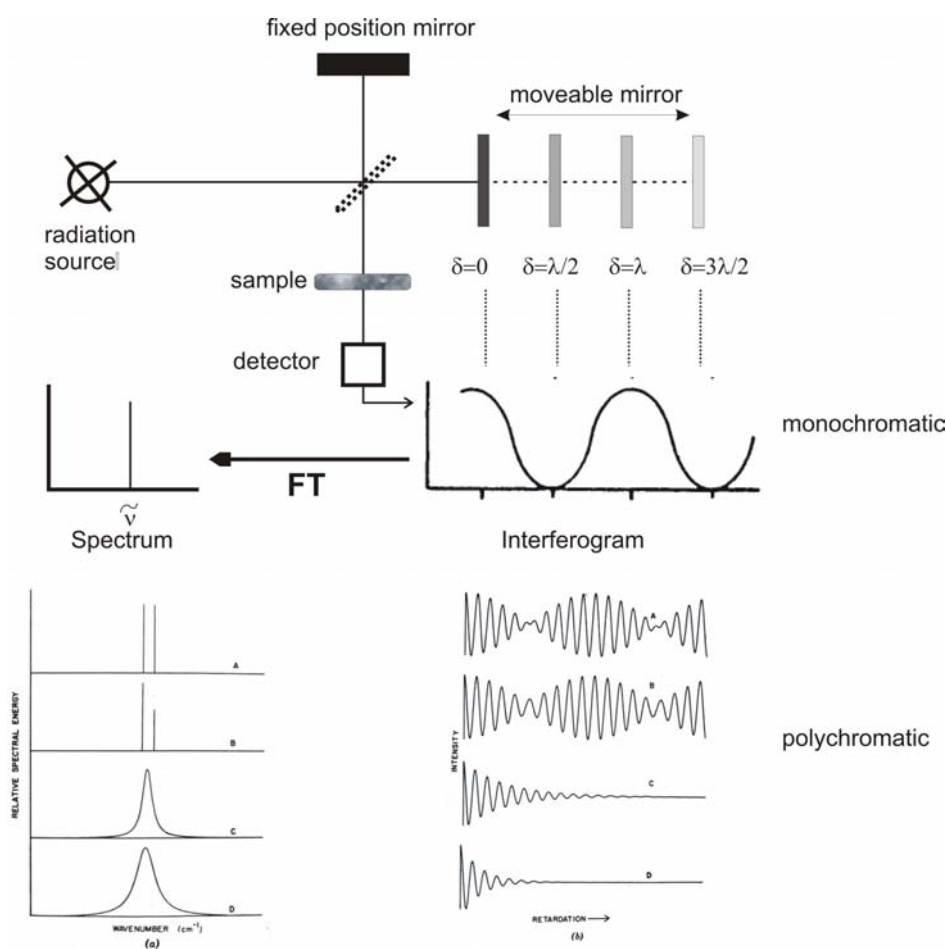


**Figure 1 Michelson Interferometer working principle**

The three main **advantages of FT-IR instruments** are:

- (1) *Felgett* or *multiplex advantage*: High light throughput, due to the lack of a wavelength range selecting slit, enabling microanalysis owing to the significantly increased sensitivity.
- (2) *Jaquinot* or *throughput advantage*: Fast spectrum acquisition and simultaneous detection of all wavelength during one scan

- (3) *Connes or calibration advantage*: High wavenumber precision. Together with (2), this allows for fast and precise signal averaging by co-adding several to hundreds of FT scans for each spectrum, improving the signal-to-noise-ratio (S/N) by the square root of number of scans.

In order to adjust the settings in a Fourier transform Infrared (FTIR) to designated measurement parameters the following has to be considered: The time for recording a spectrum is dependent on the mirror velocity and the electronics for data processing. Further, to achieve high spectral resolution the interferogram has to be recorded for long retardation, and this will of course affect the measurement time. Conversely the bandwidth of a spectrum is depending on distance of the sample points evaluated during the transformation.

The typical detectors used for the mid-IR recording are the mercury cadmium (MCT) detector and the deuterated triglycine sulfate (DTGS) detector. While the latter one is a thermal detector responding to temperature changes, which are directly proportional to the incident radiation power, the MCT belongs to the category of photon detectors responding proportional to the number of photons. The MCT has to be operated at 77 K (N<sub>lq</sub> cooled) providing a narrower range but higher sensitivity and faster response. For enhanced sensitivity in the far IR a bolometer is typically used, based on the same working principle, as the MCT but requiring He<sub>lq</sub> cooling.

Both, measuring either the reflected part or the transmitted part of the energy, exhibits information from a probed sample in infrared spectroscopy. In general it provides access to the optical properties of the sample. The optical constants of a material are given in the formula for the complex refractive index

$$\hat{n}(\tilde{\nu}) = n(\tilde{\nu}) + ik(\tilde{\nu}) \quad \text{(Eq 5)}$$

with  $n$  being the refractive index  $k$  the imaginary refractive index or more familiar the absorption index. It is generally known that the refractive index of a material changes slightly with the wavenumber, which is called the dispersion of the refractive index. When  $k$  rises shown as absorption in a spectrum the refractive index of the sample changes from the average value at positions either side of the band, where the sample does not absorb IR radiation. This is called anomalous dispersion graphically explained in Figure 2.

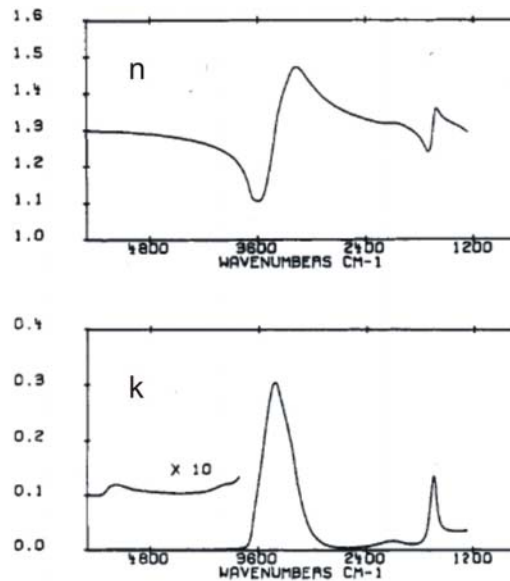


**Figure 2 Anomalous dispersion: The real  $n$  and the imaginary part  $k$  of the complex refractive index of  $\text{H}_2\text{O}$  <sup>8</sup>.**

The refractive index is of practical importance measuring in transmission several layers of different materials. When light is crossing two media of different refractive indices, the incident angle of the beam changes according to Snell's law. Furthermore, when they are significantly different, reflection of part of the rays at plane parallel surfaces occurs resulting in a standing wave effect. This leads to the interference fringe pattern, which disturbs the absorption spectra, but can be used to derive information such as the sample thickness.

The absorption index in transmission measurements the quantity actually measured in transmission measurements. The light absorbed by the sample in transmission measurement is evaluated using Maxwell's equation<sup>9</sup> of electromagnetism for calculating the intensity in a beam after it has travelled a certain distance  $r$  through a material it can be written as

$$I = I_0 \cdot e^{-4\pi\tilde{\nu}kr} \quad (\text{Eq 6})$$

with  $I_0$  the intensity reaching the detector without passing the sample and  $I$  the transmitted part of the intensity passing the sample. Replacing  $4\pi\tilde{\nu}k$  by the linear absorption coefficient  $\alpha_l$  it applies that

$$-\ln\left(\frac{I}{I_0}\right) = \alpha_l \cdot l = A_e \quad (\text{Eq 7})$$

with  $l$  the sample thickness and  $A_e$  presenting the so called Napierian absorbance (because it implements the natural logarithm), which is mostly used by physicists studying the optical properties of materials. In chemistry Lambert-Beer's law is more common, using the decade logarithm, therefore Equation 7 can be written as



$$A(\tilde{\nu}) = -\log \frac{I}{I_0} = k_c(\tilde{\nu}) \cdot c \cdot l \quad (\text{Eq 8})$$

with  $A$  being the absorption,  $T$  the transmission,  $k_c$  the molar decade absorption coefficient,  $c$  the concentration and  $l$  the sample thickness. This implies that for extracting the information of a sample it is necessary to record a background corresponding to  $I_0$ .

### 1.3 Water in IR spectroscopy

Water has importance as a solvent, a solute, a reactant structuring proteins, nucleic acids and cells. Thus water is the typical solvent for studying biochemical processes. In spite of much work, many of the properties of water are puzzling. Insight is given by understanding that water molecules form an infinite hydrogen-bonded network with localized and structured clustering. An extensive compendium on what is known about water today is given by Martin Chaplin<sup>10</sup> citing about one thousand publications dealing with water.

In IR spectroscopy water is on the one hand itself a strong absorber, which must be considered using it as solvent for investigating dissolved samples. On the other hand IR spectroscopy provides a valuable tool for studying properties and the anomalies of water providing structural information.

The IR spectrum of liquid water contains several vibrational modes, presented in Figure 3. The most dominant feature is located around  $3400 \text{ cm}^{-1}$ , which corresponds to the stretching motion of the OH bond ( $\nu_{1,3}$ ) in bulk water<sup>11;12</sup>. At  $\sim 1645 \text{ cm}^{-1}$  the HOH bending mode absorbs IR. It is a rather prominent band due to its overlap with amid I band of proteins. As a consequence, it is necessary to keep the optical path through aqueous solution short ( $\sim 8 \mu\text{m}$ ), in order to avoid total absorption at  $\sim 1645 \text{ cm}^{-1}$  and having enough light transmitting carrying the information of the protein reaching the detector. The broad band centred around  $680 \text{ cm}^{-1}$  derives from restricted rotations or rocking modes, the so-called libration mode. The band around  $2150 \text{ cm}^{-1}$  is a combination of the HOH bending vibration and the libration band around  $680 \text{ cm}^{-1}$ .<sup>13</sup> In the far IR two more bands are observed. The OH intermolecular stretching mode, found at  $\sim 180 \text{ cm}^{-1}$ <sup>14</sup> and the OH intermolecular bending mode at  $\sim 60 \text{ cm}^{-1}$

<sup>1</sup> 15;16

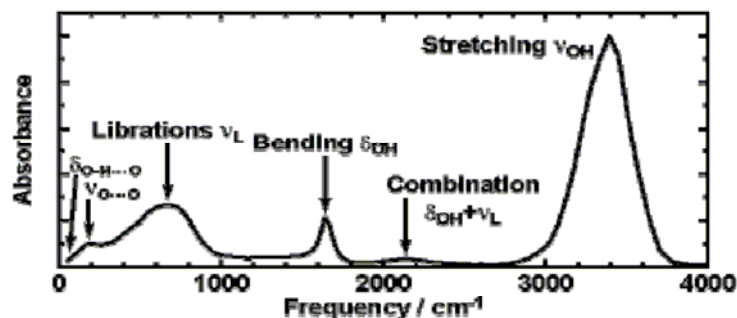


Figure 3 Vibrational bands of liquid water in the mid- and far-IR.

The typical water bands are found to be a composite of several bands deriving from the different structures that are present in liquid water. Furthermore, the H-bond network of water is breaking and forming permanently. The dynamics of these processes takes place in the picosecond time interval. As a consequence, conventional FTIR spectroscopy is too slow to see this.

As water vapour is a strong IR absorber showing many rotational modes attached to the vibrations. Therefore, it is necessary to exclude water vapour from IR spectroscopy.

Additionally it has to be considered that due to the strong absorption also the refractive index is remarkably changing with different wavenumbers. Detailed studies are provided from Zelsmann<sup>17</sup> especially in the far IR, where the refractive index climbs up to a value of 9 at 0.03 THz<sup>9</sup>.

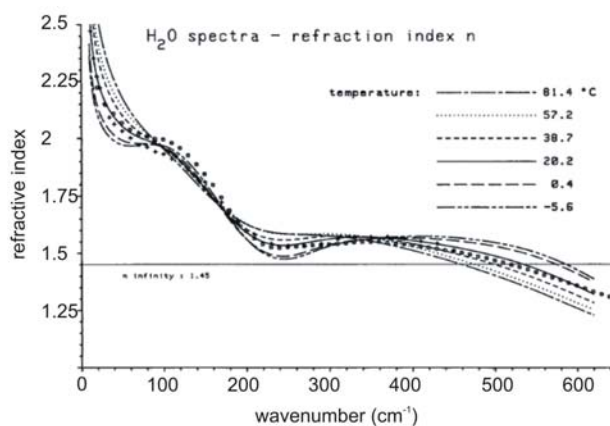


Figure 4 Refractive index for H<sub>2</sub>O in the far IR.<sup>17</sup>

## 2 Time resolved FTIR spectroscopy

Time resolved spectroscopy in the mid-IR presents a powerful tool for the investigation of dynamic processes on molecular scale. This technique provides information from a wide range of molecules without the need for labelling (as e.g. in fluorescence spectroscopy). In general, the maximum achievable time resolution is depending on the interferometric technique. In the *rapid scan mode* one interferogram is recorded for obtaining an IR spectrum. Thus giving a maximum time resolution by the time needed for recording one interferogram, which corresponds to the low ms region (60 ms common FTIR spectrometer). In this case the experiment has only to be launched once for acquiring a time resolved spectrum series. In order to achieve better time resolution the interferogram can be recorded stepwise (*step scan mode*), where for each step the start of the experiment must be repeated. The time resolution limit is set by the response time of the MCT detector<sup>18</sup> and about 1 ns time resolution can be reached.

In Biochemistry there exist processes on all various time scales starting in the fs range (the dynamics of water) up to the minute regime (bioprocesses). Exploiting the high information content of IR spectra for evolving systems offers a wide range of applications, allowing the detection and structural characterisation of transient reaction intermediates as well as the measurement of kinetic constants. Examples are the investigation of conformational changes in proteins, which give information on e.g. malfunctions that can lead to diseases<sup>19</sup> or the elucidation of the factors that make low-spin d<sup>6</sup> transition metal complexes useful as sensitizing dyes or ‘antenna molecules’ in solar energy.<sup>20</sup>

The crucial task in time resolved FTIR spectroscopy is the triggering of the events under study. External triggers such as light pulses<sup>21</sup>, temperature jumps<sup>22;23</sup> or application of electric fields<sup>24</sup> have been in use, but they all are of limited use as only a few reactions can be started with these triggers. The most universal applicable technique is starting a reaction by mixing of solutions containing the reaction partners, which is topic of this work.

## 2.1 Mixing induced time resolved FTIR spectroscopy

### 2.1.1 The microfluidic mixing system

A reaction can be induced by mixing two or more solutions containing the reaction partners. Therefore the solutions are mixed either in a mixing chamber rapidly and then transferred to an IR transmission cell (Figure 5a), or in a mixing unit that is directly integrated in the IR transmission cell (Figure 5b). The advantage of the latter approach is the absence of a transfer line, which would cause unwanted dead-time. However, while in the first approach any mixer can be used, the second approach requires a special design for FTIR spectroscopy.

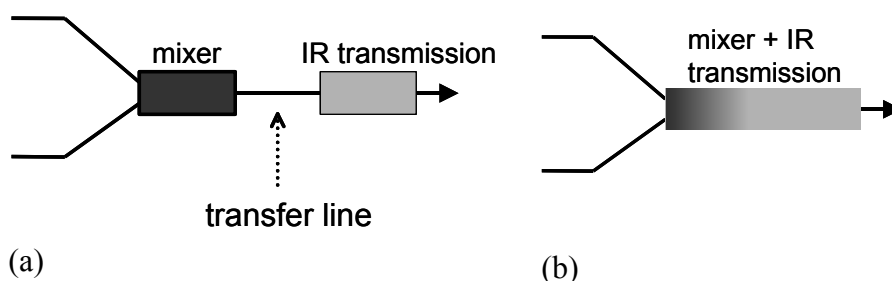


**Figure 5** Two generic concepts for implementing a mixing unit in a set-up for time resolved measurements.

Several prerequisites must be considered for setting up a mixing device for time resolved FTIR spectroscopy:

- Early access to reaction is desired. If a connection between mixing unit and transmission part for monitoring, is necessary, the distance should be kept as short as possible, to avoid dispensable dead-time.
- Furthermore, dealing with biochemical reactions the sample consumption has to be kept low. The amount of available bio-molecules of interest is limited and the concentrations required for FTIR experiments are high.
- The IR cell must be designed for aqueous solutions, as the typical solvent for investigation of biochemical systems is water based. Owing to its high absorbance the maximum optical path length is  $\sim 10 \mu\text{m}$ .
- As common to all the triggering techniques the start of the reaction has to be fast and uniform across the IR cell, in order to ensure that the reaction is of “same age” for the total probed volume

- Monitoring biochemical reactions requires a high signal-to-noise ratio (S/N), especially in case of protein folding or bio-ligand interactions as only very small spectral changes may be expected. Therefore, the mixing must be highly reproducible to allow signal averaging from experiments.

These considerations are incorporated in the construction of our design for a mixing and transmission cell. First of all, the elimination of dead time between mixing and transmission part is realised by the integration of the mixing unit in transmission cell. In this way, it also becomes possible to record spectra of both solutions prior to mixing and right from the start of the mixing process.

Further, the mixing system should be miniaturised. However, minimising the flow channels leads to low Reynolds number and therefore there are no turbulent vortices that enhance mixing, but the flow will be strongly laminar. In laminar flow regimes mixing will be solely diffusion driven, which is known as a rather slow process. The diffusion time and the time for the mixing process, respectively can be calculated by the formula derived from Fick's Law, which is valid for plane sources in semi-infinite media <sup>25</sup>

$$c(x,t) = \frac{c_0}{\sqrt{\pi Dt}} e^{-\frac{x^2}{4Dt}} \quad (\text{Eq 9})$$

with  $c$  being the concentration of a substance dissolved in the liquid, and  $c_0$  the concentration at the beginning ( $t = 0, x = 0$ ),  $D$  the diffusion constant for the substance that is spreading,  $x$  the distance of diffusion along an axis and  $t$  the diffusion time. The correlation of diffusion distance and diffusion time is given by the term  $x^2/4Dt$  in equation 1. In order to increase the speed of mixing, the distance that is to overcome by a substance driven by diffusion has as to be small as possible. This can be achieved by narrowing the streamlines of the fluidics to mix. In the thesis of Peter Hinsmann<sup>2</sup> two designs have been tested. A "spaghetti-like type" where multi-lamination is achieved by alternating streamlines (Figure 6a) and a "lasagne type", where two narrow flow sheets are superimposed (Figure 6b). Investigation revealed that for the chosen dimensions the lasagne-type mixer had a better performance in terms of mixing speed and robustness. Furthermore, this design also allows for spectroscopically more accurate absorbance measurements: When the diffusive mixing occurs in the direction of the transmitting IR light the measured absorption remains constant before and after the mixing. In case of mixing perpendicular to the passing IR beam a change in absorbance will be recorded as the intensity reaches the detector is affected by the diffusion mixing process. This effect is graphically explained in Figure 6.

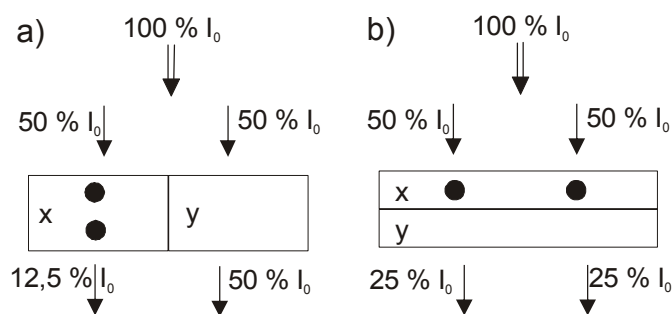


**Figure 6. Comparison of IR intensities reaching the detector after absorption for a) alternating lamination of x and y (spaghetti type) and b) superimposing flow sheets (lasagne type). It is assumed that each molecule (symbolised by the black points) in x is absorbing 50 % at half of the optical path whereas molecules in y are non-absorbing. (Publication IV)**

A sketch of the mixer chip principle based on the above-mentioned considerations is given in Figure 7.

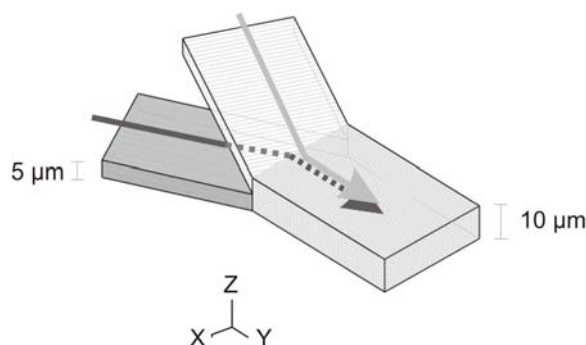


**Figure 7. Scheme of the mixing device developed for time resolved FTIR measurements**

## 2.1.1.1 Monitoring mode

### 2.1.1.1.1 Stopped-flow mode

The most obvious approach is to stop the flow once both liquids are in the mixing chamber which is also the transmission cell, and follow the reaction by repeated scans of the FTIR instrument. This mode is commonly denoted as “stopped-flow mode” and has been already extensively applied in various set-ups<sup>26-28</sup>. The discussed design was operated by Hinsmann et al.<sup>29</sup> in the stopped-flow mode. Using high flow rates, as 100 µl/min, the liquids in the mixer will not have enough time to mix while the flow is on. This gives the opportunity to measure the two liquid streams prior to mixing. By stopping the flow, the diffusion between the liquid streams leads to mixing within several 10ths of ms and then the reaction can be recorded by taking spectra one after each other.

The time resolution in this mode is depended on the scan speed of the FTIR instrument. In the thesis of Peter Hinsmann <sup>2</sup> it was demonstrated that by employing the rapid scan mode a time resolution of 65 ms could be achieved. In order to obtain a good S/N, it is necessary to repeat the stop flow process several times for accumulating scans.

This mode allows measuring at a spot size of 1 mm, which can be provided by a beam condenser attached to standard FTIR instrument. As opposed to the continuous flow mode, no moving of the cell is necessary for the measurement. Therefore one background spectrum can be used for all sample spectra.

### ***2.1.1.1.2 Continuous-flow mode***

The same type of mixing device can be used for the “continuous-flow mode” <sup>19;30</sup>. In this mode an about 100 times lower flow rate, which enables mixing while the flow is kept on. After the mixing step the reaction occurs, while the mixture flows downstream the channel. The age of the reaction mixture (i.e. the reaction time) depends on the distance between the mixing and observation point. As a consequence, the time resolution is now no longer dependent on the scan speed of the FTIR instrument, but on the following two parameters: the flow speed in the channel and the distance between adjacent sample spots.

#### Time resolution spot size determined

When the flow speed is kept constant, the time resolution is solely dependent on the distance between two adjacent measurement spots measuring downstream the channel. As a consequence, the sample spot size of the FTIR instrument will set the limitation. In order to achieve spot sizes smaller than 200  $\mu\text{m}$  an IR microscope has to be employed. Seeking for the smallest possible spot size in IR spectroscopy overlaps with other scientific area, namely imaging FTIR and synchrotron microscopy. Large improvements have been achieved on these topics. Recently, the limit in spatial resolution of IR microscopy has been enhanced by a factor of  $\sim 5$  using synchrotron light as the IR source <sup>31;32</sup>. In case of imaging, the introduction of array detectors to FTIR microscopes has brought further improvements. (See section 2.2)

#### Time resolution flow speed determined

Performing measurements at a fixed point of the observation channel, variation of the flow speed allows observing reaction volumina of different reaction time. An approach of exploiting this effect solely is demonstrated in Jensen et al <sup>33</sup> using a broad measurement spot ( $\sim 10$  mm).

The theoretical time resolution can easily be read out at a given speed of the liquid in the channel. The flow rate, which is defined as the volume of liquid pumped per time ( $\mu\text{l/s}$ ) can be converted to a linear flow rate ( $\text{m/s}$ ) by dividing the volume flow rate by the channel cross section. In the typical continuous-flow mode the focused measurement spot is moved downwards the observation channel. Increasing the flow speed, the time resolution is enhanced for a fixed distance between two adjacent sample spots. The pressure at the entrance of the mixer chip, which rises proportional with the flow rate, will provoke leaking of the set-up at a certain level. The same effect would be obtained making the channel narrower. This practical aspect limits the application of increased flow rates for enhanced time resolution.

## 2.1.2 The continuous-flow set-up

In the thesis of Peter Hinsmann<sup>2</sup>, the stopped-flow type was investigated to its capabilities and limits, revealing that the time resolution is restricted to  $\sim 65$  ms by the used FTIR instrument. Regarding the considerations above providing two variables for increasing the time resolution, the continuous-flow mode seems to be more potent for achieving higher time resolution. Therefore, the investigation of this approach is the idea of this work.

### 2.1.2.1 The mixer design

#### Design I

The continuous-flow mixer chip, which is the basis for the further work, is presented in Figure 8. A mixing unit between two  $\text{CaF}_2$  plates achieves superimposition of two streamlines. A silver layer is separating the two liquid streams until they reach the observation channel. The silver layer is operating as mask for the channel as well. The observation channel is  $300 \mu\text{m}$  broad,  $10 \mu\text{m}$  thick and  $11 \text{ mm}$  long. The cut-off of the silver layer marks the starting point with  $y = 0$ .



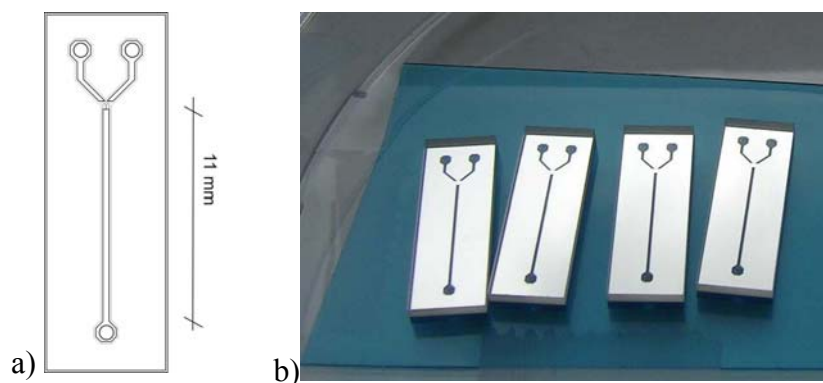


**Figure 8 Design I: (a) schematic drawing (b) new mixer chips prepared from one batch.**

The operation of the mixer chip is shown in Figure 9. The two liquid streams that contain the reaction partners are fed into the chip via Teflon tubings of 0.25 mm inner diameter driven by a syringe pump (KDS Model 200, Novodirect, Kehl Germany), which allows operating in the range of  $\mu\text{l/h}$  up to  $\text{ml/min}$ . The typical applied flow rate was  $0.5 \mu\text{l/min}$  for each syringe, resulting in the channel in a value of  $1 \mu\text{l/min}$ . This equals to a linear flow rate of  $1000 \mu\text{m}$  per  $180 \text{ ms}$  ( $0.006 \text{ m/s}$ ).

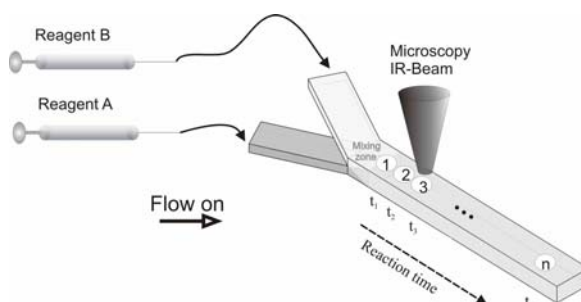


**Figure 9 Two Hamilton syringes feed the mixer chip continuously, while IR spectra can be performed on several positions downstream the observation channel.**

### Design II

A second design with an especially narrow channel was worked out (Figure 10). The observation channel dimensions are  $15 \times 10 \mu\text{m}$ . This allowed fully abandoning the superimposing principle, while simple merging the channels of three inlet channels into the  $15 \mu\text{m}$  broad observing channel was sufficient for creating  $5 \mu\text{m}$  thick flow streams. The starting point of the observation channel  $y = 0$  equals the point when the 3 inlets merge in a cross. As a consequence no silver-foil is needed, which also means that no mask for covering the outside of the channel is provided. Furthermore, the principle explained in Figure 6 is neglected.

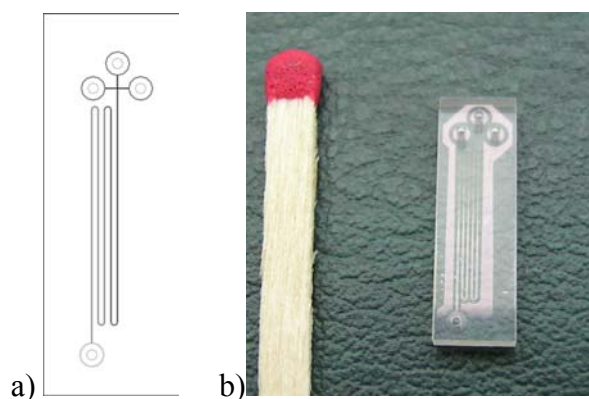


**Figure 10 Design II: (a) schematic drawing (b) mixer chip with the observation channel in serpentine.**

### Production of the microchips

The production of the chips has been carried out by Peter and Edda Svasek from the Institute of Sensor and Actuator Systems at the Vienna University of Technology. The mixer chips are consisting mainly of  $\text{CaF}_2$ , which has been chosen due to its high transparency in the mid-IR and the resistance to aqueous solutions and some more solvents. The disadvantage of this material is that it is brittle and therefore difficult to structure in the micro-meter scale. A solution for this problem has been found by forming the structure of the mixing zone and the channel by the epoxy resin SU-8, a negative photo-resist.

The mixer chips are produced in batch by using  $\text{CaF}_2$  wafers (1 mm thick, 5 in diameter) where the single chips are then cut out. For the fabrication SU-8 is spin-coated on two plates up to a height of 4  $\mu\text{m}$ . After the resin has been allowed to dry, the layer is covered by an appropriate mask in the form of the lower inlet-channel and the observation channel and exposed to UV light for hardening. Then a 2  $\mu\text{m}$  Ag-layer is deposited by evaporation on the bottom wafer carrying the structured SU-8 and patterned by wet etching with  $\text{Fe}(\text{NO}_3)_3$  using a positive photoresist layer as mask (later removed by the developer AZ400K). The unexposed and therefore not cross-linked SU-8 is then removed by dissolving it in propylene glycol monomethyl ether acetate (PGMEA). In the top  $\text{CaF}_2$  plate which carries the structure of the other inlet-channel and the observation channel the according holes for the inlets and outlet are drilled. Finally the two plates can be bonded and the ready chips can be cut out. A more detailed prescription of the fabrication of the process mixers is given in <sup>34</sup>, and for design II in **publication II**.

The according IR spectra from each compound used in this fabrication process are taken as reference (Figure 11), in order to ensure that no spectral feature later measured in the channel can be erroneously assigned to the reaction under investigation.

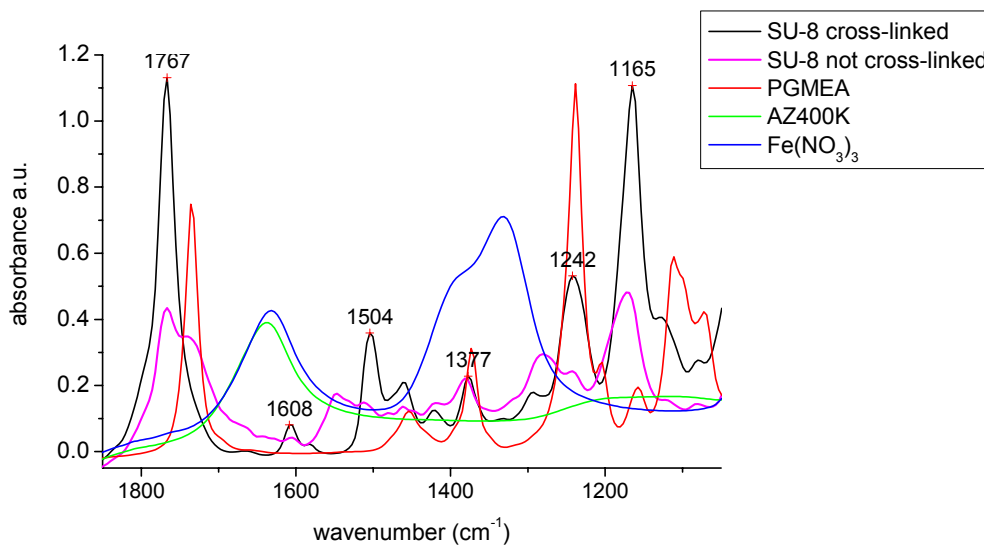
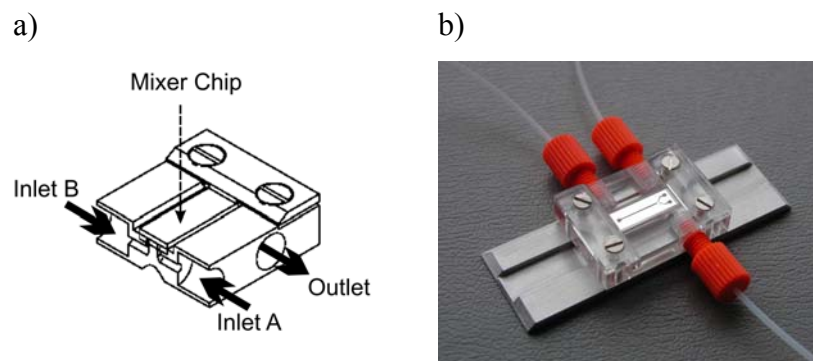


Figure 11 IR spectra of the substances used during the fabrication process of the microchip

### The support

A by no means trivial task is the connection of the mixer chip to the “real world”. Dedicated work<sup>35</sup> has been presented dealing with the problem of easy connecting lab-on-a-chip devices to medium flow-rates due to the resulting high backpressure at the inlets. Another crucial issue is the space that is available in a confocal microscope using high magnification. In the case of the Nicolet Continuum (Thermo Electron Cooperation, USA) microscope employing a 32x magnification only 7 mm above and below the focal point are available. This new demand made an adaptation and improvement of the existing support necessary<sup>2</sup>.

The new support (see Figure 12) has been made of PMMA and connects 3 tubes, two for the inlet and one for the outlet, to the holes of the mixer chip. The chip is pressed onto the support by two PMMA clamps, which can be screwed. O-rings from composition rubber are used as sealing. This support allows easy mounting and dismounting of the chip, avoiding leaking problems. Furthermore, it is only 10 mm high and holds the chip at a height of 6 mm, thus enabling focusing under the microscope even when using a 32x or 36x objective.



**Figure 12** The support for the mixer chip: (a) schematic construction (b) picture of the ready made support with the introduced mixer chip.

### 2.1.2.2 Simulations

For understanding the flow pattern and mixing behaviour in this micro-mixer, simulations are needed. Computational Fluid Dynamic (CFD) simulation have been proven to be a valuable tool for judging the performance of mixer chip <sup>29</sup> by giving detailed insight in actually occurring flow pattern and diffusion unit profiles. Employing CFD methods the geometry of the tested design is set up on the computer and transferred into a mesh by dividing it into multiple small cells. For this mesh the unsteady Navier-Stokes equations can be discretised considering the conservation equation for mass and energy as boundaries (Newtonian fluid dynamics). The resulting large set of non-linear equations is then solved by iteration.

CFD simulations for the above-described designs have been carried out in cooperation with Michael Harasek from the Institute of Chemical Engineering at the Vienna University of Technology. The whole mixer geometry is implemented into the finite volume solver FLUENT V6.2 software. For the generation of the mixer-mesh GAMBIT 2.1 is used. The geometries investigated fit to a grid consisting of up to  $9.2 \times 10^5$  cells. A laminar flow model considering Fickian diffusion is used and the multicomponent fluid system is modelled by a two-species system a liquid and a diffusing species. Fluid properties are set to the physical and thermodynamic properties of water 293 K and the boundary conditions (exit pressure, fluid inlet velocity) are set to typical experimental values. The results for velocity and mass fraction distribution in two mixer designs will be discussed here.

#### Design I

The settings for calculations on the continuous-flow mixer Design I on the diffusing species “A” and “B” are chosen as in a biochemical reaction of a drug with a peptide, both

dissolved in the same aqueous buffer. The flow rate is assumed with 0.5  $\mu\text{l}/\text{min}$  at each inlet channel resulting in a linear flow rate of  $0.006 \text{ m}\cdot\text{s}^{-1}$  in the observation channel. The physical properties are taken from the substances used later for the study of vancomycin<sup>36</sup>:

	$MW \text{ (g}\cdot\text{mol}^{-1}\text{)}$	$c \text{ (g}\cdot\text{l}^{-1}\text{)}$	$D \text{ (m}^2\cdot\text{s}^{-1}\text{)}$	$\eta \text{ (Pa}\cdot\text{s)}$
A (peptide)	372	7.5	$5\cdot 10^{-10}$	0.001
B (drug)	487	9.5	$3.6\cdot 10^{-10}$	0.001

**Table 2 Settings for the 1<sup>st</sup> simulation on design I.**

The viscosity for the solvent was set with  $\eta_{\text{H}_2\text{O}} = 0,001 \text{ Pa}\cdot\text{s}$ .

The CFD calculations gave access to the pressure, the velocity and the mass fraction profile. The velocity distribution in the observation channel is of special interest due to the expected influence on the typical parabolic flow profile being formed owing to the strongly laminar flow conditions in the micro-mixer. Figure 13 shows a cross section at  $y = 250 \mu\text{m}$  after the silver foil cut off. It reveals that the flow velocity drops not only towards the side borders in x direction, but also in z direction. In case of transmission measurements, the effect in x direction can be fully neglected by taking care that the IR beam passes only within in the inner 90 % of this channel. However, the distribution in the z-axis cannot be avoided and has to be taken into account when stating the achieved time resolution. Direct calculation of the reaction time by dividing the distance travelled in y-direction with the linear flow rate (= theoretical time axis), actually presumes a constant linear flow rate across the z-axis. The influence of the laminar flow profile leads to age distribution for the travelling fluid elements. Therefore, in one measurement position fluid elements that are assigned to different time scale are measured. Reading out the obtained values for the z-axis at the middle of the channel, it reveals that only 3 % of the fluid on this axis travel with a speed lower then 90 % of the maximum speed. Most likely, the effect is even smaller, when also the molecular diffusion of the mixed components along the z-axis could be considered.<sup>29</sup>

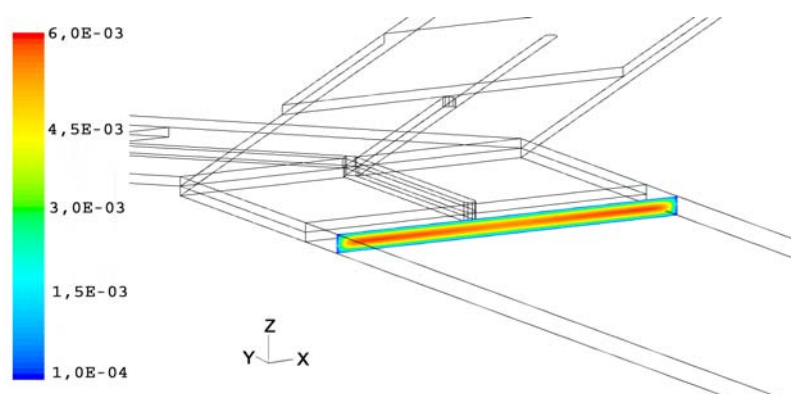


**Figure 13 The velocity profile at  $y = 250 \mu\text{m}$**

Of higher importance for the time resolution is the mixing performance of the mixer chip. Only when the mixing is finished the kinetic processes solely can be observed. Figure 14 gives the mass fraction profile of component *A*. In the simulation it was assumed that component *A* is introduced at the bottom inlet channel, visualised by the red colour for 100 % of component *A*. Further, immediately when the cut off of the silver foil that separates the two liquid streams is reached the diffusive mixing starts. Complete mixing is achieved when the mass fraction amounts 0.5, resembled by the green colour. For starting most reactions it is not necessary to reach this value. Therefore the term “mixture quality” was defined rating the mass fraction dispersion in *z*-direction. The criterion for sufficient mixing is achieved when along the channel height (*z*) all fluid elements contain a mass fraction between 0.4 and 0.6. Figure 15 illustrates this criterion by the dotted lines. Thereof it can be concluded that right at the end of the separating silver layer the mixing starts, but it takes more than 200  $\mu\text{m}$  to achieve the aimed mixture quality. This time profile dispersion as a consequence blurs the time axis that is assigned to the channel sections.

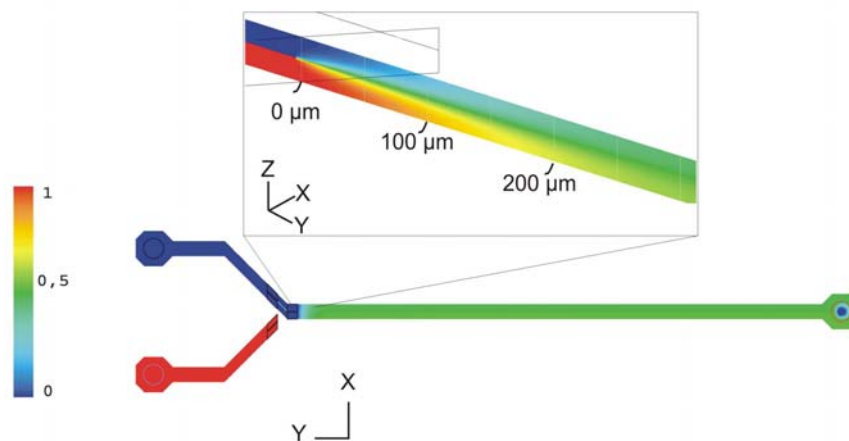


**Figure 14** Mass fraction distribution of component *A*. A zoom in the *yz*-plane at  $x = 75 \mu\text{m}$  into the mixing zone shows that it takes about 200 – 250  $\mu\text{m}$  to achieve homogeneous distribution of component *A* in the channel in *y* direction.

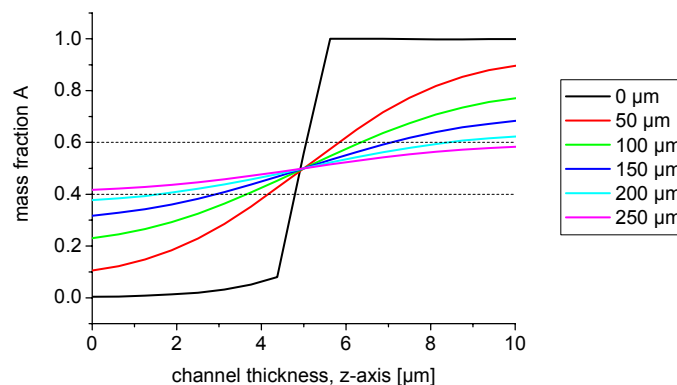


**Figure 15** The mixture quality derived from the CFD simulations presented in Figure 14

An approximation for the real time deriving from the simulations result can be written as:

$$t_{\text{real}} = t_{\text{theoretical}} + \Delta t_{\text{mix}} + 0.03 \times (t_{\text{theoretical}} + \Delta t_{\text{mix}})$$

The theoretical time is obtained by dividing the probed volume by the flow rate, the  $\Delta t_{\text{mix}}$  is the time needed for mixing (for the simulated data it amounts 45 ms) and the factor of 3 % takes the influence of the laminar flow profile into account. This formula is not universally valid, as deviations of the perfectly shaped channel assumed for the simulations are to consider as well and are not possible to be quantified.

However, even if a fully correct time axis cannot be assigned due to the effects, a relative time axis can be given with good approximation. This means that the time resolution between spectra can be read out and e.g. appearance and disappearance of reaction intermediates can be well resolved.

Once the set-up of the geometry for the CFD simulation is performed, it is possible to vary the parameters determining the physical properties of the fluids. Therefore, simulations were also carried out for various conditions. The above settings present the chemical system of the reaction under study throughout this work. In order to test the mixing performance for a conformational study on a protein the following  $\Delta$  settings were chosen:

	$MW$ ( $\text{g}\cdot\text{mol}^{-1}$ )	$w\%$	$D$ ( $\text{m}^2\cdot\text{s}^{-1}$ )	$\eta$ ( $\text{Pa}\cdot\text{s}$ )
A (protein)	37000	1	$8 \times 10^{-11}$	0.1
B (drug)	429	1	$5 \times 10^{-10}$	0.001

**Table 3 Settings for the 2<sup>nd</sup> simulation on design I.**

The flow rate was set to  $5\mu\text{l}/\text{min}$  at each inlet.

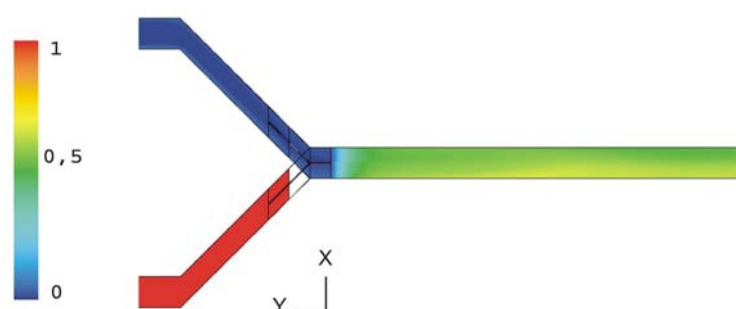


**Figure 16 Mass fraction distribution of component A resembling a protein (MW 37 000)**

The mixing performance at the beginning of the channel seems to be as good as for the 1<sup>st</sup> simulation presented by the uniform colour. However, the appearance of a mass fraction higher than 0.6 at about  $1500\mu\text{m}$  reveals that there are inhomogeneities in flow speed in the channel (not related to the laminar flow profile). The reason therefore is the  $45^\circ$  turn in the

mixer geometry. Forcing the liquids in a curve results in higher flow rates towards the outer border of the turn (similar to a river propagating in a meander pattern). This effect is observed here due to the ten times higher flow rates in combination with the different properties in viscosity and diffusion coefficient of the two mixing solutions that decelerate diffusive mixing. In order to prevent this effect to appear, either care should be taken on these two aspects (this has been obeyed throughout this work), or the influence of the 45° turn has to be removed in a new chip design.

### Design II

The flow dynamics for the mixer chip with the special narrow dimensions were also simulated. The flow velocity was set to  $8 \times 10^{-2} \text{ m}\cdot\text{s}^{-1}$  as for the observation channel and the diffusion coefficient was assumed with  $D = 10^{-9} \text{ m}^2\cdot\text{s}^{-1}$  for component A, which is introduced via the middle inlet channel.

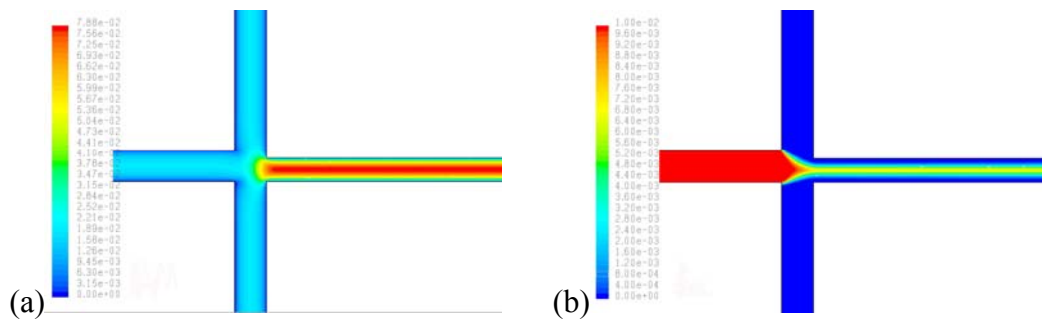


**Figure 17** CFD results for the mixing zone design II. The velocity profile (a) and mass fraction for A (b) that was introduced only in the middle inlet-channel are shown at half thickness of the mixer chip.

The picture (a) nicely visualises that by merging the three channels the flow speed is increasing by a factor of 3. The influence of the laminar profile can be very easily seen. The mass fraction profile (b) is showing a rather extended mixing area owing to the rather high flow speed. In the presented  $150 \mu\text{m}$  the aimed mixture quality is by far not achieved. Part of the reagents coming from the side inlets remain in unmixed status at the border of the beginning observation channel. Nonetheless, the solution in the middle channel is mixing completely.



### 2.1.2.3 Operation of the set-up

The feasibility of the continuous-flow mixer under experimental conditions has been tested using a model reaction. For recording the spectra a modified IR microscope type A590 (Bruker, Ettlingen Germany) available in our laboratory has been employed. Note, that it is modified by exchanging the round aperture for a manually adjustable rectangular shaped one, and the bottom mirror system was exchanged for parabolic mirror. The x,y-stage is motorised driven by Sagittarius III. As model reaction served the formation of hydroxymethanesulfonate an addition product from sulphite or bisulphite and formaldehyde in aqueous solution. This chemical reaction reveals significant spectral changes in the mid-IR and the reaction time will be somewhat lower than the time that is needed for the mixing process. The reaction takes place according to the following reaction scheme:

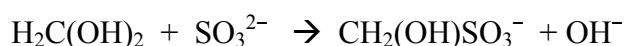
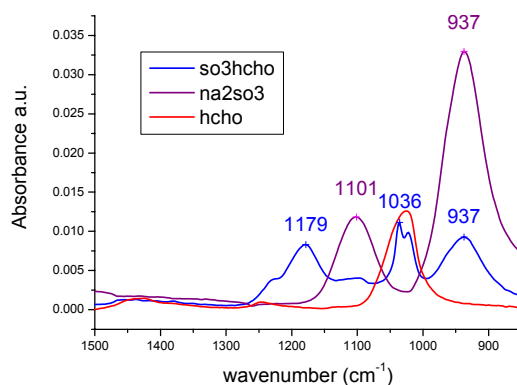


Figure 18 shows the IR spectra of the educts and the reaction product in 0.1 M concentration, acquired measured in an ATR flow cell.



**Figure 18 IR spectra of the reaction educts and the products 0.1 M. For the vibrations assignment see publication IV.**

The syringes (see Figure 9) filled with filtered water have been installed in the syringe pump and connected directly from the needle into the tubing (0.25 inner diameter) avoiding further connections, which would be a source for dead volume (refer 2.1.1). In this way the mixer has been filled with water and then the flow stopped. After the system was allowed to stabilise a set of spectra along the observation channel were recorded for the later used background. Background spectra have been recorded at stopped flow, in order to prevent the mixer chip from introduction of depositing particles, which is never completely avoidable even by passing only filtered HPLC grade water. It revealed that the difference between flow

on and flow off background spectra is marginal, as long care is taken that the conditions are stable.

Then the syringes have been filled with educts and implemented again. The flow speed has been now set to 0.5  $\mu\text{l}/\text{min}$  and the spectra recorded while the flow on. This measurement procedure has been kept the same throughout all continuous-flow measurements.

The result is shown in Figure 19. During the acquisition of spectra the measuring spot has been moved along the observation channel towards its outlet. The reaction takes place until a position of about 2000  $\mu\text{m}$ , marked by the increase of the band at 1180  $\text{cm}^{-1}$  and the decrease of the band at 936  $\text{cm}^{-1}$ .

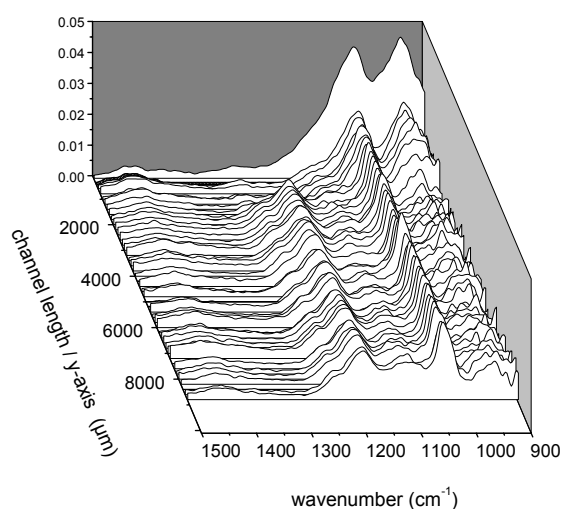


**Figure 19** Time resolved measurement on the addition reaction of formaldehyde and sulphite.

The output proves that the mixer works, showing that mixing of the solutions and on-chip monitoring of the reaction is possible. For a further performance test the flow speed was varied. Results are shown in Figure 20 giving the traces representing the integrated area of an appearing and of a disappearing peak at 1180 and 936  $\text{cm}^{-1}$ , respectively. Doubling the flow speed shifts the position where no more spectral changes are observed by approximately the double distance towards the outlet. This is expected, as the time for mixing point in this way remains almost the same.

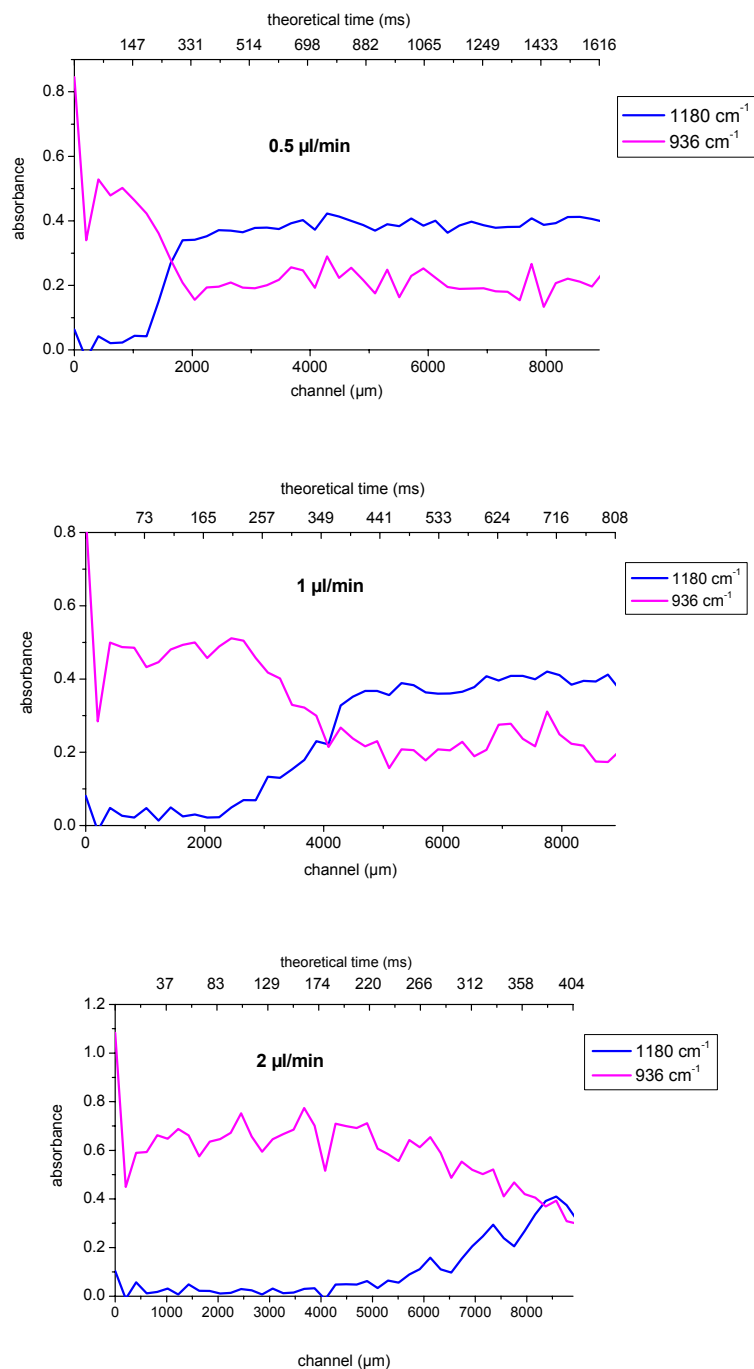


**Figure 20** Mixer operated at 3 different flow speeds presenting 2 traces obtained by integrating the according peak area. The shift of the reaction marked by the increase of the blue and the decrease of the red curve is direct proportional to the flow speed.

The unsteady shape in the beginning of the two traces is rather unexpected, but similar behaviour can be observed in several other experiments in combination with this microscope. Most likely bad alignment of the channel in the beam path is the reason therefore.

From reaction kinetic studies<sup>37;38</sup> a reaction time of about 200 ms and lower would be expected. Thus our results show that the theoretical time scale, which is directly taken from

the overall linear flow rate, present is actually too fast. However, the relative time scale remains valid.

## **2.2 IR Microspectroscopy**

The diameter of the IR beam passing the sample compartment in typical FTIR spectrometers makes up about 1 cm. Using IR for microanalysis raises the need for a more focused beam. In the work of Peter Hinsmann<sup>2</sup> a beam condenser, an optical focusing unit attached to a Bruker Equinox55 providing a spot size of 1 mm, was used for stopped flow measurements. For further reduction of the spot size an IR microscope has to be employed. For further reading note, that the spatial resolution has been achieved on the water filled mixer chip, which represents a complex sample considering its different layers.

### **2.2.1 Single point detector**

#### **2.2.1.1 The conventional IR microscope using global**

The principle of IR microscopy is based on transmission light microscopy<sup>39</sup> using a similar set-up. The light passing through the sample is coming from the FTIR instrument, where the microscope is attached. A schematic drawing of an IR microscope is presented in Figure 21. The light coming from the interferometer focused on the sample and the transmitted light is collected by the objective, and focussed onto the sample in the image plane. The illuminated spot is then reimaged onto the detector. In IR microscopy no lenses are used, but all-reflective objectives, typically in the Schwarzschild configuration.<sup>40</sup> This kind of optics allows for collecting and focusing rays of a high dynamic spectral range. Thus it is also possible to probe the sample by visible light, which is very helpful for selecting the right measurement position. Introduction of an aperture at the primary image plane for sample definition enables to set the sample spot size to defined dimensions. This can either be done manually or by computer. In this way spot sizes of 100 x 100  $\mu\text{m}^2$  probed area can be realised at an S/N that allows detection of small chemical changes in the channel.

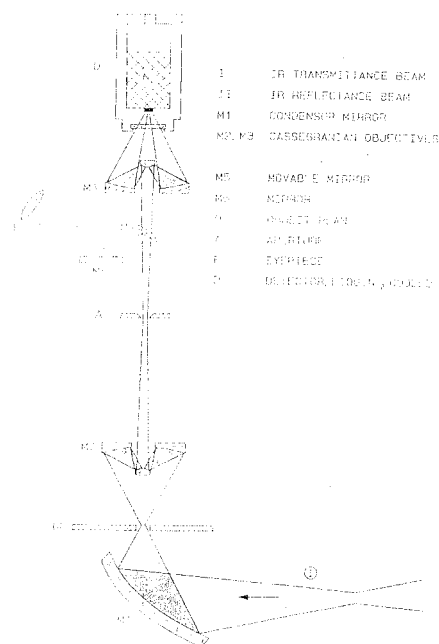


Figure 21 Schematic drawing of the IR microscope type A590 from Bruker, Ettlingen Germany.

Improvement of the spatial resolution can be achieved by a confocal arrangement. The idea of a confocal microscope is the incorporation of point-by-point illumination of the specimen and the rejection of out-of-focus light. This is realised placing a pinhole after the sample serving as a further aperture in the primary image plane and/or before the sample to limit the sample area illuminated by the IR source (see Figure 22) The advantage of this arrangement is that the light reaching the detector only stems from the sample plane of interest and by eliminating any glare deriving from its surrounding, the resolution can be increased and thus the magnification can be set higher. The limits for resolutions are theoretically diffraction limited.<sup>41;42</sup>

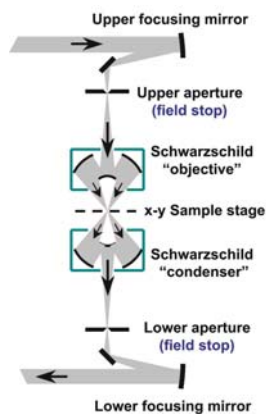
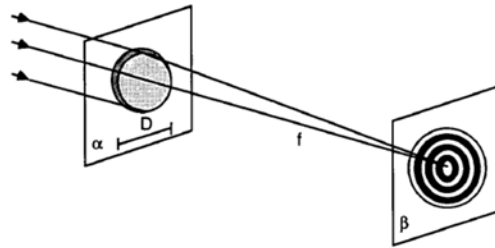


Figure 22 Sketch of a confocal arrangement for a dual aperture system (freely adapted from a Continuum Nicolet)

In an effort to understand where are the IR microscope's limitations a deeper insight in optics is necessary. Assuming that an infinitely small point source of light is possible, no lens/objective system can form a true point image, due to the fact that light is not really travelling in straight-line rays, but according to Huygen's principle of light wave propagation (saying that each point on a wave front may be considered as a source of spherical wavelets; these wavelets reinforce or interfere with each other to form the new wave front).<sup>43</sup> In case the wave front is limited by an aperture smaller than  $\lambda$ , the new wave front becomes spherical about the aperture. Thus the resulting illumination pattern consists of a bright central spot of the light surrounded by rings of rapidly decreasing intensity. This pattern is called the Airy disk (Figure 23), where the central spot contains 84 % of the intensity



**Figure 23** Airy disc pattern on screen  $\beta$  imaging emerges when light passing through an aperture or objective on  $\alpha$  with a diameter  $D < \lambda$ .<sup>41</sup>

The radius of the central spot of the airy disc, which contains most of the light that passes the aperture, is given by

$$r = \frac{1.22\lambda}{2 \frac{a}{R}} \quad (\text{Eq 10})$$

with  $R$  being the distances from the aperture to the screen and  $a$  the radius of aperture. For an objective the radius of the Airy disk is written as

$$r = \frac{1.22\lambda}{2NA} \quad (\text{Eq 11})$$

and  $NA$  the numerical aperture

$$NA = n \cdot \sin\theta \quad (\text{Eq 12})$$

with  $n$  being the refractive index of the medium and  $\theta$  half angle of the cone of illumination. The airy disc presents the smallest possible measuring spot that is achievable at a certain wavelength using a certain objective. As a result, the diffraction of the source and/or sample image through the microscope yields is defined by the superposition of the diffraction patterns

from each imaging element in the system.<sup>41</sup> In case two apertures are used, the Airy distributions are multiplying and achieving better spatial resolution.<sup>44</sup>

This is the maximum resolution that can be obtained using far field microscopy. However, its usability for IR microspectroscopy is depending on the resulting S/N. The correlation of various factors contributing to the S/N for detectors in IR microscopy is given by <sup>7</sup>

$$\frac{S}{N} = \frac{u_{\tilde{\nu}}(T) \cdot \Theta \cdot \Delta\tilde{\nu} \cdot t^{\frac{1}{2}} \cdot \xi}{NEP} \quad (\text{Eq 13})$$

with  $u_{\tilde{\nu}}(T)$  the spectral energy density for a blackbody,  $\Theta$  power received at a detector,  $\Delta\tilde{\nu}$  the spectral resolution,  $t$  the measurement time  $\xi$  the overall system efficiency.

The spectral density for a global light source is discussed in section 1.2. Due to the distribution of light far different from a point like source the losses of radiation on the sample spot (and thus the power received at the detector) increase dramatically at aperture sizes close to the diffraction limit. Another effect contributing to the deteriorated S/N is the dispersion of the light when travelling through the mixer chip composed of layers with differing refractive indices (n): from air (n = 1) through 1 mm CaF<sub>2</sub> (n ~ 1.4) 10 μm water (n ~ 1.3) and again through 1mm CaF<sub>2</sub> and again through air. The factor “overall system efficiency” includes instrument factors, such as the optical set-up.

The term NEP in Equation 14 stands for noise equivalent power of the detector, which is given by the ratio of the noise power density at the detector output divided by the detector responsivity, both measured at the appropriate modulation frequency and can also be expressed by

$$NEP = \frac{A_D^{\frac{1}{2}}}{D^*} \quad (\text{Eq 14})$$

giving the influence of the detector area on the noise by  $A_D$  being the area of the detector and  $D^*$  the “specific detectivity”, which a measure of the sensitivity of a detector. For most IR detectors the NEP is proportional to their square root of their active area.<sup>45</sup> The weak IR signal collected through small sample needs a very sensitive detector whose areas are in very good agreement with the beam size. Typically are areas of 250 x 250 μm<sup>2</sup> as used in the modified IR microscope A590 in our laboratory.

### 2.2.1.1.1 IRscope II, Bruker

A confocal IR microscope used within this work is the IRscope II attached to an IFS28B FTIR spectrometer (Bruker, Ettlingen Germany) at the Robert-Koch-Institute\*. The microscope was equipped with a x36 magnification Cassegrain (Schwarzschild-type) objective and an MCT detector with a  $100 \times 100 \mu\text{m}^2$  detector area. For removing the atmospheric water vapour the sample stage is surrounded with a box of Plexiglas® and purged with dry air as well as the instruments.

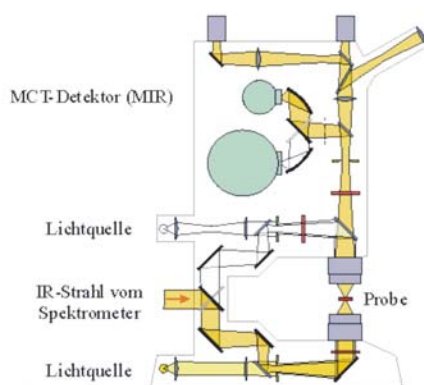
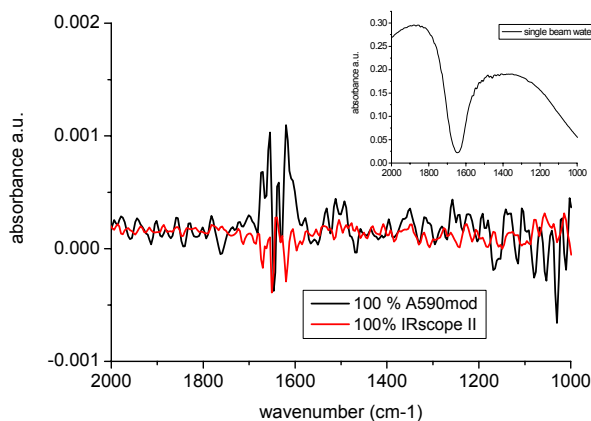


Figure 24 Sketch of the IRscope II operating in transmission mode

Due to the improved optics and detector with a smaller detector field, the IRscope II allows for measurements with good S/N at smaller spot sizes. For a comparison with the older IR microscope model, the A590, 100%-lines are here presented. These 100%-lines have been taken on the water filled mixer chip by recording the same position for background and sample spectrum. The data is shown in Figure 25. The inserted spectrum shows the single beam spectra providing information on the strength of the water absorption at  $\sim 1640 \text{ cm}^{-1}$ . Due to the little intensity in that spectral region reaching the detector the noise is higher than in remaining parts (refer to Equation 13). The calculated S/N values for the region from  $1550 - 1350 \text{ cm}^{-1}$  (thus not affected by the water absorption) are given in Table 4.

\* Robert-Koch-Institut, Berlin, Germany - <http://www.rki.de>





**Figure 25. 100 % lines on the water filled observation channel (10  $\mu\text{m}$  thick). The inserted spectrum shows the IR intensity reaching the detector.**

	<b>A590 mod.</b>	<b>IRscope II</b>
No of scans	256	265
Spectral resolution	8 $\text{cm}^{-1}$	8 $\text{cm}^{-1}$
Mirror velocity	20 kHz	100 kHz
Sample spot size	83 $\mu\text{m}$ diameter	200 x 200 $\mu\text{m}^2$
<b>S/N (RMS)</b>	<b><math>4 \times 10^{-5}</math></b>	<b><math>10^{-4}</math></b>

**Table 4 Settings for the spectra in Figure 25**

The calculated S/N values confirm nicely that the performance of the IRscope II using a round aperture giving 83  $\mu\text{m}$  spot size wins clearly over the older Bruker model employing a 200 x 200  $\mu\text{m}$  spot size regarding the noise. Note that lowering the mirror velocity of the A590 did not result in better S/N.

## 2.2.1.2 Synchrotron Infrared radiation (SIR)

### 2.2.1.2.1 Synchrotron radiation

Synchrotron radiation sources can be understood as a special light source that provides electromagnetic radiation in the range from 1 eV to >10 keV, from the FIR/THz range down to hard x-rays. It is produced when charged particles moving at relativistic velocities are accelerated.

The generation of Synchrotron radiation is explained here for the type of storage ring as found in BESSY<sup>†</sup> (Figure 26): Electrons are emitted by a diode gun in high vacuum and further accelerated on a linear accelerator with a strong high frequency electrical field in the so-called microtron. By achieving energy of several MeV the electrons pass to the synchrotron accelerator, which is containing strong magnets that accelerate the electrons by an alternating field of cavity resonator to energy of 1 GeV and more. When they are approaching the speed of light the electrons are injected via a transfer channel into the storage ring. These electron bunches are maintained in the circular orbit by a series of strong bending and focusing magnets that circumference the ring. These electron bunches are maintained in the circular orbit by a series of strong bending and focusing magnets that circumference the ring.

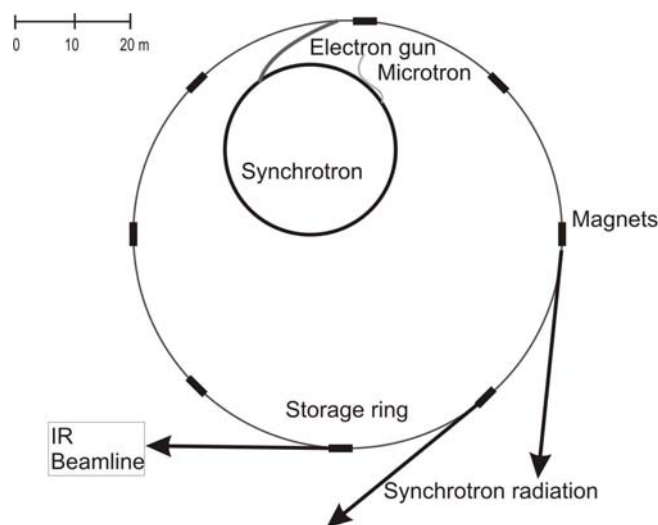


**Figure 26 Schematic view of a Synchrotron facility**

As the electrons experience a sudden acceleration for a short period of time when passing the magnetic field, this implies that the electric field created by moving electrons is also accelerated. The so caused distortion is travelling away from the electrons as electromagnetic radiation (Figure 27). This synchrotron radiation gets guided out of the storage ring at the position of the magnets to the so-called beamline. Increase of radiation is nowadays (third generation SR light sources) achieved by the insertion of undulators and wigglers, which are placed before an outlet to a beamline forcing stronger bending of the electrons' path. The energy loss due to the emission of radiation is compensated by the alternating field of one of the cavity resonators, which are part of the storage ring, each time they pass it.

<sup>†</sup> Berliner Elektronenspeicherring-Gesellschaft für Synchrotronstrahlung m.b.H., Germany - <http://www.bessy.de/>

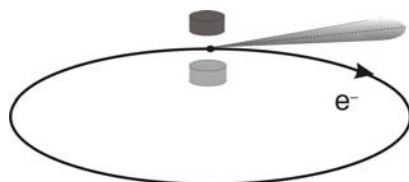


Figure 27 Emission of SIR under influence of the bending magnets.

All the different parts of a synchrotron facility (from the accelerators to the beamlines) are kept at ultra high vacuum (UHV), but even there collisions between electrons and residual gas particles occur. This is the main reason, why the ring current, the electrons circulating inside the storage ring, respectively, is decaying with time. As a consequence the beam can only be used for about maximum 12 hours before a new injection procedure has to be carried out.

In the UV and x-ray beam lines the radiation is directed by optical elements through a monochromator, a band pass selecting the energy region of interest, to the experimental end station. In case of the IR beamline using FTIR instruments a diamond window between the storage ring and the IR spectrometer shields the UHV of the storage ring from the experimental setup at the beamline. The diamond is transparent from UV to the FIR and light passing this window can be directly focused with the help of mirrors into the spectrometer (Figure 28).<sup>46</sup>

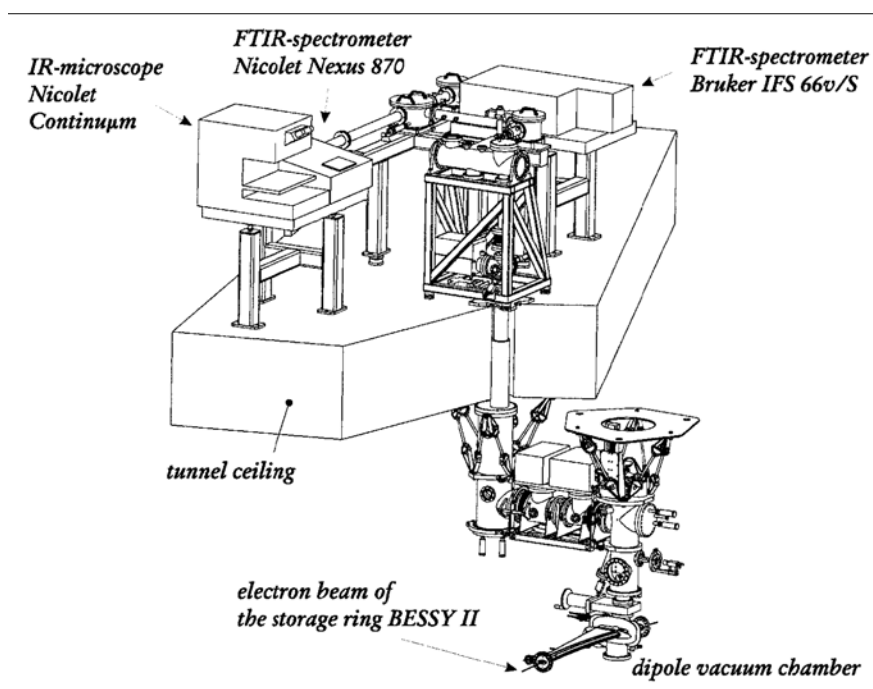


Figure 28. Layout of the beamline at BESSY. The experimental stations are placed on the concrete roof of the radiation shielding tunnel.<sup>47</sup>

The layout of the IRIS beamline at BESSY allows to use the beam for FIR experiments and ellipsometry by directing the beam to the Bruker FTIR spectrometer or alternatively it is coupled into the FTIR spectrometer from Nicolet that has the Microscope attached.

#### 2.2.1.2.2 Characteristics of SIR

The SIR provides certain special features in comparison to common IR sources like a black body. A property that derives from its way of generation is the pulsed structure. The electrons do not form a continuous distribution around the synchrotron orbit, but instead travel in ‘bunches’. These pulses can be used to probe systems exhibiting time-dependent phenomena on a sub-nanosecond time scale.<sup>31</sup> Further, SIR provides high intensity over a broad range starting from the very far IR region. Especially there, sources of high power and a high dynamic range are rare and by employing a special mode of coherent electron bunches access down to  $5 \text{ cm}^{-1}$  is provided.<sup>48;49</sup> Another advantage poses the fact that the SIR is emitted by a small source (the diameter of the radiation emitting electron-beam is in the sub-mm range) providing high photon flux in a narrow angle, thus providing high brightness. Such a brightness is quantified as ‘radiance’ (IUPAC) or ‘brilliance’ (synchrotron community) with the dimension  $\text{Wm}^{-2} \text{sr}^{-1}$ <sup>50</sup> with the definition of photon flux or power emitted into a solid angle per source area.

Together with high brilliance the SIR is also much better collimated than the radiation from a black body. Thus the source becomes more a point like source as discussed in section 2.2.1.1 and measurements down to the diffraction limit become possible.

The S/N calculation has also to be modified<sup>51</sup> replacing the black body’s term  $u_{\tilde{\nu}}(T)$  by the SIR source brightness  $B(\tilde{\nu})$ , which is no longer dependent on the temperature and by about a factor of 3 higher than the black body at 1200 K (see **Figure 29**). However, there will be additional noise deriving from fluctuations in the electron beam.

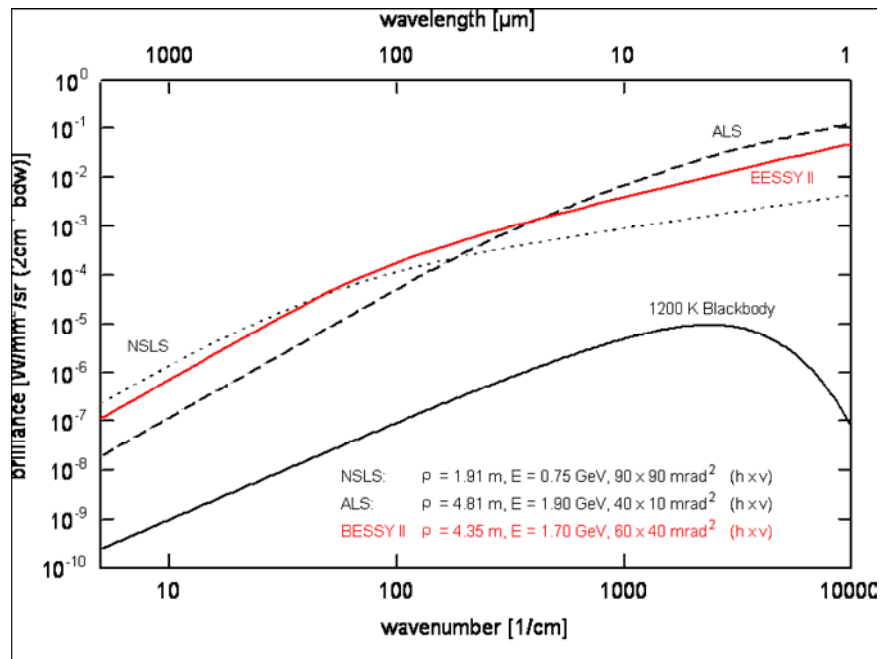


Figure 29 Comparison between a blackbody light source and 3 different synchrotron IR beamlines

Furthermore, the intensity of the SIR is decaying with time. When the current in the storage ring diminishes, also the power of the emitted radiation becomes weaker. This effect can be experienced differently strongly depending on the wavelength range. For compensation of this effect background spectra have to be taken within every 10 minutes. Alternatively external references could be used for correction.

### 2.2.1.2.3 Synchrotron IR microscopy

Two different beamlines were employed during this work: The IR beamline at ANKA<sup>‡</sup>, where our first measurements stem from **publication II** and IRIS the IR beamline at BESSY, where all of the following work was executed and which will be topic of the further manuscript. The beamline is equipped with a Nicolet Continuum IR microscope attached to Nexus 870 FTIR spectrometer (Thermo Electron Cooperation, USA) (see Figure 28). The specialty for this type of confocal microscopes is the slightly different optics, which form the image at infinity (“infinity corrected” objectives). Since the rays exiting the objective are collimated, optical accessories can be placed in the beam without affecting where the image planes occur in the microscope. The microscope is equipped with a 32x Reffachromat™ a Cassegrainian objective with a NA being 0.65.

<sup>‡</sup> Angströmquelle Karlsruhe GmbH, Germany - <http://www.anka.de>

### Comparison of globar and synchrotron

The difference of the globar and the synchrotron IR source is demonstrated measuring the water filled channel of the micromixer at varying aperture size. As for our measurements not the throughput itself, but the achieved S/N in absorption spectra is of importance, these values are given in Figure 30. The spectra were recorded as 100% lines by averaging 128 scans at 0.979 cm/s mirror velocity with a spectral resolution of 8 cm<sup>-1</sup>.

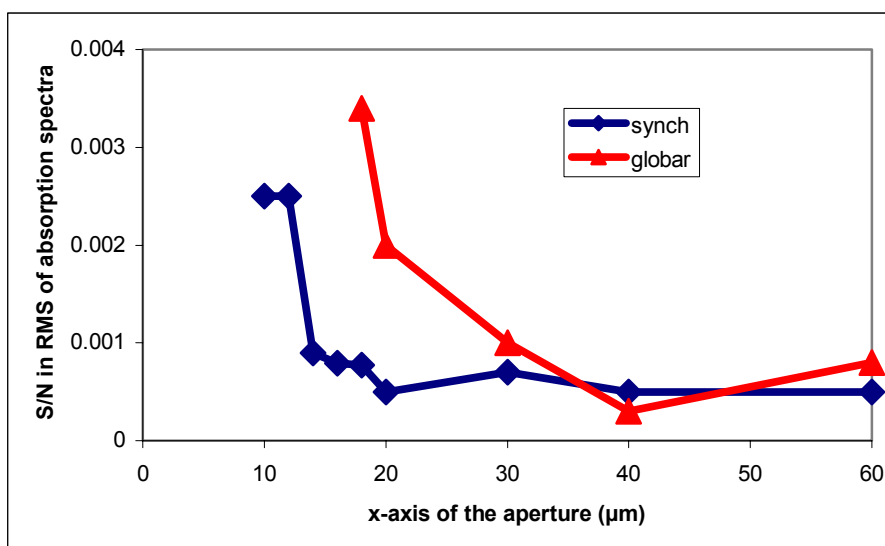


**Figure 30** The comparison of the S/N values obtained at different aperture settings over the range of 1500 – 1700 cm<sup>-1</sup>. Note that the aperture is rectangular and the x-axis in the figure gives only the length, not the diameter.

The figure clearly shows that the synchrotron light wins over the globar, but only for apertures smaller than 30 x 30 μm<sup>2</sup>. The naturally apertured focus by the 32x objective with the 0.65 NA is 1.4·10<sup>-3</sup> mm<sup>2</sup>, equivalent to a diameter of about 21 μm. As a consequence the S/N is not improving using the SIR by opening the aperture more than 30 μm. Reducing the aperture size, the increase of the S/N values for the SIR follows an unsteady trend. Even comparing 3 measurements within one aperture size showed fluctuations in the S/N values (the presented data are averaged values) The reason therefore is found in the slight instabilities in the beam of the synchrotron radiation by itself, which are noticed at small apertures. Setting the aperture smaller than 10 μm the increase in noise becomes so strong that any signal changes in aqueous solutions due to reactions cannot be observed.

#### **2.2.1.2.4 Determination of the resolution**

In general in optical microscopy the highest possible spatial resolution, the minimum distance between two objects at which they can be separated, is determined by the diffraction

limit, which lies in the order of the wavelength. From Equation 12 a definition for the separation of two image points is deduced by *Rayleigh's criterion* for resolution: Two points, each imaged as an Airy disk, can still be resolved when the centre of one Airy disk is coinciding with the first minimum of the second Airy Disk. Thus the distance is equal to Equation 12, it can be written as

$$d = 0.61 \cdot \lambda / N.A \quad (\text{Eq 15})$$

with  $d$  as the distance between objects that can be resolved according to Rayleigh's criterion.<sup>43</sup> Of course this gives only the minor limitation of lateral spatial resolution not considering the optical design that influences the SNR and therefore may deteriorate the effective resolution. However, two peaks appearing on a lateral scale fulfilling this criterion are not be baseline resolved, but correspond under ideal conditions to 26.4% of contrast value.

For the experimental determination of the contrast value for the spatial resolution in optical systems so-called resolution targets are used (see Figure 31). They provide patterns of aligned bars providing periodically zero or full transmission. Three of these alternating black and white lines are of equal width, which is defined in line pairs per millimeter written as lp/mm (Table 5).

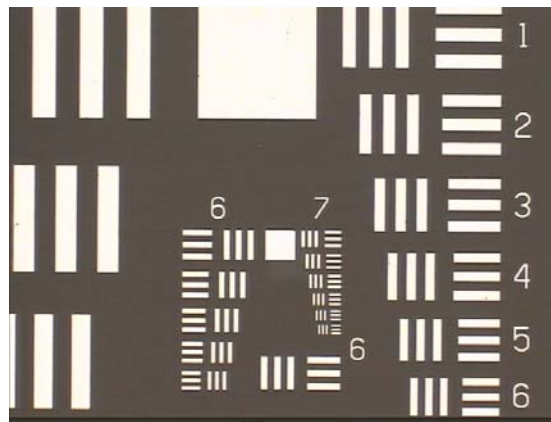


**Figure 31** Picture of a 1951USAF Glass Slide Resolution Target taken under the Continuum IR microscope at BESSY. Substrate consists of 1,5 mm soda lime glass with deposited chromium pattern

Number of Line Pairs / mm 1951								
Group Number								
Element	0	1	2	3	4	5	6	7
1	1.00	2.00	4.00	8.00	16.00	32.0	64.0	128.0
2	1.12	2.24	4.49	8.98	17.95	36.0	71.8	144.0
3	1.26	2.52	5.04	10.10	20.16	40.3	80.6	161.0
4	1.41	2.83	5.66	11.30	22.62	45.3	90.5	181.0
5	1.59	3.17	6.35	12.70	25.39	50.8	102.0	203.0
6	1.78	3.56	7.13	14.30	28.50	57.0	114.0	228.0

**Table 5** Specification table for the pattern 1951 USAF resolution target.

When such a pattern will be imaged by a line scan perpendicular to the bars, the “edges” will be “rounded off”. This gives then a sinusoidal curve, which is corresponding to the spatial frequency (Figure 32). In that way the contrast can be expressed in the image as a modulation given by <sup>43</sup>

$$\text{Modulation} = \frac{\text{max.} - \text{min.}}{\text{max.} + \text{min.}} \quad \text{Eq 16}$$

that is written in Figure 32 as percentage of the contrast. The modulation transfer function (MTF) can now be defined as the spatial frequency response of an imaging system determined by the contrast at a given spatial frequency relative to low frequencies. An MTF graph plots the percentage of transferred contrast versus the frequency (lp/mm) of the lines

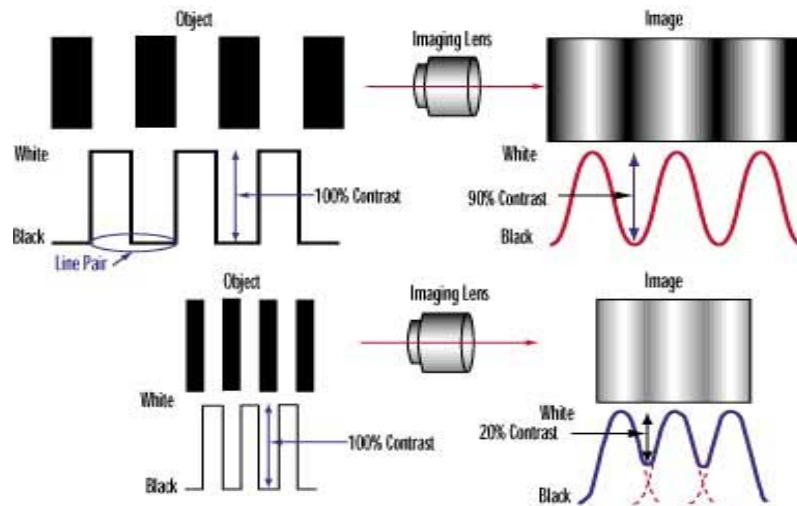


**Figure 32** Definition of the MTF

With this target the SIR microscope at BESSY has been characterised. Therefore line scans over the resolution target (**Figure 31**) has been performed. Settings are chosen as follows: 0.964 cm/s scan speed, 16 cm<sup>-1</sup> spectral resolution and 2.5 x 7.5 μm<sup>2</sup> aperture size. The line scan step size is 2.03 μm over the elements 4,5 and 6 of group 6 and of elements 1 – 7 of group 7. The measurements have been performed acquiring transmission spectra with a background that has been repeatedly taken every 5 min at a position of a part of the target without pattern order to compensate for the decay of the synchrotron light with time. In this case it is important that transmission spectra and not absorption spectra are used, as the latter would lead to distorted results in contrast by analysing data recorded on a logarithmic scale. The results for three representative wavenumbers are given in Figure 33 and Figure 34.



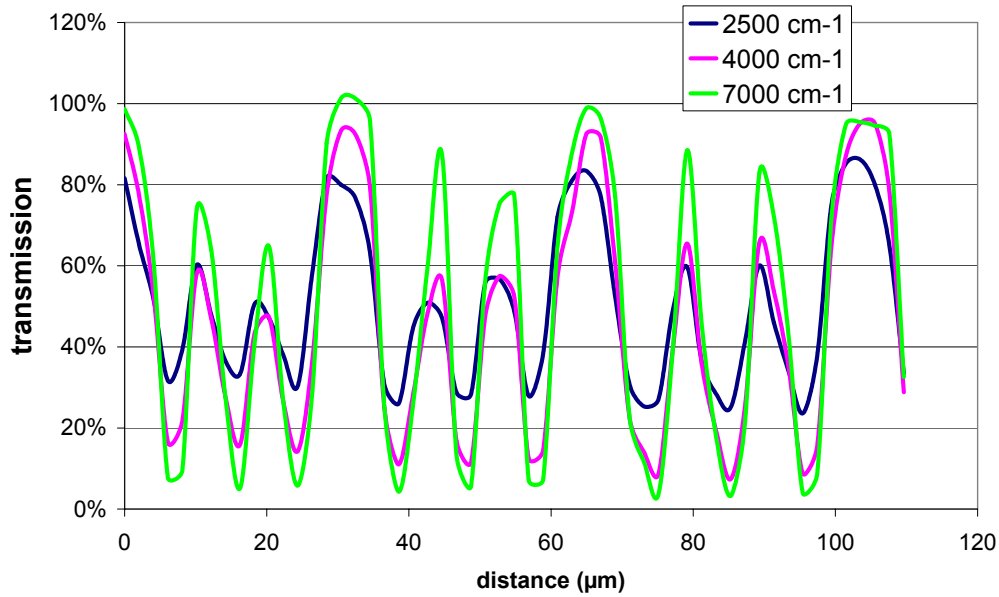


Figure 33 Line scan over the elements 4, 5 and 6 of group 7

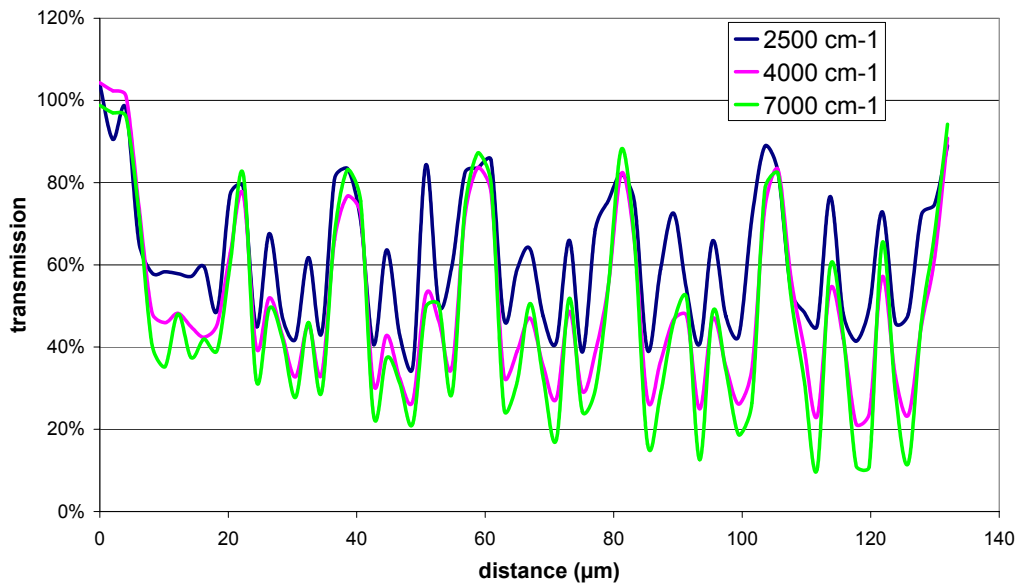
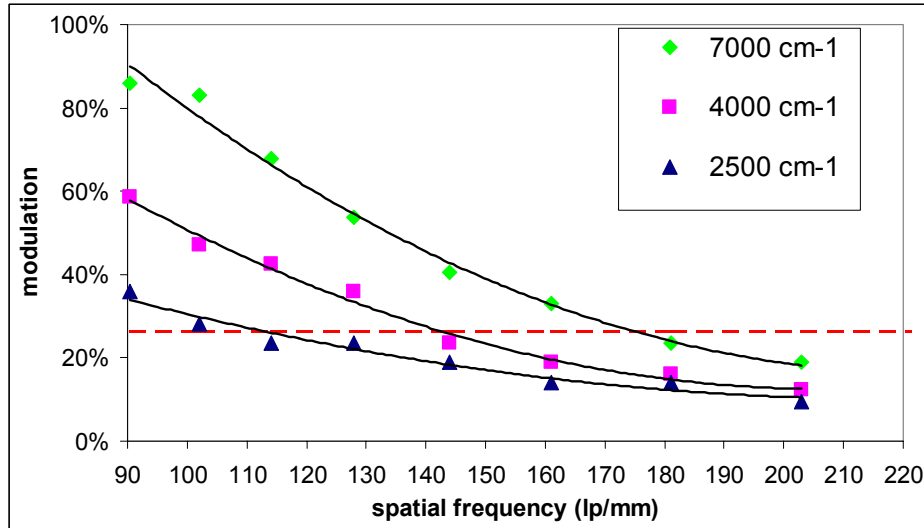


Figure 34 Line scan over the elements 1–7 of group 7.

At a first sight it is clear that the resolution is strongly dependent on the wavelength, which is in agreement with Equation 16. For  $7000\text{ cm}^{-1}$  which corresponds to a wavelength of  $1.4\text{ }\mu\text{m}$  even the smallest pattern with a line pair size of  $4.4\text{ }\mu\text{m}$ , a bar thickness of  $2.2$  respectively, can be discerned. The step size chosen is actually too large for the smallest element regarding the Nyquist-Shannon sampling theorem, which says that the sampling interval should not be larger than one-half the size of the smallest frequency – in this case line pair width. The effect of its violation is a flattening of the curve as it happened for the element 7 in group 7 is aliasing to appear as of lower frequency. Furthermore a shift of the modulation

curves in position owing to the wavenumber can be discerned from the line scans. This is an effect of the wavelength dependency of the refractive index of the glass, where the light is travelling through.

From these line scans the MTF was obtained shown in Figure 35. This curve allows easy comparison with other MTF characterising microscopes.



**Figure 35** MTF derived from the line scans in Figure 33 and Figure 34. The red line marks the value for the Rayleigh criterion

Note, that the performance of the microscope employing SIR is strongly depended on the properties of the Synchrotron light itself, which vary by means, and on appropriate adjustment. From the MTF the minimum resolution according to the Rayleigh criterion can be read out Table 6.

Wavenumber (cm <sup>-1</sup> )	Wavelength (μm)	Frequency (lp/mm)	Distance (μm)
2500	4	112	4.5
4000	2.5	142	3.5
7000	1.4	174	2.9

**Table 6.** Values for the resolution limit according to Rayleigh's criterion received by the MTF

It is necessary to state here that the Rayleigh criterion is solely a benchmark used for comparison of instruments and estimation of achievable spatial resolution. Comparing the MTF with the line scans shows that the minimum distance for resolution defined by the Rayleigh criterion, can be under-run and features spaced by 2.2 μm can be distinguished at 7000 cm<sup>-1</sup>. For using wavelengths below 2500 cm<sup>-1</sup> the limit will be between 2.5 and 3 μm.

However, this type of resolution targets was actually developed for light microscopy. It only gives the possibility of light passing through or not, but no spectral features had to be

detected. For this reason the spatial resolution could be set to the rather high value of  $16\text{ cm}^{-1}$ . Furthermore quartz cuts all frequencies below  $2200\text{ cm}^{-1}$ . In IR spectroscopy it would be more appropriate to investigate the resolution on an IR sensitive pattern deposited on a substrate that is transparent in the region of interest, namely below  $1800\text{ cm}^{-1}$ .

### 2.2.1.2.5 Application of SIR microspectroscopy

#### Test of design II

Design II was especially developed for the SIR microspectroscopy. The channel width of  $15\text{ }\mu\text{m}$  presents the very limit of what is detectable regarding the studies in the sections before. First spectra of  $\text{D}_2\text{O}$  and  $\text{H}_2\text{O}$  in this channel were recorded at ANKA in 2003 showing that it is possible to acquire IR information from about  $2\text{ pl}$  of a substance (**publication II**). In later attempts at BESSY we could also succeed in testing the mixer for its mixing capabilities.

For this experiment the aperture has been set to  $8 \times 25\text{ }\mu\text{m}$ , in order to get the best signal from the channel solely and exclude influences from structures from the sidewalls. Note, that design II does not have a silver foil that acts as mask where the light can only pass through the channel. As a consequence, IR information from outside the channel will carry signals from SU-8. Two syringes have been filled with aqueous solution of  $0.25\text{ M NaOH}$  connected to the sideways inlets and one syringe filled with  $0.5\text{ M acetic acid (HAc)}$  to the middle inlet. The flow speed has been set to  $0.1\text{ }\mu\text{l/min}$ . Spectra were taken at 4 different positions along the channel. The background had been acquired at the same positions previously with the channel filled with water. The result is presented in Figure 36. For all 4 positions bands deriving from the reaction product acetate ( $1560$  and  $1420\text{ cm}^{-1}$ ) are observed proving that the mixing is taking place. However, part of the educt HAc ( $1715$  and  $1288\text{ cm}^{-1}$ ) is still present and only decaying with time. From the simulations it is known that complete mixing is difficult to achieve in the first  $200\text{ }\mu\text{m}$  with this design, but from this data it seems that complete mixing is even not taking place even after  $8000\text{ }\mu\text{m}$  (equalling a theoretical reaction time of  $0.8\text{ s}$ ). It is possible that the small particles ( $< 1\text{ }\mu\text{m}$ ) that have deposited in the observation channel are the reason for the deteriorated mixing performance. It has shown that also consequent filtering of the solutions by  $0.2\text{ }\mu\text{m}$  pore size filters could not avoid this problem.

Further to see in Figure 36 is a baseline shift due to the time delay between background measurement and sample measurement. As the change is not dramatically here, compensation therefore was omitted. The negative peak at about  $1640\text{ cm}^{-1}$  derives from water. The region of the water band is very delicate, because even by using only  $10\text{ }\mu\text{m}$  sample thickness the

strong absorption of water absorbs most of the intensity (refer section 1.3). Thus even little changes like e.g. temperature changes, changes in thickness on the sub- $\mu\text{m}$  scale due to pressure and the replacement of water in solutions by solutes, affect the signal in absorption spectra. Another two peaks hardly higher than the noise can be discerned at 1610 and about 1480  $\text{cm}^{-1}$  originating from the channel forming SU-8 (refer Figure 11). This provides indication that the positions of the background and the sample spectrum are not exactly the same, thus the x.y-stage is not moving precisely enough. This problem and others like detectability of only high concentrations and not perfect mixing performance, the accumulation of particles in the channel have lead to the decision to stop working on this design and to go back to the more robust design I.

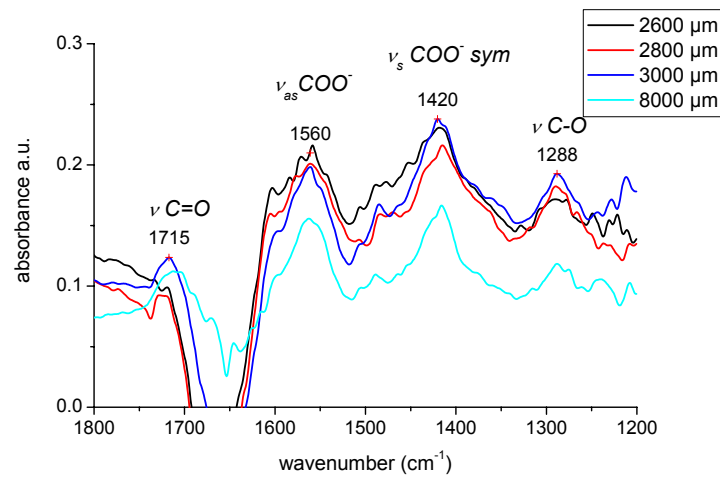


**Figure 36** Measurements along the channel axis of design II while the flow was kept on. (32,5 ms,

### Performance test of design I

The small sample spot size of the SIR microscope allows a performance study of the design I mixer chip also in x-direction. Simulations propose that the concentrations are distributed homogenously for the inner 90 % of the full 300  $\mu\text{m}$  channel width, or at least symmetric to the middle axis as for a typical laminar flow profile. This means that at position  $x = 50 \mu\text{m}$  and  $x = 250 \mu\text{m}$  the spectra should look the same. This hypothesis was tested by the chemical system of an ester hydrolysis. The reactions partners are methyl monochloracetate and Sodium hydroxide both in aqueous solutions. The according spectra of reaction educts and product are shown in Figure 37.

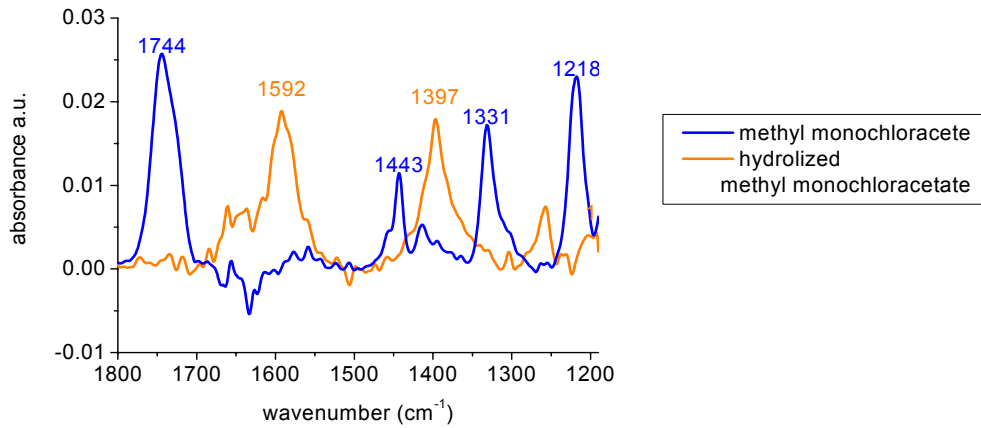


**Figure 37. Spectra of MCA 0.15 M before and after hydrolysis acquired in the observation channel.**

For the performance test the educts are fed into the mixer with a flow rate of  $0.5 \mu\text{l}/\text{min}$  and  $4 \times 5$  measurements positions in x and y direction respectively are acquired. The traces for two wavelengths, either deriving from a band of the educt or the product, are shown in Figure 38. It is clearly seen that reaction is taking place moving downwards the observation channel (y direction) but the concentration profile for the x direction is not homogeneous and not symmetrically to the middle axis either considering that  $150 \mu\text{m}$  presents the channel's middle axis.

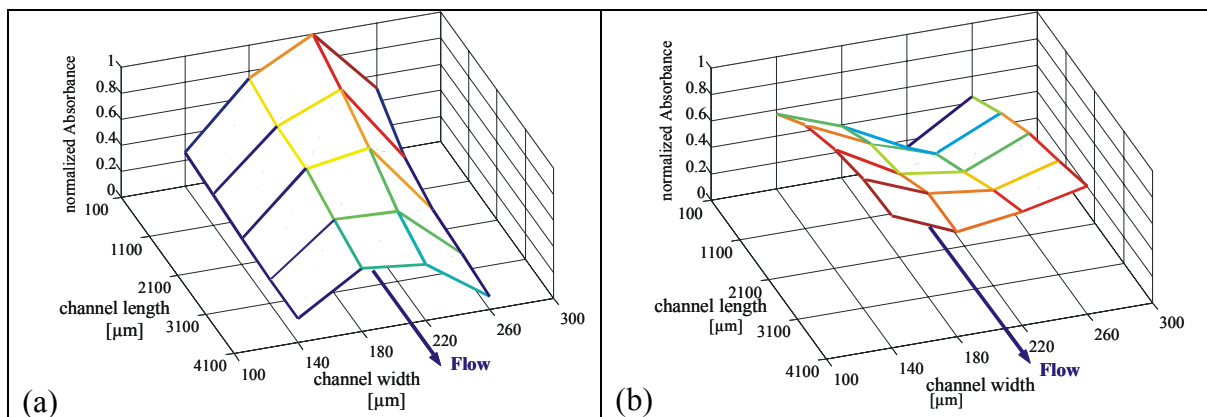


**Figure 38 (a) Peak height distribution over the channel at  $1744 \text{ cm}^{-1}$  representing the ester concentration (b) Peak height distribution over the channel at  $1592 \text{ cm}^{-1}$  representing the concentration of the hydrolyzation product**

The deviation of the experimentally obtained result from the simulations can be explained by changes in the channel, such as deposition of introduced and deposited particles or residues of the fabrication process, which are transported into the observation channel. The inhomogeneous concentration profile arises due to the inhomogeneous velocity profile.

The conclusion is that the theoretical time axis not given as calculated by flow rate divided by sample spot volume is not valid, a. However, for measuring along a certain x-axis the relative time axis is still valid.

### 2.2.2 Array detector

Another development in FTIR-spectroscopy that aims at measuring smallest possible spot sizes is the use of multichannel detectors for FTIR imaging. In the 90s imaging detectors for IR the so-called focal plane array detectors (FPA) originally developed for military and surveillance application have become commercially accessible.<sup>52</sup> These detectors consist of  $n \times m$  fields of photon detector elements (i.e. pixels) most commonly from MCT or indium antimonide (InSb). The working principle is shown in Figure 39. The performance of a microscope equipped with an FPA differs a little from conventional single point detector microscopes. The spatial discrimination is achieved by the detector elements themselves, rather than by an aperture. In this way it becomes necessary to illuminate the investigated area evenly. Furthermore reading out a large amount of data given by a data matrix of  $n \times m \times$  wavenumber requires more time for data processing per scan. Most instruments do not have electronics that are fast enough to read out such large data amounts during a scan and therefore use the step scan mode.<sup>53</sup> This means that for reading out the detectors array the moving mirror is stopped.



Figure 39 Schematic drawing FPA detector

The spatial resolution is not diffraction limited due to the lack of an aperture as in the single point detector microscopes.<sup>54</sup> On the one hand this means that no light is lost due to diffraction at an aperture. On the other hand, overlap of the information imaged onto the pixel

grid has to be taken into account. Therefore, the spatial resolution of such systems cannot directly be given by the pixel element size for certain magnification.

Comparisons of the spatial resolution of microscopes equipped with FPA detector and single point detectors operating in the confocal arrangement have been performed.<sup>44;54</sup> These references reveals that the confocal single point arrangement is winning over the FPA detector without aperture with respect to the spatial resolution. However, such comparisons have to be read carefully, as these results are strongly depending on the instruments employed. A soon coming work by Peter Lasch will show by presenting the MTF curves for different instruments that the latest Hyperion3000™ with FPA detector and 32x Cassegrain objective provides a slower decaying MTF curve than even our presented data from the confocal single point microscope using SIR (Figure 35). Higher spatial resolution can be realised by using the FPA technique in combination with attenuated total reflection (ATR)<sup>55;56</sup> exploiting the magnification from a special geometry and the high refractive index of a germanium crystal acting as focusing unit.

Apart from the rather good spatial resolution the biggest advantage of the FPA detector instrument is the fast recording of multiple spectra. In order to deal with such large amount of data the spectra are usually immediately integrated over the spectral region of interest and then presented in an  $m \times n$  three-dimensional plot. For more complicated samples chemometric methods are applied (see section 2.2.2.1).

The possibility of a combination of the FPA measurements with our continuous-flow set-up was worked out (see Figure 39) on a Hyperion3000 (Bruker, Ettlingen Germany).

### Application

The measurements within this work were performed at the Ludwig-Bolzmann Institute of Osteology at the Hanusch Hospital (Vienna, Austria) on a Hyperion 3000 (Bruker, Ettlingen Germany) equipped with an FPA of 64x64 detector elements allowing probing a 266x266  $\mu\text{m}$  area by the use of a 15x Cassegrain objective. The data recorded with a nominal spatial resolution of 4.2  $\mu\text{m}$  are presented in **publication IV**.



Figure 40 Picture of the Hyperion3000 equipped with an FPA detector (right top side)

For elaboration of the exact spatial resolution it has been tried to define the overlap, which must occur when the sample is imaged with a wavelength of 9 – 10  $\mu\text{m}$  onto 4.2  $\mu\text{m}$  size pixels. Therefore the calculation of the according point spread function should be performed.<sup>43</sup> This allows estimation of the spread of a point like source by considering the optical beam path, such as objective diameter, numerical aperture and further optical arrangement including the sample. However, due to the policy of Bruker (Ettlingen, Germany) it was not possible to get sufficient information on the optical set-up, which would allow performing this calculation.

### 2.2.2.1 Chemometric data evaluation for time resolved FTIR spectroscopy

Chemometric data analysis is the tool of choice for extracting information that is contained in complex large data matrices. This applies to IR spectroscopy considering the high information content on molecular structure presented in various bands of substances. Chemometrics were extensively applied in the CAVS-group,<sup>57-59</sup> especially within the thesis of Josef Diewok.<sup>1</sup> In this work the method of multivariate curve resolution-alternating least squares (MCR-ALS) was successfully applied and discussed for FTIR data, and established as a standard method for analysing evolving systems in the CAVS-group. The MCR-ALS analysis takes advantage of known chemical and mathematical information about the data set through the use of constraints and decomposes the data set into concentration profiles and spectra for each modelled component. In this way a large data matrix is reduced to a few spectra that carry the information of the changing substances and intermediates can be identified.



The time resolved measurements on the mixer chip present a typical evolving data matrix. Therefore application of MCR-ALS was attempted throughout this work. However, subjecting the data of vancomycin presented in section 2.2.1.1 revealed to be rather difficult, mainly due to the problems of the baseline shift. The same applied for the data of the SIR measurements. The MCR-ALS procedure seems to fail, when the data is affected by fluctuating influences that cannot be modelled to a clear trend. The only successful application was achieved on the presented data in **publication IV**. The spectral changes of the model reaction were strong enough and time resolved data obtained using an FPA detector in combination with a microfluidic mixing device could be presented.

### 2.3 Investigation of a drug's reaction mechanism

The task is to monitor the binding of vancomycin a glycopeptide antibiotic to a bacterium's cell wall analogue. Vancomycin, deriving from *Streptomyces orientalis* binds to a sequence of pentapeptide precursors, the tripeptide N <sup>$\alpha$</sup> -diacetyl-L-lysyl-D-alanyl-D-alanine (Ac<sub>2</sub>KAA) produced during bacterial cell wall biosynthesis, thereby inhibiting the establishing of bacterial enzymes.<sup>60</sup> The structure of vancomycin and the peptide is depicted in Figure 41. The lines indicate the formation of hydrogen bonds upon complexation. The binding mechanism proceeds via a co-operative array of hydrogen bonds and hydrophobic interactions, namely the binding of the carboxylate of the peptide with three amide N-H groups of vancomycin, formation of amide-amide hydrogen bonds and hydrophobic interactions of the methyl groups of the peptide with the aromatic rings of the antibiotic.<sup>60</sup> It is proposed that this reaction mechanism is taking place in two steps.<sup>61;62</sup> However, little is known about the kinetics and about the role of the binding centres involved.

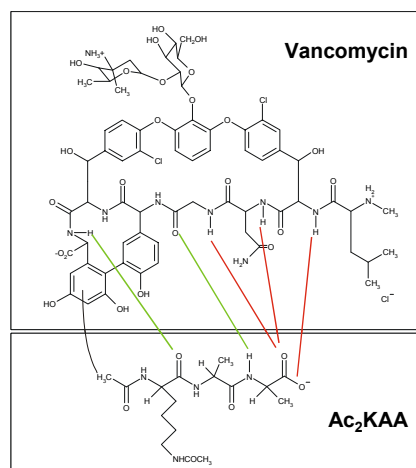
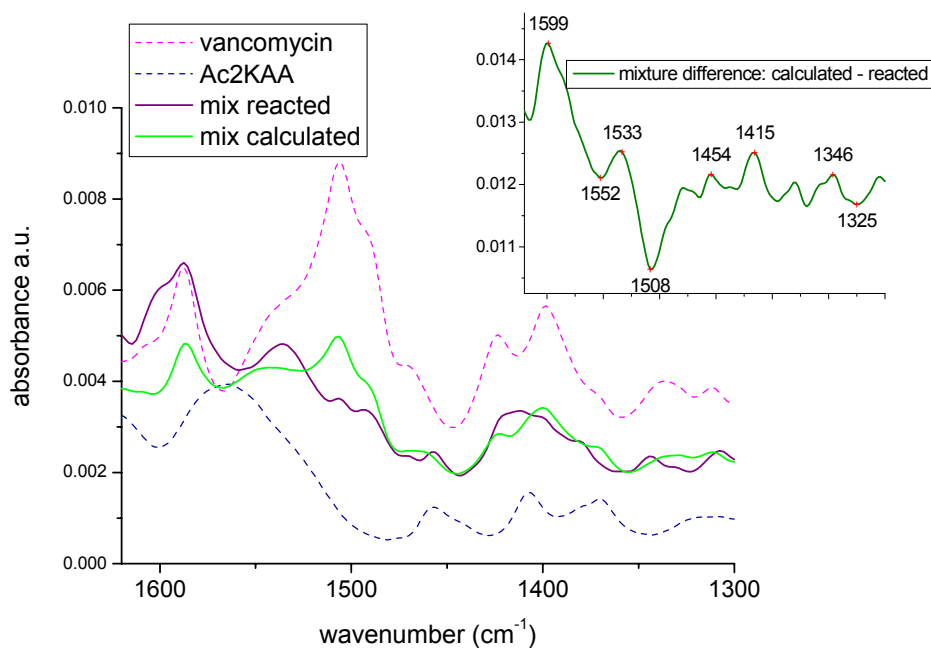


Figure 41 Interaction of Vancomycin and N <sup>$\alpha$</sup> -diacetyl-L-lysyl-D-alanyl-D-alanine (Ac<sub>2</sub>KAA)

Spectra of the pure solutions of 10 mM Vancomycin and 10 mM Ac<sub>2</sub>KAA (for preparation see **publication I**) are presented in Figure 42. There is a clear difference between the mixture before and after the reaction, which can be well observed in the according difference spectrum.



**Figure 42** Spectra of the reaction partners and the according mixture. The black spectrum is at random scale depicting the difference of the reacted mixture minus the calculated one.

A detailed investigation on the spectral differences between the vancomycin and the tripeptide before and after the reaction in steady state was performed. An excerpt of the band assignment for the two reaction partners shall be given in Figure 43 and Figure 44. Measurements were performed at the ATR.

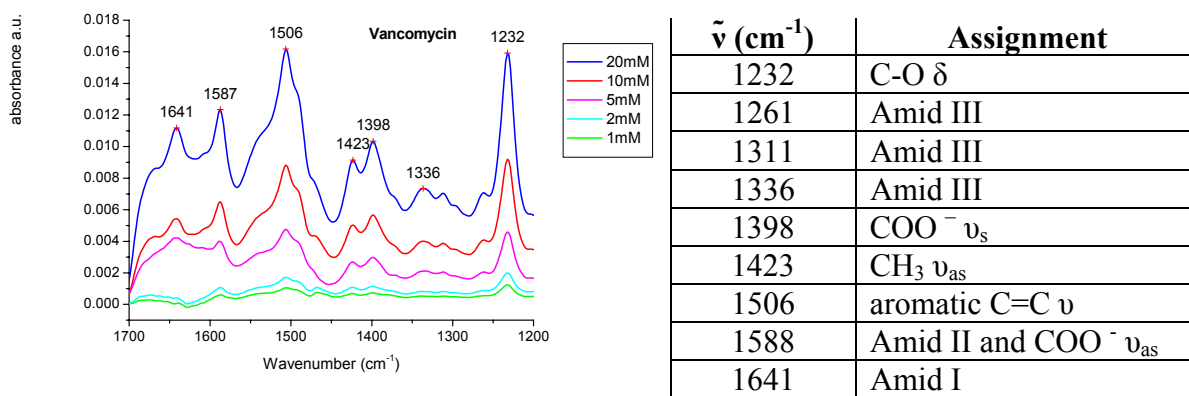


Figure 43 IR spectra of vancomycin at various concentration together with the according band assignment

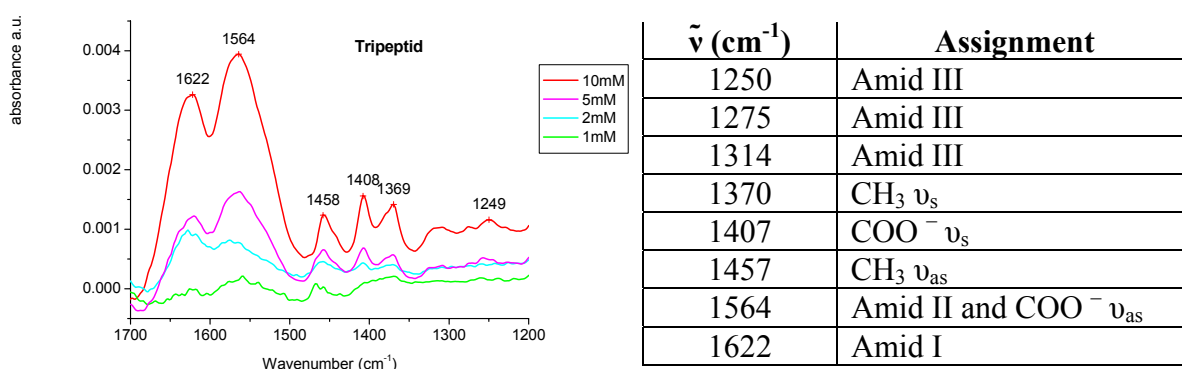


Figure 44 IR spectra of Ac<sub>2</sub>KAA at various concentration together with the according band assignment

Using obtained spectra mixtures were calculated and compared with spectra taken from real reacted solutions. The according difference spectra are shown in Figure 45.

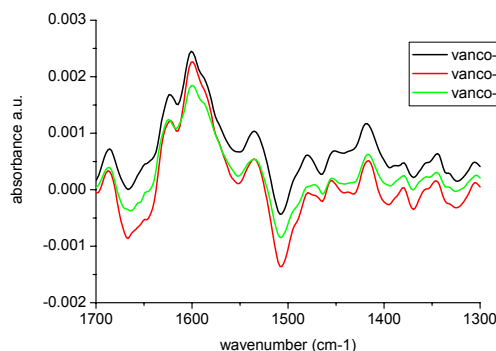


Figure 45. Difference spectra of measured and calculated spectra on mixtures of Tripeptide and Vancomycin in different ratio.

The three presented spectra from different mixture ratios show hardly any difference. Thereof it follows that the reaction is not concentration dependent once it is in steady state

and the dimerisation of vancomycin stated in literature<sup>60</sup> is not observed in these experiments. Thus, it is concluded that solely the binding of vancomycin to tripeptide provokes the spectral changes.

First time resolved measurements were already achieved by the use of the stopped-flow mixing approach<sup>2</sup>, but data for the confirmation of the proposed mechanism are still lacking. Using of the continuous-flow mixer these experiments have been repeated.

### 2.3.1 Time resolved reaction of vancomycin using the modified A590

The first instrument in use for time resolved experiments on the vancomycin system is the IR microscopy modified A590. A spot size of 200  $\mu\text{m}$  on the observation channel was chosen and the stage was programmed to move in 200  $\mu\text{m}$  steps. For the background the chip was filled with phosphate buffer and spectra recorded for 1 mm length while the flow was on. For the sample measurement the syringes were filled with 10 mM Vancomycin and 10 mM Tripeptide, respectively and the flow set to 0.5  $\mu\text{l}/\text{min}$ . The recorded spectra are presented in Figure 46 as difference spectra to the first position. Note, that they are cut at 1620  $\text{cm}^{-1}$  due to disturbing influence of high noise in the water band. A decay at  $\sim 1505 \text{ cm}^{-1}$  and an increase at  $>1600 \text{ cm}^{-1}$  are observed in good agreement with the spectra in Figure 42. A slight decrease at  $\sim 1550 \text{ cm}^{-1}$  can be discerned as well, but the other expected features below 1500  $\text{cm}^{-1}$  (e.g. the band at 1410  $\text{cm}^{-1}$ ) are most likely hidden in the noise.

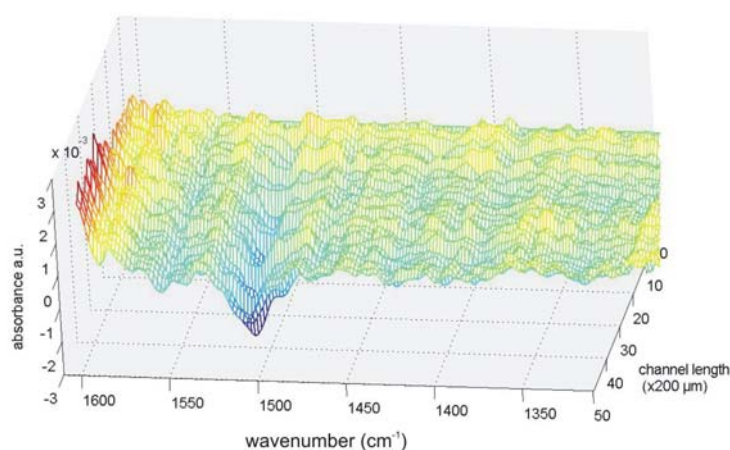


Figure 46 Time resolved measurement of vancomycin and Ac<sub>2</sub>KAA at 0.5  $\mu\text{l}/\text{min}$  flow rate

Furthermore, due to the low S/N ratio it is difficult to judge, whether the band change appear synchronously or sequentially shifted, which would indicate the two-step binding mechanism. The observed trends in the time resolved profile are not constant enough for kinetic evaluation. It can only be stated that the reaction is still going on at 10000  $\mu\text{m}$ , which

equals a theoretical reaction time of 1.8 s. This value is still in agreement with data presented in the thesis of Peter Hinsmann.<sup>2</sup>

### 2.3.2 Time resolved reaction of vancomycin using the IRscope II<sup>§</sup>

Tests with the water filled mixing cell in the spectral region of interest 1800 – 1200  $\text{cm}^{-1}$  have been performed (see 2.2.1.1.1). The highest mirror velocity that can be chosen without losing significantly intensity was 20 kHz, which corresponds to 0.63 cm/s. The limit for probing the chip measures about 50  $\mu\text{m}$  sample spot size in diameter giving for the current settings single measurements an S/N of  $8 \cdot 10^{-5}$  RMS noise on 100% absorbance measurements recorded with 8  $\text{cm}^{-1}$  spectral resolution 200 scans (52 sec). However, for measurements on the biochemical system the scan time has to be reduced in order to keep the sample consumption low ( $< 50 \mu\text{l}$  for one experiment). For compensation in the S/N resolution, measurements are performed with an aperture of 83  $\mu\text{m}$  in diameter. Carrying out the time resolved experiment absorbance spectra along the channel were recorded while the flow speed was set to 0.5  $\mu\text{l}/\text{min}$  resulting in a theoretical time resolution of 15 ms. For better visualisation of the spectral changes difference spectroscopy is used. Therefore first a spectrum at the beginning of the channel ( $y = 37 - 120$ ), where the solutions are considered as unmixed, is taken, which is then subtracted from the following spectra. In this way only the changes that occur during reaction are monitored. The background spectra recorded for each sample position have been acquired from phosphate buffer with the flow on. This adaptation of the experimental procedure has been carried out, as first test measurement showed problems with the baseline stability and the conditions for the sample and the background spectra have been tried to be kept exactly the same. Note, that the region 1630 – 1700  $\text{cm}^{-1}$  is skipped due to the high noise (refer Figure 25). For the sake of clarity, Figure 47 shows only an excerpt of the measurements along the observation channel. Several changes in the spectra between 1630 and 1300  $\text{cm}^{-1}$  are observed. Within the first 1500  $\mu\text{m}$  a decay at 1554 and 1508  $\text{cm}^{-1}$  and an increase at 1610 as well as at  $\sim 1450$  and 1350  $\text{cm}^{-1}$  in absorption intensity can be seen. In the following part of the channel further peaks at 1481 and 1419  $\text{cm}^{-1}$  appear.

---

<sup>§</sup> performed at the Robert-Koch Institute

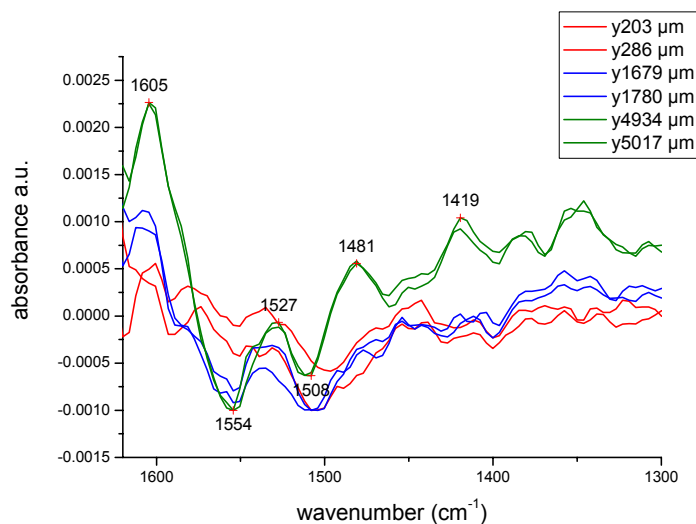


**Figure 47** Time resolved difference spectra of the Vancomycin-Tripeptide-reaction

A problem in the evaluation of this information is the encountered rather high noise – especially for the first spectra (red colour) – together with a sloping baseline, which may derive from the fact that the x,y-stage is not moving precisely enough and even very small differences in the channel position for the background and the sample measurement affect the beam path. The baseline-shift in the region below  $1500\text{ cm}^{-1}$  is stronger than at higher wavenumbers. Correction therefore is partly performed in Figure 47, but revealed to be difficult owing to the feature rich spectrum.

However, despite these problems the spectra contain a lot of information. The changes from the red to the blue spectra corresponding to about 260 ms theoretical reaction time, are similar to the difference spectrum in Figure 42, showing an increase at  $1600\text{ cm}^{-1}$  for the amid I and the asymmetric stretch vibrations together with a slight decrease at  $1554\text{ cm}^{-1}$  for the amid II and a strong decrease for the C=C vibrations at  $1504\text{ cm}^{-1}$ , while the asymmetric stretch vibration of the carboxylate groups is not observed at  $1415\text{ cm}^{-1}$ . In the later spectra corresponding to about 850 ms the behaviour a band at  $1417\text{ cm}^{-1}$  is rising, which could be taken for the symmetric carboxylate vibration, accompanied by an further increase at  $\sim 1590\text{ cm}^{-1}$ . However, an additional band at  $1481\text{ cm}^{-1}$  is rising as well, which has not been encountered in any spectra of the vancomycin system so far. This leads to the conclusion that this is either an intermediate or deriving from a substance not related to the reaction found in the observation channel. Checking the signals of the substances used for the fabrication of the mixer in Figure 11 no spectral feature at exactly  $1481\text{ cm}^{-1}$  is present, but the SU-8 shows two bands close to it. A look to the region  $> 1700\text{ cm}^{-1}$  in Figure 48 lacks a possible SU-8 band at

1767  $\text{cm}^{-1}$ , albeit a low and broad peak around 1745  $\text{cm}^{-1}$  is observed, which is not related to the vancomycin system. Considering that SU-8 that is brought into the observation channel simply by applying linear flow rates of 0.006 m/s of water, it must be a matter of non or only partly crosslinked SU-8. If this is the case, deviations of the exact positions are not surprisingly and the band at 1481  $\text{cm}^{-1}$  can be related to depositing modified SU-8 in the channel when the chip is in use for longer time.

Repeating the same measurements with another mixer showed similar deviation from the expected difference IR spectrum at certain positions in the observation channel. Under a conventional light microscopy deposited material could be seen. Attempts for recording spectra of the deposited material solely failed, because the signal was very weak and overlapping with spectral band deriving from the also deposited sample. Investigation of the deposit by electron probe x-ray microanalysis (EPXMA) revealed that it is organic material containing phosphor (which can be assigned to the phosphate buffer) and some means of iron.

A look at the background spectra, which were recorded before the sample measurements, reveals that a band appears around 1481  $\text{cm}^{-1}$ , which indicates that there is a substance already in the channel before the two reactant containing solutions are brought into the mixer. In case this substance would be stable in the channel, correction for it would be carried out by calculating the absorbance spectra. However, this substance in the channel is either moving or the x,y-stage is not moving precisely enough for recording background and sample spectrum in the same position. Therefore, it cannot be corrected for it and interference with the signal from the vancomycin-system hinders the evaluation thereof.

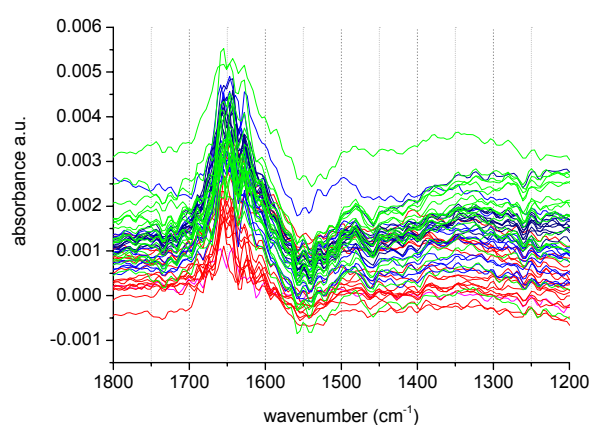


**Figure 48** The background measurement of 80 mM phosphatebuffer. The colours are assigned to the position where the spectra have been recorded: blue = 120 - 1614  $\mu\text{m}$ , red = 1679 - 3523  $\mu\text{m}$  and green = 3606 - 5183  $\mu\text{m}$

Apart from the conclusion that this charge of mixer may suffer from a fabrication deficiency exhibiting when the chip is in use, the reaction between Vancomycin and Ac<sub>2</sub>KAA is monitored by according band changes. Due the discussed problems it is not possible to make a statement regarding a confirmation or rejection of the data monitoring a two-step binding mechanism in the work of Peter Hinsmann.<sup>2</sup>

### 2.3.3 Time resolved reaction of vancomycin using SIR (Continuum)

The small sample spot-size in Synchrotron IR microscopy was also exploited for the already presented biochemical system of vancomycin. Due to the high noise, which is strongly increasing below 1500 cm<sup>-1</sup> only the rising band at 1600 cm<sup>-1</sup> could be monitored with a theoretical time resolution of 3 ms. The data is given in **publication I**.

## 2.4 Outlook - the next generation of micromixers

In order to set up an optimised mixing system the first question to address is continuous-flow mode or stopped-flow mixer. Both systems have their advantages and their drawbacks. The stopped-flow system is in general easier to realise. The crucial step with this kind of flow apparatus will be the stopping of the flow, which means setting the flow velocity from ~ 1 m/s to 0 μm/s within 60 ms. If the reduction of the flow velocity takes longer, the time profile is disturbed due to supply of unreacted sample in the monitoring chamber. In the worst case the results obtained can even be wrong, when only one of the substances is re-squeezing, because of some pressure differences in the system resulting in changes of the ratio of the reactants in the monitoring chamber. However, in other set-ups<sup>27</sup> these problems are kept small. A problem, which is usually the biggest enemy dealing with microfluidic systems, is the appearance of air bubbles in the system. Due to mostly complex set-ups it is difficult to locate the problem and get rid of it, which results in the mentioned pressure influence that hinders reliable measurements.

Two major aspects that let the stopped-flow mode fall behind the continuous-flow mode are the rather higher sample consumption and the lower time resolution. While in our presented continuous flow set-up only 50 μl are necessary for one measurement campaign (rinsing the lines included), the according stopped flow measurement, will need approximately 500 μl.



### 2.4.1 The continuous-flow mode of the future

As the presented measurements revealed the continuous-flow set-up is capable of time resolved measurements, but it is not yet optimised. Therefore I would like to give a list of points that should be considered for improving the performance in future mixer designs.

#### *Chip design:*

- For improving the mixing performance a homogenous flow rate over the whole broadness of the channel already at the entrance to the observation channel should be provided. This can be achieved by straightening the two inlets, as curved or bended channel geometries will always lead to velocity distributions in the fluid elements.
- The thickness of the observation channel should be lowered, best 8  $\mu\text{m}$  thick, for enabling good measurements of the amid I band in water. This would also result in faster mixing because only 4  $\mu\text{m}$  distance has to be overcome by diffusion. However, in the same way this reduces the absorption of the sample, but this can be compensated by higher concentrations.
- The broadness of the channel can be reduced to 100  $\mu\text{m}$  in combination with a state-of-the-art well purged microscope. It is supposed that reducing the ratio broadness to thickness will lead to more stable flow sheets and probably hinder reduces effects as seen in the 2<sup>nd</sup> simulation (Figure 16), but this assumption should be confirmed by CFD simulations. (The argument of lower sample consumption due to lower flow rates for the same speed, applies here as well.)
- The silver foil marking the border of the channel is obligatory and should not be left out undertaking any design changes. It ensures that no SU-8 signal deriving from the channel walls is disturbing

#### *Fluidics connection:*

- The volume in the connections from the syringe to the mixer chip shall be reduced. An attempt has been made by using tubings of 0.17 mm inner diameter, but better results could be conceived using capillaries. Commercial connections therefore exist (Upchurch Scientific, Oak Harbor WA, USA). Lowering the internal volume from the syringe to the mixer, less sample is consumed for changing from background solution to sample and back.
- This latter point in combination with a valve before support inlet that allows switching between background solution and sample without opening the system (airbubbles!) would be preferable. In this way the lines could be rinsed up to the support inlets without unnecessarily ageing the mixer.

- The support should be ideally made from peek providing higher chemical resistance and better durability compared to Plexiglas<sup>®</sup>. The visible non-transparency of peek can be accepted.
- The design of the support is already rather optimised, however care must be taken that there is enough space for access of the IR beam stemming from an objective with large NA. The current opening is a bit too limited.

#### *Mount on x,y-stage*

- It is very important that the mixer is perfectly fixed on the moving sample stage. Cluing by adhesive tape is not sufficient! The positions of the mixer must be absolutely producible. Perfect alignment to the y-axis would help in online screening in the difference spectroscopy mode; in combination with a homogenous observation channel probably background measurements for every position can be omitted.

#### *Specials*

- Ideally, for measurements in aqueous solutions the mixer should be thermostatised as little changes in temperature affect the absorption of water.<sup>63;64</sup> A solution could be to introduce a thermostatic unit into the support.
- The icing on the cake would be mixer that can be disassembled for cleaning.

Considering all these points the mixing performance will be optimised, but an external problem that arises in continuous-flow measurements is not ruled out yet. Moving the mixer changes the matrix effects on the sample measurements. Even by taking background spectra at the same position, as this means that exactly the same position has be accessed precisely by the x,y stage. Furthermore, using the mixer usually particles smaller than 1  $\mu\text{m}$  is usually in the mixing zone, but if any particle is depositing in the observation channel sample and background measurement do not match anymore.

### **2.4.2 Both concepts into one**

The optimum could be reached by a design that combines both operating modes, the continuous-flow mode and the stopped-flow mode. This would allow obtaining high time resolution in the beginning of the reaction operating the chip in the continuous flow mode. Stopping the flow at the spot equivalent to e.g. 1 second reaction time, spectra could be recorded consecutively at one position. A time resolution of 1 sec could be obtained by using the rapid scan mode (e.g. 10 scans recorded into one buffer, and data processing performed after the measurement campaign).

The proposed valve can be used for stopping, by having only the capillaries and no further volume, stopping of small volume should be less difficult. Furthermore, in this way the sample consumption will be kept as low as possible. For ensuring abrupt stop of the flow, a third valve at the outlet should be implemented, which closes the outlet synchronic with shutting the inlets.

### 3 Water in the very far Infrared region

The far IR region down to the microwaves is studied since the 40's<sup>65</sup>, but the possibilities were very limited from the instrumental side. Due to the developments of more powerful sources and better performing instruments in the last decade, the interest in this region providing a lot of information has increased again.<sup>4,16</sup> Mainly physicists have employed this region to measure physical properties, but by the appearance of powerful broadband instruments the full FIR region is accessible for performing analytical spectroscopy of biochemical systems. The far IR region down to  $1\text{ cm}^{-1}$  (the region between 1 and  $100\text{ cm}^{-1}$  often called the THz region (see 1.2) offers a little studied range, where e.g. intermolecular vibrations of hydrogen bonds are expected<sup>4</sup>. This is of interest for biochemical investigations with respect to large and versatile connected molecules such as proteins. However as this region is so rarely exploited from a chemist's view it is necessary to first get more information on how the solvent for protein solutions, water, behaves in this region.

#### 3.1 Measurements using Terahertz pulsed Spectroscopy (TPS)

##### 3.1.1 Instrument

The instrument employed in this work is the TPI™ spectra 1000 from TeraView Limited (Cambridge, UK). It is based on photoemission of a semiconductor. Therefore an ultra-short laser pulse from a 75s bandwidth-limited titanium sapphire laser (800 nm at 80 MHz repetition rate) is focused on a GaAs photoconductive switch, a so-called Auston switch, where electron-hole pairs are generated and further accelerated. This results in emission of short bursts of broadband coherent radiation in the very far IR. This light is then collected by a silicon lens and focused onto the sample by additional mirrors. The detection of the transmitted radiation is achieved using an optically gated semiconductor receiver similar to the emitter. Gating this switch with the same laser, a certain time delay between the terahertz and the optical pulses is varied to measure a waveform comprising the terahertz signal as a function of time. This obtained waveform results by Fourier transformation in a spectrum with a wavenumber range from 1 up to  $150\text{ cm}^{-1}$ . A scheme of the instrument is presented in Figure 49

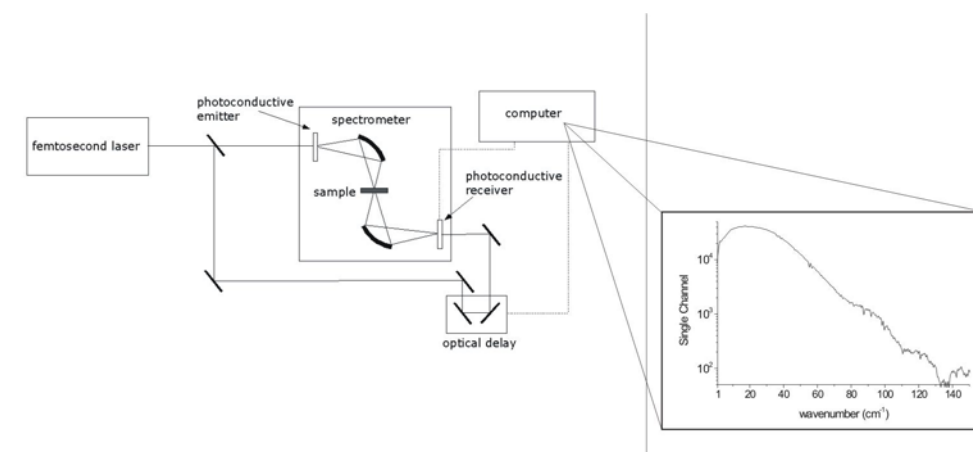


**Figure 49 Schematic drawing of the terahertz pulsed spectrometer. It provides radiation in the region below  $133\text{ cm}^{-1}$ , which is here presented on logarithmic scale.**

This type of instrument found so far mainly application on solids like pharmaceuticals<sup>66;67</sup>, whereas our approach is to use this instrument for spectroscopy on a standard liquid flow cell as established in mid-FTIR.

### 3.1.2 Characteristics of the TPI™ 1000

The instrument output is a spectrum equivalent to that measured by a Michelson Interferometer. Instead of a two mirror system the optical delay for generating the power spectrum is achieved by gating a semiconductor at different times on the femtosecond timescale. As a consequence the settings for a spectrum are difficult to compare. For instance, the spectral resolution cannot easily be changed and is set for fixed value, which makes up nominated  $1\text{ cm}^{-1}$ . Measurements at higher spectral resolution are stated to be possible and such as using a step scan mode for high time resolution as well.<sup>67</sup> The big advantage of the instrument is the high spectral power density down to  $1\text{ cm}^{-1}$ , which enables measurements of liquid water in transmission. In order to get rid of atmospheric water vapour, which would show rotational modes in this region, the sample compartment is  $\text{N}_2$  purged. No cooling neither by liquid helium nor by liquid nitrogen for the detector is needed.

Typical settings for the measurements were averaging of 180 scans at a spectral resolution of  $1\text{ cm}^{-1}$ , which takes about 1 min.

### 3.1.3 Application for aqueous solutions

The flow cell was equipped with polyethylene (PE) windows (replacing the CaF<sub>2</sub> for the mid-IR) showing high transparency apart from a lattice mode at  $\sim 72 \text{ cm}^{-1}$  (Figure 50). The windows are of 4 mm thickness each, in order to prevent from the so-called etalon effect. In case the wavelength is of same length as the thickness of the window, this would lead by reflection between the two surfaces to a standing wave effect, which would result in disturbing interference patterns.

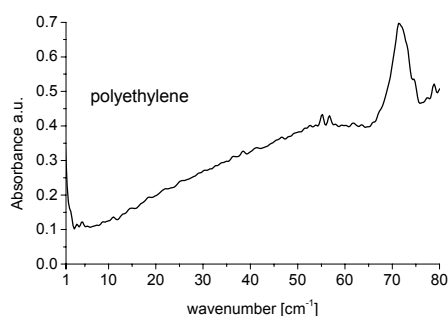


**Figure 50 Spectrum of PE in the THz-region**

A spectrum of pure water from  $1 - 100 \text{ cm}^{-1}$  is presented in Figure 51. The region above  $60 \text{ cm}^{-1}$  shows a poor signal-to-noise ratio due to the low intensity provided by the spectrometer in this region.

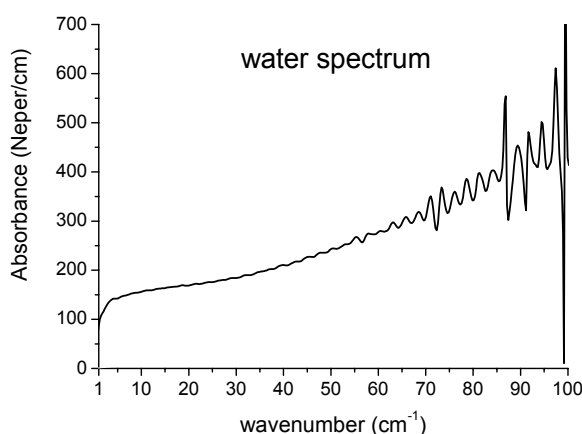


**Figure 51 Water spectrum in the THz region**

Despite the long time water is under study in this region there are still scientists working on this topic elucidating the “real shape” of the spectrum.<sup>68;69</sup> For a better comparison with other literature data the absorbance here is given as attenuation of power  $P$  ( $\alpha(\omega)$ ) in Neper per cm.<sup>70</sup> It describes the attenuation applying the natural logarithm to

the ratio of  $P$  and  $P_0$ , similar the linear absorptivity ( $\alpha_L$ ) in Equation 7 but using the signal amplitude  $F$  and not the power. The conversion is given by  $P(\omega) = F(\omega)^2$ . From there it follows, that the relation between the according to Lambert Beer received absorbance value ( $A$ ) can be translated to

$$\alpha(\omega) = \frac{2}{l} \cdot 2.303A \quad (\text{Eq 17})$$

Obtaining  $\alpha$  ( $33,3 \text{ cm}^{-1}$ ) = 224 from Figure 51 is in very good agreement with literature.<sup>69;71</sup> From Raman measurements and simulations a band around  $55 \text{ cm}^{-1}$ <sup>10;16</sup> is expected, but it seems only hardly, if at all, discernible using broadband spectroscopy at room temperature.<sup>14;17</sup>

Measurements of various salts have shown that their either “kosmotropic” or “chaotropic” effect on water is expressed in this region by an overall decrease or increase in absorbance. Results are presented in **publication V**. Furthermore an observed slope change in the region between  $20 - 40 \text{ cm}^{-1}$  is directly related to the ionic conductivity contribution,<sup>71</sup> often expressed by physicists in terms of the dielectric constant.<sup>9</sup>

Although spectra are recorded down to  $1 \text{ cm}^{-1}$  fluctuations in the region below  $15 \text{ cm}^{-1}$  were evoked only by the instrument itself and thus, make an interpretation of the spectra in this region questionable.

Attempts of monitoring changes of hydrogen bonding or long-range intramolecular vibrations in proteins failed. The digestion of albumin by the enzyme trypsin did not give significant changes higher than the noise of the instrument.

### 3.2 Synchrotron far infrared radiation

The generation of synchrotron radiation is explained in section 2.2.1.2. The IR beam emitted by the electrons is usually made of incoherent electromagnetic waves of arbitrary phase relation, ranges down to the microwave region. However, the transmittance of the mirror system collecting the synchrotron radiation is strongly decaying at about  $25 \text{ cm}^{-1}$  towards smaller wavenumbers because of diffraction effects. The intensity can be increased proportional to the number of electrons circulating in the storage ring. However, by operating shorter electron bunches in the ring, which have the length of the radiation of interest, the generated waves can superimpose in phase and the electric fields of these waves are adding up. This results in a radiation power growing as the square of the number of circulating electrons.<sup>72</sup> Considering the large number of electrons in a bunch

(typically  $10^8 - 10^{11}$ ) the intensity gain compared to incoherent synchrotron radiation is huge. This so-called coherent synchrotron radiation (CSR) is provided several times a year at BESSY for experiments using only the region from  $\sim 5$  to  $< 40 \text{ cm}^{-1}$  at high power.<sup>48</sup>

### 3.2.1 Instrumentation

At IRIS (BESSY) the synchrotron radiation can be coupled into a Bruker IFS 66v/s FTIR spectrometer (Figure 28). Additionally to the external light source the spectrometer is equipped with a standard globar for the mid-IR and a mercury lamp as alternative light source far IR. For switching from one region to the other, the beamsplitter for the interferometer can be exchanged. Typically, the KBr beamsplitter for the mid-IR is replaced by mylar-beamsplitter at various thickness for the far IR.<sup>73</sup> The type and thickness determines the cut-off in the low wavenumber-region and the position of the zero-points in transmission. The characteristic intensity curves for 3 different beamsplitter are presented in Figure 52.

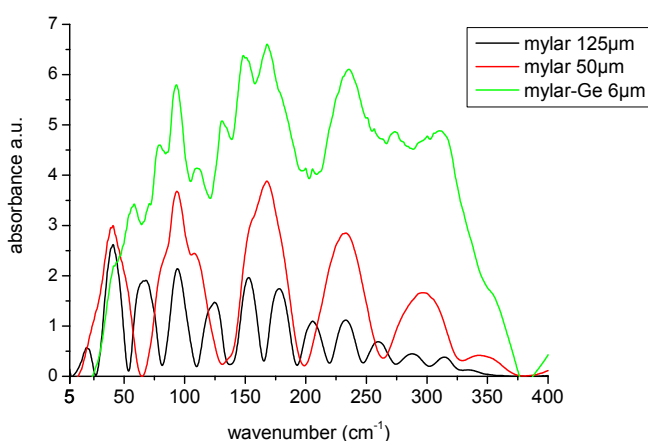


**Figure 52. Beamsplitter-test for SIR. The intensity distribution shows that the 6  $\mu\text{m}$  mylar beamsplitter with a layer of Germanium provides most constant intensity, but the 50 and the 125  $\mu\text{m}$  mylar beamsplitter have a lower cut-off**

Apart from the internal DTGS and MCT detector a liquid-helium cooled (4 K) bolometer as FIR detector is attached. The latter detector has a low frequency cut-off at  $\sim 20 \text{ cm}^{-1}$ . Gaining sensitivity in the low wavenumber region is possible by operating this type of detector at  $\sim 1.5 \text{ K}$  which is achieved by pumping the liquid helium to bring it to its superfluidic phase. In this way the frequency cut-off is given at  $\sim 5 \text{ cm}^{-1}$ . The instrument parameters for adjusting e.g. scan speed or spectral resolution can be set as with any FTIR-spectrometer. However, attention has to be paid at some settings, such as



the zero-filling, which do not have a high influence on the broad spectral region of the mid-IR, but can lead to misinterpretation in the narrow range of the low wavenumber regime.

In order to get rid of the atmospheric water vapour the whole spectrometer is evacuated for measurements.

### 3.2.2 Characteristics

The big advantage of the light source SIR is its high dynamic spectral range covering the lowest wavenumber region up to the near infrared. The limitation for recording the whole spectral IR region at once is only set by the instrument equipment such as beam splitter, detectors or cuvette material. Compared to other FIR sources like the mercury lamp the synchrotron light provides higher power in the region below  $\sim 50 \text{ cm}^{-1}$ . The biggest advantage of the synchrotron is exploited when operated in the CSR mode providing high intensity between  $0.3 - 1 \text{ THz}$  ( $\sim 5 - 35 \text{ cm}^{-1}$ ), which is even saturating the detector. Furthermore, the high brilliance of this type of radiation was used for near-field experiments.<sup>74</sup>

The appearance as a point-like source, which is similarly exploited for the spatial resolution in section 2.2.1, is in the same way enabling measuring at high spectral resolution. By setting it down to  $0.2 \text{ cm}^{-1}$  narrow spectral features can be resolved, which would appear as undefined noise by using lower resolution. However, as usually it must be considered that increasing the resolution is only possible at the expense of scan time. This can be crucial for synchrotron radiation, as the decay in intensity related to the beam current will be interfering with the information deriving from the sample. For compensation it is necessary to perform periodic reference measurements of the empty sample compartment determining the current available beam intensity.

### 3.2.3 Application

Using the SIR the water spectrum from about  $400$  down to  $20 \text{ cm}^{-1}$  could be recorded. Especially for water it is of high interest to see the little studied low wavenumber region ( $< 70 \text{ cm}^{-1}$ ) in context with the known water band at  $180 \text{ cm}^{-1}$  and the tail of the broad band at  $680 \text{ cm}^{-1}$  (libration mode). The spectrum recorded on  $25 \text{ }\mu\text{m}$  layer of water

between two 4 mm thick PE windows measured with  $1 \text{ cm}^{-1}$  of resolution is given in Figure 53. For the resulting spectra 512 scans were averaged taking 180 sec.

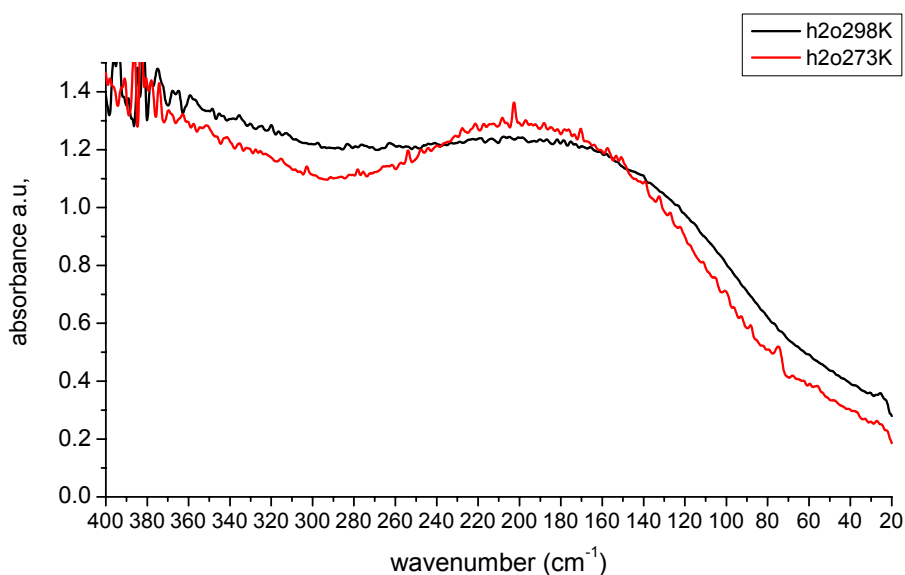


**Figure 53 Spectrum of pure water with the empty cell as background in dependence of two different temperatures**

The temperature dependence and the therewith related change in shape of the connectivity band at  $\sim 200 \text{ cm}^{-1}$ , deriving from the intramolecular stretching mode of water (H-O...H), is in agreement with literature<sup>14;17;64</sup> (although it is sometimes denoted as a band at  $\sim 175 \text{ cm}^{-1}$ )<sup>16</sup>. The exact band position is determined actually by the several subjacent water bands related to the different water structures typically present in liquid water.<sup>64</sup> Comparing this spectrum to the results in **publication V**, it shows that the effect of solutes on the water spectrum discovered in the region  $10 - 60 \text{ cm}^{-1}$  using the TPI instrument (see section 3.1.3) is overlaying with the border region of the connectivity band. In literature<sup>17</sup> a rather broad and smeared feature in the water spectrum at low temperatures is identified as the discussed band, which is also found by simulations.<sup>75;76</sup> However, the predicted band at  $\sim 60 \text{ cm}^{-1}$  cannot be discerned here, as well as in other references.<sup>77</sup> It is stated that the intermolecular H-bond bending motions causes this band due to the fluctuations of the polarisability anisotropy and therefore it is stronger in Raman and hardly IR active.<sup>78</sup> The band at  $\sim 200 \text{ cm}^{-1}$  occurs due to intermolecular H-bonds as well, but it arises from the translational modes and this involves fluctuations both in the dipole moment and the polarisability.

In order to corroborate the results obtained at TeraView and to apply our theory to more solutes, the measurements performed at the TPI™1000 were repeated at the synchrotron facility. The main feature to observe is shift in absorbance either to higher or lower values with respect to pure filtered water. It is necessary to carefully compensate for intensity drift of the synchrotron. For these measurements this was done by acquiring a background water spectrum for the background before and after the sample measurement, which were averaged and used as the background spectrum. For avoiding any influence of temperature (which would be expected to express in the spectrum regarding Figure 53) a thermostatisable cell was used connected to an oil bath keeping the temperature constant of 20 °C. The settings of the instrument are the same as in the water measurement before. Due to instrument problems, the beamsplitter of 6 μm had to be changed during the campaign for the 50 μm. This affects the noise in the absorption spectra for the wavenumber regions where the transmission is zero (for reference see Figure 52).

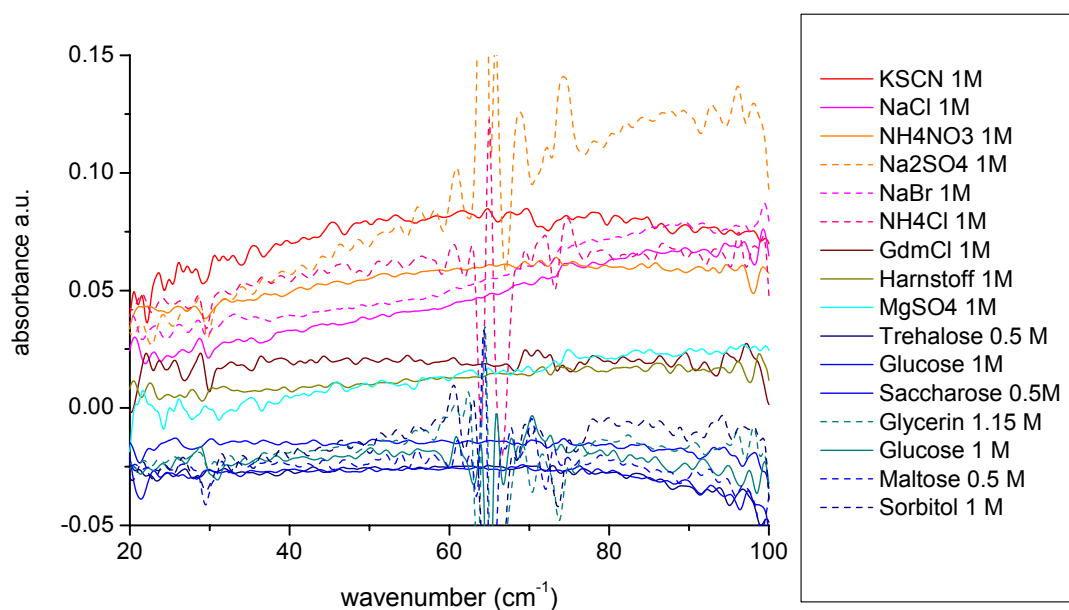


**Figure 54 Spectra of aqueous solutions against pure water. The concentrations are chosen for easy comparison with publication V.**

The resulting spectra clearly confirm our theory made on absorbance spectra in the region between 20 and 60  $\text{cm}^{-1}$  saying that “chaotropic” solutes shift the absorbance values up (reddish colour) and that “kosmotropic” (bluish colour) lead to decreased absorption. However a closer look to this graph provides even more information: The access to the region  $> 60 \text{ cm}^{-1}$  reveals that, for instance, the graph of the dissolved KSCN

or  $\text{NH}_4\text{NO}_3$  is describing a slight decay in this region. This trend gives evidence that the influence of the structural behaviour of solutes is not depending on the connectivity band at  $180\text{ cm}^{-1}$ , but may probably be in relation with the expected band at  $\sim 60\text{ cm}^{-1}$ . Furthermore, the relation between ionic strength and slope in the spectra is clearly to see. For  $\text{Na}_2\text{SO}_4$  providing higher ionic conductivity than  $\text{MgSO}_4$  at the same concentration the graph is much steeper, while only for larger ions the decay towards higher wavenumbers can be seen. Thus it could be confirmed that this region provides access to two overlaying effects, namely the polarity and the structural changes in water. However, this fact hinders at the same time a good evaluation of the structural effects of solutes on water.

While these measurements could only be performed down to  $20\text{ cm}^{-1}$ , the TPI instrument gave access down to  $1\text{ cm}^{-1}$ . However, due to instabilities of the spectra especially in the lower region we had to omit the part below  $20\text{ cm}^{-1}$  for evaluation of the spectra (**publication V**). The possibility of using CSR at the synchrotron can fill up this gap. Therefore the same samples were measured at the synchrotron using the pumped bolometer. The result is given in Figure 55.

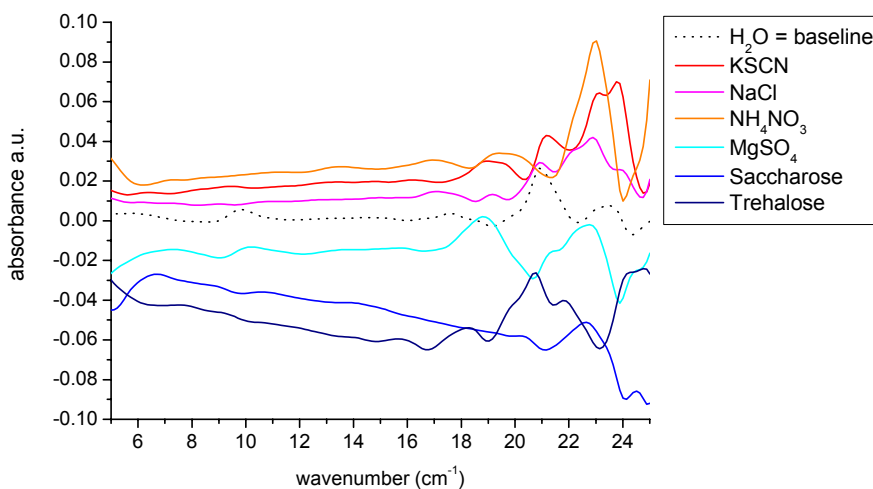


**Figure 55.** The measurements from Figure 54 were repeated using the CSR. All concentrations are 1 M.

In general, the spectra show an extended effect of shifts in absorption intensity. However, the strong decay for the two tested carbohydrates is observed from  $7$  to  $16\text{ cm}^{-1}$ , contradicts the obtained results from the TPI (**publication V**), where a horizontal shift in absorption was observed. Interpretation here fore can only be tentative and may be related either instrumental differences in combination with the complex information of water and the carbohydrates themselves in this region. The features at  $> 18\text{ cm}^{-1}$  are not

reproducible, and therefore are related to the noise, which is due to the lower intensity of the synchrotron in this region (Equation 13).

What was not taken into account so far, as well as in the measurements at the TPI, is the increasing refractive index of water when approaching small wavenumbers (see 1.3). This of course, must result into interference pattern that occur when light travels in media of different refractive indices. This shall be discussed by the next experiment.

For a deeper look into the “noise” the spectral resolution is enhanced to a value of  $0.2 \text{ cm}^{-1}$ . Note that an increase of the spectral resolution requires a “more point like” source, comparable to the need for good spatial resolution (refer 2.2.1.1). This can be achieved by lowering the aperture size in front of the interferometer. This may be more troublesome owing to the causing loss of intensity. In this case the synchrotron light source providing high power in this region clearly poses an advantage.

The recorded spectra are shown in Figure 56. The spectra so far were recorded at  $1 \text{ cm}^{-1}$  spectral resolution represented by the red line.

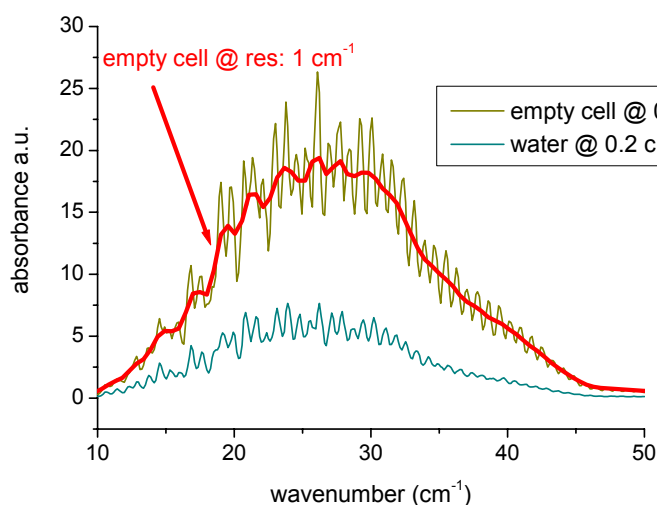


**Figure 56.** The transmitted intensity measured at  $0.2 \text{ cm}^{-1}$  spectral resolution. The “smoothed” red curve is deriving from a measurement performed with spectral resolution  $1 \text{ cm}^{-1}$ .

The enhanced resolution enables to see the features that appear smoothed at  $1 \text{ cm}^{-1}$ . It can be seen that the spectra contain a fringe pattern resulting from the defined thickness in the beam path. Comparing the better resolved spectra of water and empty cell it can be seen apart from the fact that the water layer of  $25 \text{ }\mu\text{m}$  is absorbing 75 % of the intensity, that there are some similarities as some differences as well in the pattern. Introducing

water with its increasing refractive index towards lower wavenumbers (refer section 1.3), it can be expected that fringes appear and this will lead to problems for calculating an absorbance spectrum out of these two.

A closer look to such occurring fringe pattern provides Figure 57. A typical interferogram containing a wide range of frequencies shows the large center burst and a continuous decay on both sides. This presented interferogram shows inhomogeneities at several positions, each of them deriving from an other “disturbing” layer in the beam path. These may stem from the sample, the sample windows, the diamond window separating the beamline from the storage ring system or the bolometer window.

The explanation for the appearance of such patterns is given by presence of the etalon effect. Passing two reflecting surfaces a part of the beam will suffer multiple reflections, which lead to constructive and destructive interferences, similar to a Fabry-Perot Interferometer. Considering that an interferogram develops not until reaching the detector, the modulated beam carrying the information of several units, which act as interferometer, will give a complex interferogram. However, the main modulation occurs in the Michelson interferometer where the beam is split nearly in a 50:50 ratio, whereas the further materials in the beam path only retard a small part, depending on the reflecting property. As a consequence the etalon effect only provokes “small interferograms” overlaying with the main one from the Michelson interferometer.

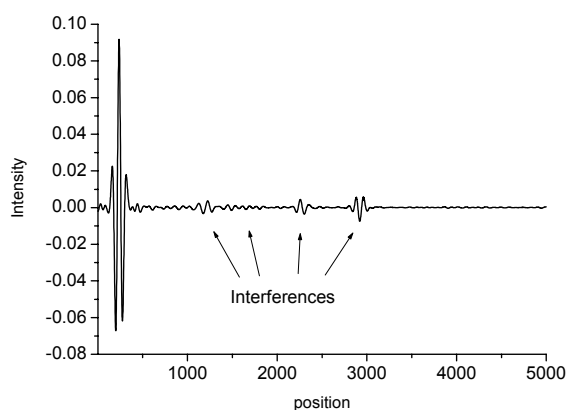


**Figure 57** Detailed look at the interferogram of water spectrum. Several interferences can be discerned.

Considering several overlaying interferences, it becomes obvious why the pattern in Figure 57 is only slightly changing when an item with a changing refractive index is brought into the beam path. If further, the resolution is lowered, such pattern cannot be resolved and broad spectral features will appear, which cannot be interpreted. This must

be taken into account when a sample with refractive index differing of the background is introduced and absorption spectra thereof are calculated.

Such problems were not observed acquiring spectra using the TPI instrument. Of course it could be that the interferences are not appearing due to careful arrangement of the optics. However, it can also be the case that the spectra appear so smooth, because the spectrometer without further aperture system is not capable of performing real  $1\text{ cm}^{-1}$  resolution and smoothes the interferences away by low actual resolution. Both considerations would explain, why it was possible to measure the water against the empty cell (equals a change in refractive index from  $\sim 1.5$  to 1, refer Figure 4), which did not lead to interferences.

### **3.3 Conclusion and Outlook for aqueous FIR measurements**

The aim of these studies was testing the capabilities of the THz region for performing biochemical experiments in water. Very recent literature claims to successfully record information in this region of aqueous protein and DNA solutions.<sup>79;80</sup> While DNA reveals distinct features, protein solutions show only broad band absorption. So far, the observed spectral feature cannot be assigned to certain vibrations as common in the mid-IR and the evaluation of the overall protein absorption is strongly dependent on the consideration of the changing water due to solvation shell effects. Facing the complexity of simple water in this region, which was demonstrated within this work, it is clear how delicate measurements on aqueous solution are. Furthermore, the intermolecular interactions carry information of the structure of water, a topic that still lacks full understanding. A basic consideration is the fact that water generally is a rather strong absorber and it will be difficult to distinguish spectral changes that only derive from protein molecules.

Albeit it seems possible to get information related to e.g. DNA<sup>79</sup> it deserves, from my point of view, much more fundamental studies on water in this region before it becomes possible to use the vibrational information from spectroscopy in the very far IR as we do it since decades for the mid-IR.

## 4 References

1. Diewok, J. M. *Advanced Multivariate Data Evaluation for Fourier Transform Infrared Spectroscopy*. Inst. of Chem. Technologies and Analytics, Vienna University of Technology, 2002.
2. Hinsmann, P. Novel microfluidic chips with Fourier transform infrared spectroscopic detection for reaction and separation monitoring in miniaturised analysis systems. Inst. of Chem. Technologies and Analytics, Vienna University of Technology, 2002.
3. Kellner, R.; et al *Analytical Chemistry*, Wiley-VCH: Weinheim, 1998; 541-567.
4. Griffiths P. R. *Handbook of Vibrational Spectroscopy*; John Wiley & Sons: New York, 2002; Chapter Vol.1, pp. 229-239.
5. Colthup, N. B. *Introduction to Infrared and Raman Spectroscopy*, third ed.; Academic Press: San Diego, CA, 1990; IX-547.
6. Nakanishi, K. *Infrared Absorption Spectroscopy*, Holden-Day: San Francisco, 1962; IX-233.
7. Griffiths, P. R.; de Haseth, J. *Fourier Infrared Transform Spectroscopy*, John Wiley & Sons: New York, 1986.
8. Bertie, J. E.; Ahmed, M. K. *Journal of Physical Chemistry* **1989**, *93*, 2210-2218.
9. Bertie J. E. *Handbook of Vibrational Spectroscopy*; John Wiley & Sons: New York, 2002; pp. 89-100.
10. Chaplin, Martin. Water: Structure and Behaviour. <http://www.lsbu.ac.uk/water> . 2006.
11. Venyaminov, S. Y.; Prendergast, F. G. *Analytical Biochemistry* **1997**, *248*, 234-245.
12. Bertie, J. E.; Lan, Z. *Applied Spectroscopy* **1996**, *50*, 1047-1057.
13. Libnau, F. O.; Kvalheim, O. M.; Christy, A. A.; Toft, J. *Vibrational Spectroscopy* **1994**, *7*, 243-254.
14. Hasted, J. B.; Husain, S. K.; Frescura, F. A. M.; Birch, J. R. *Chemical Physics Letters* **1985**, *118*, 622-625.
15. Walrafen, G. E.; Chu, Y. C. *Journal Physical Chemistry* **1995**, *99*, 11225.
16. Nielsen, O. F. *Annual Report on Progress of Chemistry: Section C: Physical Chemistry* **1997**, *93*, 57-99.
17. Zelsmann, H. R. *Journal of Molecular Liquids* **1995**, *350*, 95.
18. Smith G. D.; Palmer, R. A. *Handbook of Vibrational Spectroscopy*; John Wiley & Sons: New York, 2002; Chapter Vol.1, pp. 621-640.
19. Kauffmann, E.; Darnton, N. C.; Austin, R. H.; Batt, C.; Gerwert, K. *Proceedings of the National Academy of Sciences of the United States of America* **2001**, *98*, 6646-6649.



20. Palmer, R. A.; Smith, G. D.; Pingyun, C. *Vibrational Spectroscopy* **1999**, *19*, 131-141.
21. Rammelsberg, R.; Hessling, B.; Chorongiewski, H.; Gerwert, K. *Applied Spectroscopy* **1997**, *51*, 558-562.
22. Georg, H.; Wharton, C. V.; Siebert, F. *Laser Chem.* **1999**, *9*, 233-235.
23. Reinstädler, D.; Fabian, H.; Backmann, J.; Naumann, D. *Biochemistry* **1996**, *35*, 15822-15830.
24. Friedrich, M.; Gieß, F.; Naumann, R.; Knoll, W.; Ataka, K.; Heberle, J.; Hrabakova, J.; Murgida, D.; Hildebrandt, P. *Chemical Communications* **2004**, *21*, 2377.
25. Crank, J. *The mathematics of diffusion*, 2. ed.; Oxford Univ. Press: Oxford, 1986; VIII-414.
26. Dunn, B. C.; Eyring, E. M. *Applied Spectroscopy* **1999**, *53*, 292-296.
27. Masuch, R.; Moss, D. A. *Applied Spectroscopy* **2003**, *57*, 1407-1418.
28. White, A. J.; Drabble, K.; Wharton, C. W. *Biochemistry Journal* **1995**, *306*, 843-849.
29. Hinsmann, P.; Frank, J.; Svasek, P.; Harasek, M.; Lendl, B. *Lab on A Chip* **2001**, *1*, 16-21.
30. Konermann, L. *Journal of Physical Chemistry* **1999**, *103*, 7210-7216.
31. Carr, L. *Vibrational Spectroscopy* **1999**, *19*, 53-60.
32. Dumas, P.; Miller, L. *Vibrational Spectroscopy* **2003**, *32*, 3-21.
33. Floyd, T. M.; Schmidt, M. A.; Jensen Klavs F. *Ind.Eng.Chem.Res.* **2005**, *44*, 2351-2358.
34. Svasek, P.; Svasek, E.; Lendl, B.; Vellekoop, M. J. *Sensors and Actuators A* **2004**, *115*, 591-599.
35. Morishima, K.; Yoshida, Y.; Kitamori, T. *Proceedings of  $\mu$ TAS 2004* **2004**, *1*, 171-174.
36. Bleicher, K.; Lin, M.; Shapiro, M. J.; Wareing, J. R. *Journal of Organic Chemistry* **1998**, *63*, 8486-8490.
37. Deister, U.; Neeb, R.; Helas, G.; Warneck, P. *Journal of Physical Chemistry* **1986**, *90*, 3213-3217.
38. Rao, T. S.; Salunke, S. B. *React.Kinet.Catal.Lett.* **1984**, *26*, 273-277.
39. Sommer A. J. *Handbook of Vibrational Spectroscopy*; John Wiley & Sons: New York, 2002; Chapter Vol.2, pp. 1369-1393.
40. Amelinckx, S. *Handbook of microscopy: applications in materials science, solid-state physics and chemistry*, Wiley-VCH: Weinheim, 1997.
41. Sommer, A. J.; Katon, J. E. *Applied Spectroscopy* **1991**, *45*, 1633-1640.
42. Carr, L. *Review of Scientific Instruments* **2001**, *72*, 1613-1618.
43. Smith, W. J. *Modern Optical Engineering*, McGraw-Hill: New York, NY [u.a.], 1966; XII-476.
44. Nishikida, K. *Thermo Electron Corporation, Application Note* **2005**.
45. Theocharous E.; Birch, J. R. *Handbook of Vibrational Spectroscopy*; John Wiley & Son: New York, 2002; Chapter Vol.1, pp. 348-361.

46. Schade, U.; Roeseler, A.; Korte, E. H.; Bartl, F.; Hofmann, K. P.; Noll, T.; Peatman, W. B. *Review of Scientific Instruments* **2002**, *73*, 1568-1572.
47. Schade, U.; Peatman, W. B. *Journal of Biological Physics* **2003**, *29*, 309-312.
48. Abo-Bakr, M.; Feikes, J.; Holldack, K.; Kuske, P.; Peatman, W. B.; Schade, U.; Wustefeld, G.; Hubers, H. W. *Physical Review Letters* **2003**, *90*.
49. Carr, G. L.; Martin, M. C.; McKinney, W. R.; Jordan, K.; Neil, J. R.; Williams, G. P. *Journal of Biological Physics* **2004**, *29*, 101-108.
50. Gensch, M.; Hinrichs, K.; Roeseler, A.; Korte, E. H.; Schade, U. *Anal. Bioanal. Chem.* **2003**, *376*, 626-630.
51. Williams G. P. *Handbook of Vibrational Spectroscopy*; John Wiley & Sons: New York, 2002; Chapter Vol.1, pp. 341-348.
52. Lewis, E. N.; Treado, P. J.; Reeder, R. C.; Story, G. M.; Dowrey, A. E.; Marcott, C.; Levin, I. W. *Analytical Chemistry* **1995**, *67*, 3377-3381.
53. Schultz, Christian. Precision Infrared Spectroscopic Imaging: The Future of FT-IR Spectroscopy. [www.spectroscopyonline.com](http://www.spectroscopyonline.com) 16[10], 24-33. 2001.
54. Miller, L. M.; Smith, R. J. *Vibrational Spectroscopy* **2005**, *38*, 237-240.
55. Chan, K. L. A.; Kazarian, S. G.; Mavraki, A.; Williams, D. R. *Applied Spectroscopy* **2005**, *59*, 149-155.
56. Lewis, L. L.; Sommer, A. J. *Applied Spectroscopy* **2000**, *54*, 324-330.
57. Domínguez-Vidal, A.; Saenz-Navajas, M. P.; Ayora-Canada, M. J.; Lendl, B. *Analytical Chemistry* **2006**, *78*, 3257-3264.
58. Muik, B.; Lendl, B.; Molina-Díaz, A.; Ortega-Calderón, D.; Ayora-Canada, M. J. *J. Agric. Food. Chem.* **2004**, *49*, 6055-6060.
59. Diewok, J.; de Juan, A.; Maeder, M.; Tauler, R.; Lendl, B. *Analytical Chemistry* **2003**, *75*, 641-647.
60. Williams, D. H.; Bardsley, B. *Angew. Chem* **1999**, *111*, 1264-1286.
61. Popienik, P. H.; Pratt, R. F. *Journal of the American Chemical Society* **1988**, *110*, 1285-1286.
62. Williamson, P. M.; Williams, D. H.; Hammond, S. J. *Tetrahedron* **1984**, *40*, 569-577.
63. Rahmelow, K.; Hübner, W. *Applied Spectroscopy* **1997**, *51*, 160-170.
64. Brubach, J. B.; Mermet, A.; Filabozzi, A.; Gerschel, A.; Roy, P. *Journal of Chemical Physics* **2005**, *122*.
65. Kimmitt, M. F. *Journal of Biological Physics* **2003**, *29*, 77-85.
66. Taday, P. F.; Bradley, I. V.; Arnone, D. D.; Pepper, M. *Journal of Pharmaceutical Science* **2002**, *92*, 831-838.
67. Taday, P. F.; Newnham, D. A. *Spectroscopy europe* **2004**, *16*, 20-24.
68. Woods, K. N.; Wiedemann, H. *Chemical Physics Letters* **2004**, *393*, 159-165.

69. Xu, J.; Allen, S. J.; Plaxco, K. W. *Journal of Chemical Physics* **2006**, *124*, 036101 .
70. Mills, I. M.; Taylor, B. N.; Thor, A. J. *Metrologia* **2001**, *38*, 353-361.
71. Zoidis, E.; Yarwood, J.; Besnard, M. *Journal of Physical Chemistry A* **1999**, *1003*, 220-225.
72. Abo-Bakr, M.; Feikes, K.; Holldack, K.; Kuske, P.; Peatman, W. B.; Schade, U.; Wustefeld, G.; Hübers, H.-W. *Physical Review Letters* **2003**, *90*, 094801-1-094801/4.
73. Griffiths P. R.; Homes, C. C. *Handbook of Vibrational Spectroscopy*; John Wiley & Sons: New York, 2002; Chapter Vol.1, pp. 326-340.
74. Schade, U.; Holldack, K.; Kuske, P.; Wüstefeld, G.; Hübers, H.-W. *APPLIED PHYSICS LETTERS* **2004**, *84*, 1422-1424.
75. Madden, P. A.; Impey, R. W. *Chemical Physics Letters* **1986**, *123*, 502-506.
76. Padro, J. A.; Marti, J. *Journal of Chemical Physics* **2003**, *118*, 452-453.
77. Guillot, B. *Journal of Chemical Physics* **1991**, *95*, 1543-1551.
78. Vij, J. K.; Simpson, D. R. J.; Panarina, O. E. *Journal of Molecular Liquids* **2004**, *112*, 125-135.
79. Globus, T. R.; Khromova, T.; Gelmont, B. L.; Woolard, D. L.; Tamm, L. K. *Proceedings of SPIE-The International Society for Optical Engineering* **2006**, *6093*, 609308-609320.
80. Xu, J.; Plaxco, K. W.; Allen, S. J. *Protein Science* **2006**, *15*, 1175-1181.

## ***Publication I***

*N. Kaun, S. Kulka, J. Frank, U. Schade, M. J. Vellekoop M. Harasek and B. Lendl*

*„Towards Biochemical reaction monitoring using FT-IR Synchrotron radiation”*

*Analyst, 131,( 2006) 489–494*

# Towards biochemical reaction monitoring using FT-IR synchrotron radiation

N. Kaun,<sup>a</sup> S. Kulka,<sup>a</sup> J. Frank,<sup>c</sup> U. Schade,<sup>b</sup> M. J. Vellekoop,<sup>d</sup> M. Harasek<sup>e</sup> and B. Lendl<sup>\*a</sup>

Received 5th October 2005, Accepted 6th January 2006

First published as an Advance Article on the web 27th January 2006

DOI: 10.1039/b514102h

A lab-on-a-chip device made of CaF<sub>2</sub> windows and SU-8 polymer was used for fluid lamination to achieve rapid mixing of two streamlines with a cross section of 300 × 5 μm each. Time resolved measurements of the induced chemical reaction was achieved by applying constant feeding low flow rates and by on-chip measurement at defined distances after the mixing point. Synchrotron IR microscopic detection was employed for direct and label-free monitoring of (bio)chemical reactions. Furthermore, using synchrotron IR microscopy the measurement spot could be reduced to the diffraction limit, thus maximizing time resolution in the experimental set-up under study. Based on computational fluid dynamic simulations the principle of the set-up is discussed. Experimental results on the basic hydrolysis of methyl chloroacetate proved the working principle of the experimental set-up. First results on the interaction between the antibiotic vancomycin and a tripeptide (Ac<sub>2</sub>KAA) involved in the build up of the membrane proteins of gram-positive bacteria are presented.

## Introduction

Fourier transform infrared (FTIR) spectroscopy provides *direct* molecular specific information on systems ranging from small molecules to complex systems such as proteins.<sup>1</sup> The information obtained can be a global one like the secondary structure of a protein but it can also be highly specific for single functional groups in a large molecule. Especially in the field of protein analysis, FTIR spectroscopy has emerged as a powerful method for studying the secondary structure of proteins and subtle changes in the protein structure.<sup>2–7</sup> The use of time resolved (TR) FTIR enabled workers to obtain kinetic data on conformational changes in proteins with a time resolution down to a few nanoseconds<sup>8</sup> in the case of photo-initiated reactions. In this context it is important to note that kinetic studies have been restricted to reactions which can be initiated by suitable triggering techniques, such as light pulse,<sup>9,10</sup> temperature jump<sup>11,12</sup> or pressure jump.<sup>13</sup> This limitation has been partly overcome by the development of solution mixing techniques suitable for TR-FTIR, giving way to a general applicable technique for label-free (bio)chemical reaction monitoring.

For mixing two reactants quickly and monitoring the reaction with mid-IR spectroscopy, certain prerequisites have to be fulfilled: A device has to be used that should be capable of reproducible and rapid mixing to start a reaction of two

substances dissolved in two liquid streams. Further, it should be possible to record spectra of both solutions immediately prior to mixing and right from the start of the mixing process. The typical conditions for samples in biochemistry are pH buffered aqueous solution. As a consequence, the optical path length for mid-IR measurements should be kept below 10 μm in order to avoid the absorption of all IR intensity by water. This applies especially around 1640 cm<sup>-1</sup> where both the information rich amid I band and the water bending vibration absorb. Miniaturization of the system is also highly desirable as often the amount of available biomolecules of interest is limited and high concentrations are required for the FTIR experiment. Measuring small changes in IR absorption, such as are observable in biochemical reactions, needs a high signal-to-noise-ratio (S/N ratio), which can be obtained by signal averaging. In the case of FTIR spectroscopy this requires averaging of scans, which is a time consuming process. Therefore, to achieve both a short time scale and a high S/N ratio, repetition of the process is necessary. In the case of biochemical reaction monitoring this translates to repeated initiation of the mixing process. The small size of the mixer, due to both the small channel height for the mid-IR spectroscopy in aqueous solution and to the low internal volume, together with low flow rates for little sample consumption, results in a Reynolds Number <1, which means laminar flow. Without turbulence the mixing process will be determined by diffusion, which is known to be a rather slow process. The diffusion time and the time for the mixing process, respectively, can be calculated by the formula derived from Fick's Law, which is valid for plane sources in semi-infinite media

$$c(x,t) = \frac{c_0}{\sqrt{\pi Dt}} e^{-\frac{x^2}{4Dt}} \quad (1)$$

with  $c$  being the concentration of a substance dissolved in the liquid, and  $c_0$  the concentration at the beginning ( $t = 0$ ,  $x = 0$ ),

<sup>a</sup>Institute of Chemical Technologies and Analytics, Vienna University of Technology, Getreidemarkt 9-164, 1060 Vienna, Austria.

E-mail: bernhard.lendl@tuwien.ac.at

<sup>b</sup>BESSY, 12489 Berlin, Germany

<sup>c</sup>Institute of Materials Chemistry, Vienna University of Technology, 1060 Vienna, Austria

<sup>d</sup>Institute of Sensor and Actuator Systems, Vienna University of Technology, 1040 Vienna, Austria

<sup>e</sup>Institute of Chemical Engineering, Vienna University of Technology, 1060 Vienna, Austria

$D$  the diffusion constant for the substance that is spreading,  $x$  the distance of diffusion along an axis and  $t$  the diffusion time. In order to increase the speed of mixing, which is indispensable for monitoring a reaction uncoupled from the mixing process, the distance that a substance has to overcome driven only by diffusion has to be small as possible. The correlation of diffusion distance and diffusion time is given by the term  $x^2/4Dt$  in eqn. 1.

All these requirements were already achieved in Hinsmann *et al.*<sup>14</sup> a mixer chip superimposes two streamlines of low thickness (5–7.5  $\mu\text{m}$  each), such that even the slow diffusion process is fast enough to finish mixing in the ms region (depending on experimental conditions) so that only the ongoing reaction as changes in spectra with time can be followed. The channel is 10–15  $\mu\text{m}$  high and is confined by two 1 mm thick  $\text{CaF}_2$ -plates which allow IR transmission measurements of the liquids inside (Fig. 1). Owing to its structure, made of SU-8 stabilizing a silver foil as separating membrane, the set up geometry allows steadily reproducible mixing just by applying constant flow. So far, the mixer was used in the “stopped-flow mode”.<sup>14,15</sup> This means the liquids were pumped into the chip, where they started mixing and then the flow stopped, so, after several tens of milliseconds for finalising the mixing process, the reaction could be followed by acquiring spectra over time. The limit for the time resolution is therefore set by the scan speed of the instrument (Fig. 2). The beam of the recording instrument needs to be no smaller than the broadness of the channel (in Hinsmann *et al.*<sup>14</sup> 1 mm).

With the availability of high precision low flow-rate pumps and an FTIR microscope equipped with a moveable stage, the mixer design also can be used in the “continuous flow” mode.<sup>16</sup> The two liquids are pumped at up to 100 times lower flow-rates into the mixer, where the mixing occurs within the first part of the channel and afterwards just the changes in the chemical system are observed along the channel. This can actually be considered as a transfer of the time scale axes into a lateral axis. Thus, the time resolution is dependent on the distance and the size of the sample spots along the channel and is no longer limited by the scan speed, as in the stopped flow experiment. Alternatively, only the flow rate need be varied as recently shown in ref. 17.

Synchrotron infrared radiation (SIR) allows measurement of sample spot sizes at the diffraction limit which lies in the  $\mu\text{m}$ -range; the reason for this is its high brilliance.<sup>18</sup> So far,

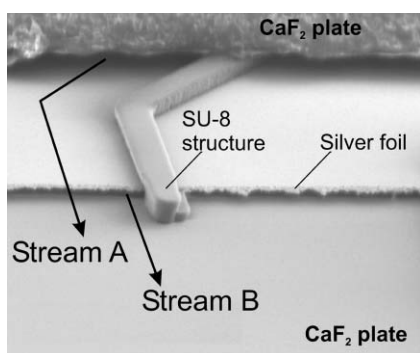


**Fig. 1** Image of the assembly of the mixer chip. A, Stopped flow mode. B, Continuous flow mode.

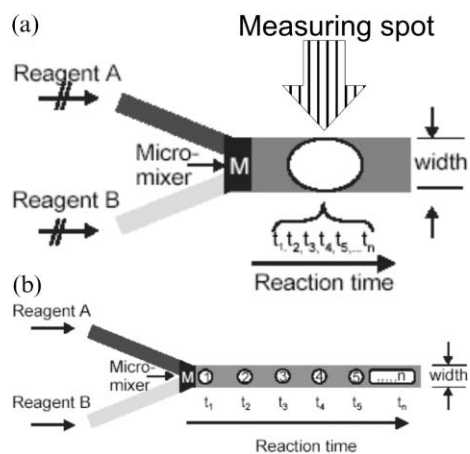


**Fig. 2** Schemes for measuring modes for reaction monitoring: (a) stopped flow mode; (b) continuous flow mode.

advantage of the high spatial resolution is taken in biochemical analytics, mainly for the imaging of complex samples,<sup>19,20</sup> such as tissues, with great success. In this work the small sample spot size will be used for achieving high time resolution in the continuous flow mode.

The mixing device is tested by computational fluid dynamic (CFD) simulations. Apart from visualising the strengths and weaknesses of the continuous flow approach, CFD simulations also help to determine the time and therefore the distance required for full mixing. The feasibility of the whole set-up is demonstrated by an ester hydrolysis, which serves as a simple model reaction. In addition, first studies on a biochemical system are presented. The system of interest is the interaction of the antibiotic vancomycin, belonging to the group of glycopeptide antibiotics, and the peptide  $N^{26}$ -diacetyl-L-lysyl-D-alanyl-D-alanine ( $\text{Ac}_2\text{KAA}$ ). This peptide represents the terminating segment of a cell wall precursor during bacteria biosynthesis. Binding of the antibiotic to this sequence inhibits the action of bacterial enzymes that would use these termini for formation of further bacteria.<sup>21</sup> Already in the early 1990s Popieniek *et al.* had proposed kinetics based on an at least 2 step binding process.<sup>22</sup> However, researchers are still working on the elucidation of the mechanism for the stereospecific molecular recognition.<sup>23</sup>

## Experimental

### Mixing devices

The basic design and constructions of the employed mixers has been described by Hinsmann<sup>14</sup> and Svasek,<sup>24</sup> recently. The mixer for this study differs in the dimensions of the channel, which in these experiments are a width of 300  $\mu\text{m}$  and 10  $\mu\text{m}$  height.

For the connection to the liquids, the chip was mounted into a special fabricated support made of PMMA (Fig. 3) that can be fixed onto the microscope stage. It connects 3 tubes, two for the inlet and one for the outlet, to the openings in the top  $\text{CaF}_2$  plate of the mixer chip. The chip is pressed onto the support by two PMMA clamps which can be screwed. O-rings from composition rubber are used as sealing around the openings.

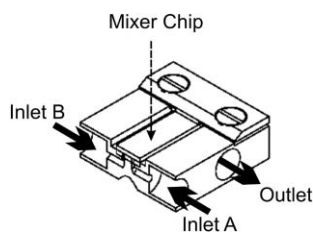


Fig. 3 Cross section through the mixer-chip support.

This support allows easy mounting and dismounting of the chip, avoiding leaking problems due to pressure. Furthermore, the support also fulfills the demand that the fully operational chip including connected tubings fits under the microscope's  $\times 32$  objective, which requires a working distance of 7 mm. The liquids were pumped into the chip by a syringe pump (Novodirect, KDS Model 200) equipped with Hamilton syringes, providing high stability in flow rates.

### Synchrotron light source and FTIR microspectroscopy

All presented measurements were performed at the infrared microscope (Thermo Nicolet Continuum and Nexus<sup>®</sup>) at the IR Synchrotron Beamline (IRIS) at BESSY.<sup>25</sup> The  $32\times$  objective has a numerical aperture of 0.65. This results in a naturally apertured focus of  $1.4\cdot 10^{-3}$  mm<sup>2</sup>, equivalent to a diameter of about 21  $\mu$ m. The aperture of  $16 \times 16$   $\mu$ m gave an optimum between small spot size for the high time resolution and enough intensity throughput that was not yet affected by the diffraction limit.

All the spectra were acquired as single beam spectra as an average of 128 scans at a mirror velocity of  $1.89$  cm s<sup>-1</sup>. The spectral resolution was set to  $4$  cm<sup>-1</sup>, as in routine measurements for biochemical systems. As the apodization function Happ-Genzel was provided in the instrument. These settings resulted in a scan time of 65 s per spectrum. The *xy*-stage was programmed to record spectra in certain steps along the channel. In that way the set of water spectra as background were acquired and later used as background spectra, according to the position. Then the two liquids containing the samples were pumped in and single beam spectra at the same positions as the background were recorded. The shift of the baseline was corrected after the calculation of the absorbance spectra using the OPUS software.

### Chemicals

The chemicals for the performance test reactions were NaOH, ClCH<sub>2</sub>COOCH<sub>3</sub>, and water, HPLC grade from Fluka. For the biochemical reaction vancomycin and the tripeptide solutions, 20 mM each, were prepared in 20 mM phosphate buffer using D<sub>2</sub>O at pD 7. The D<sub>2</sub>O 99.9 atom% D was purchased at Aldrich. The buffer and the test solutions were filtered through 2  $\mu$ m pore filters in order to avoid bringing in depositing solids, which would lead to a deterioration of the mixing performance.

### Computational fluid dynamics (CFD)

In order to visualize the fluid flow in the mixer device and to explore the mixing behaviour, fluid dynamic simulations were

performed. The whole mixer geometry was implemented into a CFD model using the finite volume solver FLUENT<sup>®</sup> V6.2 to make the equations of fluid flow on the mesh achieved from the GAMBIT<sup>®</sup> 2.1 preprocessor discretisation. Fluid properties were set to the physical and thermodynamic properties of water at 293 K. For the simulation of the mixing behaviour, two diffusing species "A" and "B" were defined containing the physical properties of the two substances that would be later used for the biochemical study of vancomycin. "A", resembling vancomycin, was introduced and added to one of the feed streams at a concentration of  $7.5$  g L<sup>-1</sup>. The substance in the stream of the other inlet, "B", was assumed to be the tripeptide Ac<sub>2</sub>KAA at a concentration of  $9.5$  g L<sup>-1</sup>. Under consideration of the thermodynamic properties of water at 293 K the binary diffusion coefficients of both substances were set to  $D = 5 \times 10^{-10}$  m<sup>2</sup> s<sup>-1</sup>.<sup>26</sup> The viscosities were assumed to approximately equal to those of water and therefore set to  $\eta = 0.001$  Pa s.<sup>27</sup> The flow speed for the calculation was  $0.5$   $\mu$ L min<sup>-1</sup> at each inlet.

### Results and discussion

The diffusion equation (1) allows an estimation of the mixing time. However, in order to consider the mixer geometry and the velocity distribution, and hence the residence time of the fluid streams, CFD simulations were carried out. Using the physico-chemical parameters of a biochemical system, the calculations were set up. The results for each substance introduced in one channel in aqueous solution show the spreading by diffusion over time along the channel. As a consequence of the laminar flow profile a gradient in linear flow velocity is observed (Fig. 4). Due to the rather broad channel (300  $\mu$ m) measurements at a spot size of  $16 \times 16$   $\mu$ m

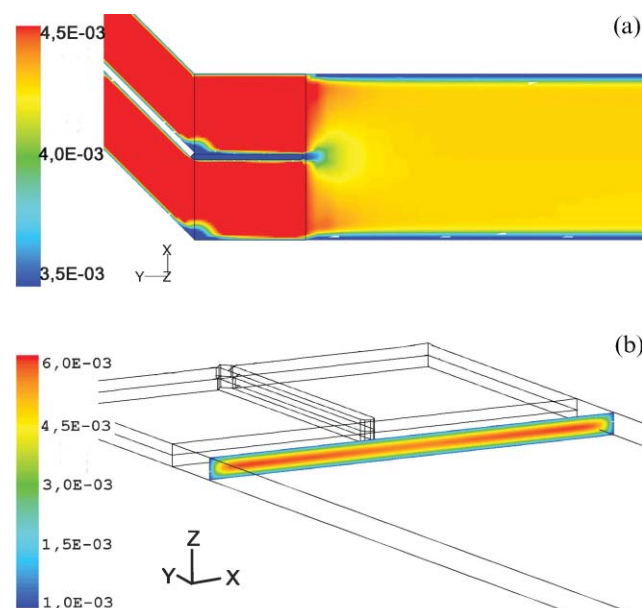
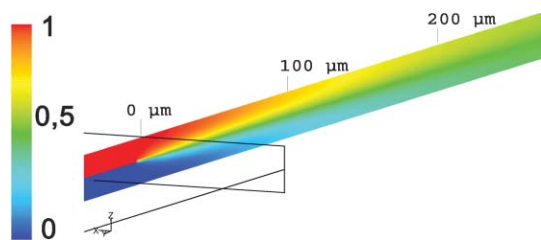


Fig. 4 Velocity profiles. (a) The CFD calculation of the velocity profile of a layer in the channel at  $3.75$   $\mu$ m from the middle showing the influence of the laminar flow profile in the *xy* plane. (b) The velocity profile of the *xz* plane at  $250$   $\mu$ m after the mixing point. The velocity is given in m s<sup>-1</sup>.



**Fig. 5** Mass fraction profile. The CFD calculation gives the mass fraction of one substance from 1 (red) to 0 (blue) at a total flow rate of  $1 \mu\text{L min}^{-1}$

in the middle of the channel are not affected by the resulting velocity dispersion at the sides. However, dispersion of the flow velocity resulting from the top and bottom borders cannot be avoided. As we are regarding the channel axis as the time axis of the reaction, only in the case of uniform flow speed across the probed sample can the reaction time be calculated by dividing the channel volumes by the flow rate. Because of the laminar flow profile this is not the case. Thus, this time scale only serves as an estimate. In Fig. 5 the mass fraction profile in the channel of one species is presented as layer in the  $y$ - $z$ -plane. It can be seen that after the silver-film cut off the mixing starts immediately. The complete mixed status equals 0.5 of the mass fraction of one substance spreading from one inlet over the channel, which is illustrated by the green colour. Table 1 gives the mixture quality, which is defined as the area of mass fraction between 0.4 and 0.6 with reference to the whole channel cross section. This means that right after the channel inlet the mixing starts, but it takes more than  $200 \mu\text{m}$  to complete the mixing process. This fact poses another blurring in the time scale. However, Fig. 5 proves that the chip design is capable of fast mixing, and although no absolute time at the channel can be given, the model of the time resolution still remains in a relative way.

To demonstrate the feasibility of the set-up under experimental conditions tests were performed, carrying out as model reaction an ester hydrolysis, which had already been studied by Hinsmann *et al.*<sup>28</sup> This kind of reaction, when not acid catalysed, is known as a very slow reaction, and therefore allows the checking of its performance for reaction monitoring purposes in the continuous flow mode after the mixing.

First pure water and then 300 mM solutions of methyl monochloroacetate and sodium hydroxide were pumped into the chip at a flow speed of  $0.5 \mu\text{L min}^{-1}$  at each channel inlet. Spectra were recorded every  $1000 \mu\text{m}$  with a  $20 \times 20 \mu\text{m}^2$  spot size. Fig. 6 shows that the characteristic ester bands ( $\nu\text{C}=\text{O}$  at  $1744 \text{ cm}^{-1}$ , at  $1330 \text{ cm}^{-1}$  the  $\text{CH}_3$  bending vibrational band

**Table 1** The mixture quality as a percentage of mass fraction values between 0.4 and 0.6

Distance from channel outlet	Mixture quality
0 $\mu\text{m}$	0.10%
50 $\mu\text{m}$	16.80%
100 $\mu\text{m}$	29.40%
150 $\mu\text{m}$	41.36%
200 $\mu\text{m}$	71.60%
250 $\mu\text{m}$	100.00%

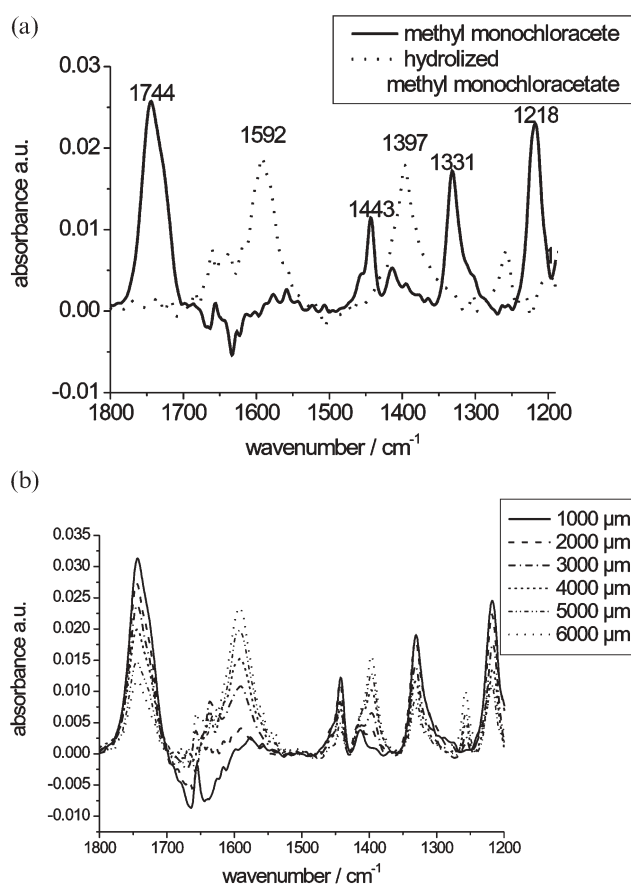


**Fig. 6** Hydrolysis of methyl monochloroacetate: (a) presenting the IR spectra of the ester and the hydrolysed products; (b) showing the reaction time resolved.

and the asymmetric stretching vibration of ester  $\text{C}-\text{O}-\text{C}$  at  $1218 \text{ cm}^{-1}$ ) are present at the beginning of the channel but decrease measuring along the channel towards the outlet, while an increase of the carboxylate band of the forming deprotonated acid (asymmetric and symmetric acetate stretching vibration at  $1591$  and  $1397 \text{ cm}^{-1}$ ) is recorded. According to the flow speed and the mixer dimensions spacing of the measurement spot at  $1000 \mu\text{m}$  corresponds to a relative time resolution of 90 ms between the spots. The mixing process is considered complete after  $250 \mu\text{m}$  (see Fig. 5). Any changes in spectra later in the channel must derive from changes in the structure of the molecules inside due to a reaction. Fig. 6 shows clearly that the hydrolysis of methyl monochloroacetate by NaOH and IR spectra can be measured at different states of the reaction, which corroborates the functioning of the experimental set-up.

In the way in which the ester hydrolysis was monitored the set-up was also capable of mixing organic substances of biochemical interest: The reaction of the antibiotic vancomycin and the tripeptide  $\text{Ac}_2\text{KAA}$  is known to be of 2nd order kinetics.<sup>22</sup> The two substrates bind with each other on several sites, therefore it could be estimated that the two-step mechanism could be followed in the IR. First, solutions of 20 mM vancomycin and 20 mM  $\text{Ac}_2\text{KAA}$  in  $\text{D}_2\text{O}$  phosphate buffer were injected into the channel and spectra of the pure solutions were recorded (Fig. 7(a)). A numerical comparison



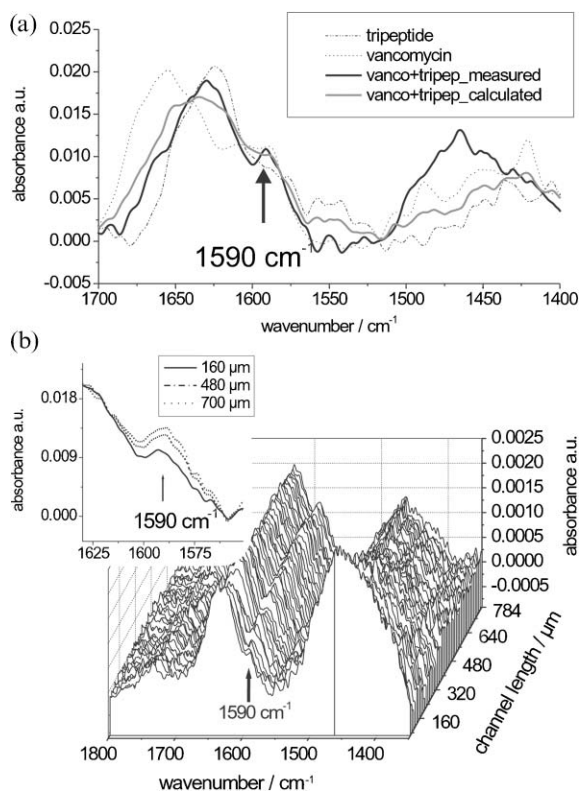


**Fig. 7** (a) The IR spectra of 20 mM vancomycin and 20 mM Ac2KAA, together with the mixture spectra. (b) The reaction of vancomycin and Ac2KAA time resolved. The distance of 16  $\mu\text{m}$  between the spectra equals 3 ms. While the larger spectrum shows the spectra with a spatial resolution of 16  $\mu\text{m}$  giving a well resolved increase of the band at 1590  $\text{cm}^{-1}$ , the small spectrum better visualizes this phenomenon using the average spectra of the first five, the middle five and the last five spectra.

of the calculated mixture from the absorbance spectra of the individual components and an offline prepared mixture gave spectral changes. Most changes were due to the reaction of the amide groups. At 1590  $\text{cm}^{-1}$  a new band was even appearing, which was tentatively assigned to the asymmetric carboxylate stretch vibration. The accompanying symmetric stretch vibration also changes, but is only a little recognisable in the lower region of the spectrum (around 1415  $\text{cm}^{-1}$ ).

Next a set of 50 spectra with 16  $\times$  16  $\mu\text{m}$  sample spot size with a flow of 0.5  $\mu\text{L}$  was acquired. These settings result in a relative time resolution of 3 ms. For the background the pure buffer was recorded at the same positions and from the two single beam spectra the absorbance spectra were calculated. Fig. 7(b) shows the time resolved reaction. The increase of the band at 1590  $\text{cm}^{-1}$  can be observed strongly in the first 5 spectra and a continuing increase is also observable at longer reaction times. Counting the time required for diffusion based mixing, as obtained from CFD simulations, it follows that at the very beginning the observed reaction and mixing overlap. However, as the spectral changes continue after the mixing process has been completed, it can be concluded that the reaction can be monitored using the developed system. Apart from the observed increase at 1590  $\text{cm}^{-1}$ , other spectral changes are most likely present in the recorded spectra, which

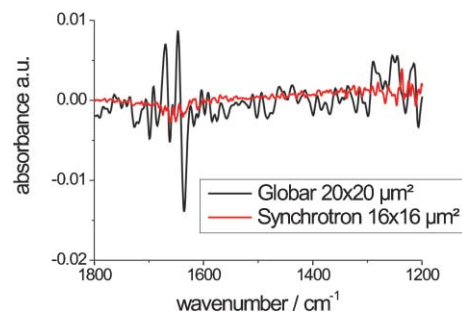


**Fig. 8** Comparison of the radiation sources: two 100% lines recorded from the water filled mixer channel.

might be attributed to the chemical reaction. However, in order to discuss these in a meaningful way a further improved S/N ratio needs to be obtained. The low optical throughput of our experiment resulting from the strong IR absorption of the sample and the aimed for high spatial resolution in the mixing channel drastically reduces the photon flux reaching the detector, even using an almost diffraction-limited synchrotron radiation source. It should be mentioned here that the experiment presented would not have been possible using a standard spectroscopic Globar source. Fig. 8 gives a comparison of the Synchrotron IR and the Globar. Still, noise in the IR flux typical for IR synchrotron sources and originated by electron beam motion in the storage ring deteriorates the S/N ratio. However, further future improvements of the S/N ratio of the mixer-IR synchrotron microscopy experiment are planned, in order to provide a highly useful tool to study the kinetics of (bio)chemical reactions.

## Conclusion and outlook

We have set up a tool at an IR Synchrotron microscope that enables reaction monitoring with a total sample consumption of 10–50  $\mu\text{L}$  (depending on experimental conditions). The vancomycin system presents a good example of a drug-protein reaction, where use of this tool can be made. Also, further biochemical systems such as conformational studies of proteins or in changing conditions could be carried out. The best achievable time resolution with the current set up would amount to 0.5 ms, limited by the measurement spot size and the applicable flow rates. Due to the long channel and the possibility of varying the flow speed we have access to a high dynamic time range, starting from milliseconds up to the minute region by combination with stopped flow measurements. An absolute time-scale cannot be assigned, because the mixing itself blurs the accuracy in reaction time. In addition, the laminar flow-profile present in such small devices has always to be considered. However, a rather good estimation can be derived from the simulations and the time resolution can be easily read out in a relative way.

So far, the S/N ratio achieved with this set-up limits the interpretation of spectral changes smaller than  $4 \times 10^{-4}$  rms of absorption spectra (considering a baseline noise at the region of 1600–1300  $\text{cm}^{-1}$  of  $1.5 \times 10^{-4}$ ), as they are typical in biochemical reactions. However, within this study the S/N

ratio could already be improved and further work on this issue is planned from the IRIS beamline at BESSY.

## Acknowledgements

Financial support by the Austrian Science Fund within the project FWF 15531 is gratefully acknowledged. This work was supported further by the European Community—Research Infrastructure Action under the FP6 “Structuring the European Research Area” Programme (through the Integrated Infrastructure Initiative “Integrating Activity on Synchrotron and Free Electron Laser Science”—Contract R II 3-CT-2004-506008). B. L. and M. V. acknowledge support received from TU Vienna within the “Innovative Project 2003”.

## References

- 1 H. Fabian and W. Mänteles, in *Handbook of Vibrational Spectroscopy*, eds. J. M. Chalmers and P. R. Griffiths, John Wiley and Sons, Ltd., Chichester, 2002, pp. 3399–3425.
- 2 J. L. R. Arrondo and F. M. Goñi, *Prog. Biophys. Mol. Biol.*, 1999, **72**, 367.
- 3 A. Troullier, D. Reinstädler, Y. Dupont, D. Naumann and V. Forge, *Nat. Struct. Biol.*, 2000, **7**, 78.
- 4 R. Vogel and F. Siebert, *Curr. Opin. Chem. Biol.*, 2000, **4**, 518.
- 5 W. Mänteles, *Trends Biochem. Sci.*, 1993, **18**, 197–202.
- 6 A. Barth and C. Zscherp, *FEBS Lett.*, 2000, **477**, 151.
- 7 K. Gerwert, *Curr. Opin. Chem. Biol.*, 1993, **3**, 769.
- 8 R. Rammelsberg, B. Heßling, H. Chornigiewski and K. Gerwert, *Appl. Spectrosc.*, 1997, **51**, 558.
- 9 F. v. Germar, A. Barth and W. Mänteles, *Biophys. J.*, 2000, **78**, 1531.
- 10 C. Zscherp and J. Heberle, *J. Phys. Chem.*, 1997, **101**, 10542.
- 11 H. Georg, C. W. Wharton and F. Siebert, *Laser Chem.*, 1999, **19**, 233.
- 12 J. Backmann, H. Fabian and D. Naumann, *FEBS Lett.*, 1995, **364**, 175.
- 13 H. Heberhold and R. Winter, *Biochemistry*, 2002, **41**, 2396.
- 14 P. Hinsmann, J. Frank, P. Svasek, M. Harasek and B. Lendl, *Lab Chip*, 2001, **1**, 16.
- 15 R. Masuch and D. A. Moss, *Appl. Spectrosc.*, 2003, **57**, 1407.
- 16 E. Kauffmann, N. C. Darnton, R. H. Austin, C. Batt and K. Gerwert, *Proc. Natl. Acad. Sci. U. S. A.*, 2001, **98**, 6646.
- 17 T. M. Floyd, M. A. Schmidt and K. F. Jensen, *Ind. Eng. Chem. Res.*, 2005, **44**, 2351.
- 18 L. Carr, *Vib. Spectrosc.*, 1999, **19**, 53.
- 19 J. Kneipp, L. M. Miller, M. Joncic, M. Kittel, P. Lasch, M. Beekes and D. Naumann, *Biochim. Biophys. Acta*, 2003, **1639**, 152.
- 20 P. Dumas and L. Miller, *Vib. Spectrosc.*, 2003, **32**, 3.
- 21 H. R. Perkins, *Biochem. J.*, 1969, **111**, 195.
- 22 P. H. Popieniek and R. F. Pratt, *J. Am. Chem. Soc.*, 1991, **113**, 2264.
- 23 S. Jusuf and P. H. Axelsen, *Biochemistry*, 2004, **43**, 15446.
- 24 P. Svasek, E. Svasek, B. Lendl and M. Vellekoop, *Sens. Actuators, A*, 2004, **115**, 591.
- 25 U. Schade, A. Röseler, E. H. Korte, F. Bartl, K. P. Hofmann, T. Noll and W. B. Peatman, *Rev. Sci. Instrum.*, 2002, **73**, 1568.
- 26 K. Bleicher, M. Lin, M. J. Shapiro and J. R. Wareing, *J. Org. Chem.*, 1998, **63**, 8486.
- 27 <http://webbook.nist.gov>.
- 28 P. Hinsmann, M. Haberkorn, J. Frank, P. Svasek, M. Harasek and B. Lendl, *Appl. Spectrosc.*, 2001, **55**, 241.

## ***Publication II***

S. Kulka, N. Kaun, J. R. Baena, J. Frank, P. Svasek, D. Moss, M.J. Vellekoop and B. Lendl

*„Mid-IR synchrotron radiation for molecular specific detection in micro-chip based analysis systems”*

Analytical and Bioanalytical Chemistry (2004), 378(7), 1735-1740

S. Kulka · N. Kaun · J. R. Baena · J. Frank · P. Svasek  
D. Moss · M. J. Vellekoop · B. Lendl

## Mid-IR synchrotron radiation for molecular specific detection in microchip-based analysis systems

Received: 2 October 2003 / Revised: 30 January 2004 / Accepted: 2 February 2004 / Published online: 2 March 2004  
© Springer-Verlag 2004

**Abstract** Microstructures constructed from SU-8 polymer and produced on CaF<sub>2</sub> base plates have been developed for microchip-based analysis systems used to perform FTIR spectroscopic detection using mid-IR synchrotron radiation. The high brilliance of the synchrotron source enables measurements at spot sizes at the diffraction limit of mid-IR radiation. This corresponds to a spatial resolution of a few micrometers (5–20 μm). These small measurement spots are useful for lab-on-a-chip devices, since their sizes are comparable to those of the structures usually used in these devices. Two different types of microchips are introduced here. The first chip was designed for time-resolved FTIR investigations of chemical reactions in solution. The second chip was designed for chip-based electrophoresis with IR detection on-chip. The results obtained prove the operational functionality of these chips, and indicate the potential of these new devices for further applications in (bio)analytical chemistry.

**Keywords** Synchrotron radiation · Time resolved IR spectroscopy · Capillary electrophoresis · Lab-on-a-chip · SU-8

### Introduction

Miniaturization of chemical analysis systems remains a major driving force in the development of advanced instrumentation for analytical chemistry. Frequently, the ultimate goal of miniaturization is seen as the development of self-contained sensor-like analysis systems known as “lab-on-a-chip” devices or micro total analysis systems. However, to obtain significant advantages from chip-based liquid handling, complete miniaturization of the whole analysis system is not usually required.

Especially when dealing with instrumentally complex detection systems like mass spectrometry [1], nuclear magnetic resonance [2] or vibrational spectroscopic techniques (infrared and Raman) [3, 4], microchips may be viewed rather as valuable add-ons to these powerful detectors rather than as stand-alone micro-systems. In many cases, an appropriate microchip for fluid handling may extend the problem-solving capabilities of these detectors due to the added degree of experimental flexibility. An example of this is the use of microchips for the study of (bio)chemical reactions with high time resolution and minimum sample consumption via Fourier transform mid-infrared spectrometry [4, 5, 6]. In this case, miniaturization and integration of micro-mixers in IR transmission cells enables fast diffusive mixing by the generation of short diffusion distances inside the mixer. These devices allow complete diffusive mixing of two solutions in less than 100 ms and the simultaneous recording of the reaction-induced spectral changes on-chip. From these changes, details about the reaction under study may be deduced, and intermediates characterized. In a similar way, fast mixers have been used to study chemical reactions via mass spectrometry, although in this case with substantially lower time resolution since only off-chip measurements are possible [7].

Within the group of optical techniques based on absorption measurements, mid-IR detection holds a special position; in contrast to absorption measurements at shorter wavelength (UV-Vis or NIR spectrometry) no loss in sensitivity is incurred upon miniaturization. This is because

---

S. Kulka · N. Kaun · J. R. Baena · J. Frank · B. Lendl (✉)  
Institute of Chemical Technologies and Analytics,  
Vienna University of Technology,  
Getreidemarkt 164-AC, 1060 Vienna, Austria  
e-mail: blendl@mail.zserv.tuwien.ac.at

P. Svasek  
Ludwig Boltzmann Institute of Biomedical Microtechnology,  
Vienna, Austria

D. Moss  
Institute for Synchrotron Radiation,  
Forschungszentrum Karlsruhe,  
Postfach 3640, 76021 Karlsruhe, Germany

M. J. Vellekoop  
Institute of Industrial Electronics and Material Science,  
Vienna University of Technology,  
Gusshausstrasse 27–19, 1040 Vienna, Austria

mid-IR detection is already confined to small path-lengths in normal-sized systems due to strong solvent absorption. This especially applies for water, as for measurements in the information-rich fingerprint region the optical path must be kept in the region of  $10\ \mu\text{m}$ . Even shorter paths ( $<8\ \mu\text{m}$ ) are required if the amide I band from proteins is to be measured too [8, 9], because this band heavily overlaps with the bending vibration of the water molecule ( $1640\ \text{cm}^{-1}$ ). An alternative solution would be the use of heavy water, where the solvent absorption bands are shifted away from the amide I band, towards lower frequencies [10]. However, even in this case optical paths must still be kept within the low- $\mu\text{m}$  region.

Therefore, a reduction in the detection volume for on-chip mid-IR detection can only be realized by reducing the beam diameter. The use of an economical beam-condenser already allows a parallel beam taken from an FTIR spectrometer to be focused to a spot diameter of about  $1\ \text{mm}$ , resulting in a probed volume of  $\sim 8\ \text{nl}$  when considering an optical path of  $10\ \mu\text{m}$ . Such a detection volume is rather big for chip-based analysis systems, but appropriate for the time-resolved analysis of a chemical reaction in solution using a microchip device operated in the stopped-flow mode [4, 5]. Such a detection volume has also proven to be adequate for successful on-line FTIR detection in capillary zone electrophoresis [11] and micellar electrokinetic chromatography [12]. For these applications, a dedicated IR transparent chip for detection has been connected to conventional capillaries (i.d.  $75\ \mu\text{m}$ ). However on-chip injection and detection using a chip for infrared detection has not yet been demonstrated. If the beam-condenser is replaced by an IR microscope attached to an FTIR spectrometer, the spot size may be reduced to  $\sim 100\ \mu\text{m}$  without facing degradation in the signal-to-noise ratio due to reduced optical throughput. In this case, again assuming an optical path of  $10\ \mu\text{m}$ , the probed volume can be reduced to  $80\ \text{pl}$ . Such a configuration can already be used to probe different positions on a chip device [6]. This opens up the possibility of studying chemical reactions in solution with better time resolution than stopped flow technique, using continuous flow experiments instead. In such experiments the time resolution is defined by the distance between the mixing point and the sample spot, as well as by the flow rate applied. A further reduction in spot size can be achieved (while still maintaining a high signal-to-noise ratio) if the light source of the FTIR spectrometer (global) is replaced by a synchrotron radiation source [13, 14]. Although the number of photons emitted per second in the mid-IR spectral region by the global is comparable to the number emitted by the synchrotron source, the synchrotron has a distinct advantage over the global source in that it naturally produces a highly collimated beam of small diameter. Therefore, the brilliance of a synchrotron source, in terms of photons emitted per second and per solid angle, is significantly higher than that of a global – although the throughput advantage of the synchrotron source over a global obviously only applies if measurements are to be performed on a small spot size [14]. Using an FTIR microscope and synchrotron radiation, high quality measure-

ments at spot sizes close to the diffraction limit of a given wavelength are possible. For mid-IR detection in a  $10\ \mu\text{m}$ -thick micro-channel with a spot size of  $10\ \mu\text{m}$ , we can achieve a probed volume of only  $0.8\ \text{pl}$ . The realization of this very small volume for mid-IR detection is highly-applicable to chip-based separation and detection systems, as well as to time-resolved experiments with high time resolution and low sample consumption.

It was the aim of this study to produce microchips containing small channels and test them at the new IR beam-line of the synchrotron radiation source ANKA in Karlsruhe (Forschungszentrum Karlsruhe, Germany). For this purpose, two different chip designs, one designed for time-resolved FTIR spectroscopy and the other for on-chip capillary electrophoresis, have been produced. In this paper, the first experimental results obtained from them are reported.

## Experimental

### Microchip fabrication and packaging

Two different microchip geometries have been produced on 4 inch-wide  $\times$  1 mm-thick  $\text{CaF}_2$  wafers. Because standard materials for microchip fabrication, such as silicon, glass or polymer materials, are not transparent in the mid-IR spectral region,  $\text{CaF}_2$  must be used instead. Due to its insolubility in water,  $\text{CaF}_2$  is an appropriate material for producing IR chips [4, 5, 11, 12].

By applying SU-8 technology, structures have been realized on the wafers, and the wafers have been bonded. The geometries of the structures produced are shown in Fig. 1. Design A was intended for time-resolved FTIR spectroscopy in the continuous flow mode, and design B was made for on-chip electrophoresis. For the latter application it was considered important to produce channels made out of one type of material. Therefore, prior to producing the SU-8 structures on the  $\text{CaF}_2$  wafers, they were coated with a  $0.5\ \mu\text{m}$  thick SU-8 layer, and exposed to oxygen plasma for two minutes to make them hydrophilic so that another layer of SU-8 could be deposited (Fig. 2a). Due to the thin nature of the SU-8 layer, the throughput for mid-IR measurements was not impaired despite the fact that the SU-8 characteristic bands were clearly visible in the recorded single beam spectra.

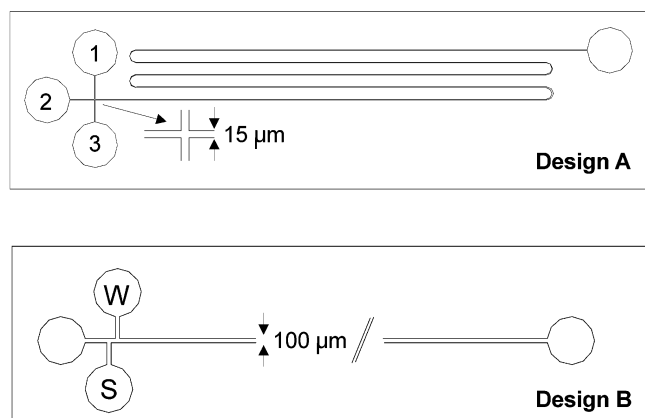
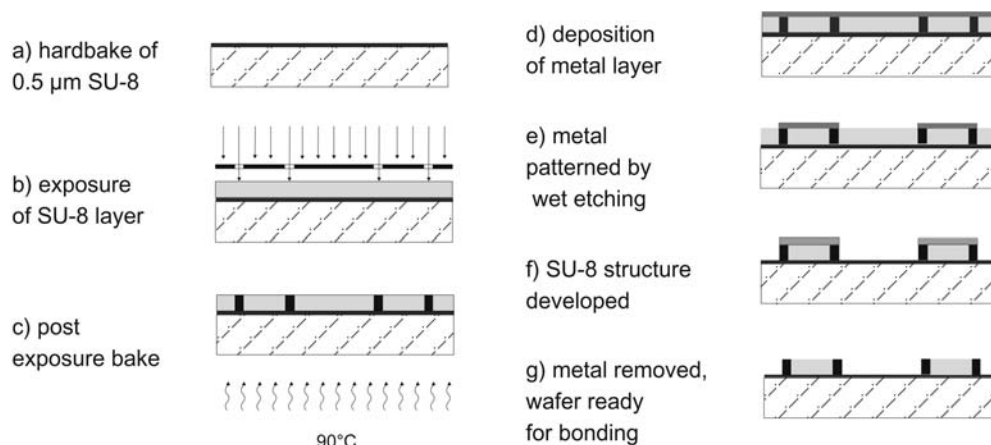


**Fig. 1** Schematic drawing of the structures made on  $\text{CaF}_2$  wafers. Design A was made for time-resolved FTIR spectroscopy of chemical reactions in solution. The reagents are introduced at the inlets 1, 2 and 3. Design B was made for electrophoretic separations with on-chip IR detection. The device is loaded by introducing the sample via hydrodynamic pumping from port S to waste (W)

**Fig. 2** Schematic of the production of micro-devices on  $\text{CaF}_2$  wafers using SU-8 structuring technology. For details see text



The flow channel was formed by two lines of epoxy-based photoresist SU-8 (Microchem Corp. Newton, MA), each of them 60  $\mu\text{m}$  wide. The distance between two lines, and therefore the width of the channel formed, was 15 and 100  $\mu\text{m}$  for designs A and B respectively. The height of the SU-8 lines were about 10  $\mu\text{m}$ , equivalent to the desired optical path. One of the  $\text{CaF}_2$  wafers already carrying the 0.5  $\mu\text{m}$  thick SU-8 layer was spin-coated with SU-8 and softbaked (90  $^\circ\text{C}$ , 30 min). After UV-exposure for 30 s using a SUSS MJB3 mask aligner (Suss Microtech, Munich, Germany) and an appropriate photomask, the resist was post-exposure-baked at 90  $^\circ\text{C}$  for 10 min (see Fig. 2b and c). A metal layer (1  $\mu\text{m}$  Ag) was deposited by evaporation on this wafer (Fig. 2d). This layer was patterned by wet etching (Fig. 2e). The areas where unexposed SU-8 was necessary for bonding were surrounded by narrow lines of exposed (hard) SU-8 and covered by metal. After development of the SU-8 with propylene glycol monomethyl ether acetate (PGMEA), the metal layer was removed (Fig. 2f and g). The unexposed and therefore not crosslinked areas of SU-8 were dissolved during the development process. The reason for covering some areas with the metal is to prevent them from getting exposed and to keep them soft, and also to make sure that they are not removed during the development process. The two wafers, with one carrying the structure, were aligned in an EVG AL6 mask aligner (EV group, Schärding, Austria) and the wafer stack was inserted into an EVG 501 wafer bonder (EV group). Bonding was accomplished by applying a contact force of 1000 N while the temperature was increased up to 180  $^\circ\text{C}$  with a ramp of 3  $^\circ\text{C}/\text{min}$ , and left for 1 h. Finally the temperature was decreased to room temperature with a ramp of 2  $^\circ\text{C}/\text{min}$  and the contact force was removed. This procedure is necessary to induce a complete crosslinking of SU-8 and to develop full mechanical strength and chemical resistance. The soft parts of SU-8 were used to fill small gaps caused by non-uniform layer thickness, meaning that less contact force is necessary when the gaps are filled and so the structures are not deformed and their correct height and shape is maintained during the bonding process. The resulting microchips were placed in dedicated supports made out of PMMA, to facilitate the supply of the chips with reagents and the electrodes as required for the experiments. The connections to the support were all standard flow injection threaded fittings for simple liquid handling. The openings of the chips were sealed to the support with commercially-available O-rings (Zorzi, Vienna, Austria) to ensure tightness. This arrangement made it possible to exchange the microchips easily. The supports carrying the microchips were screwed onto a metal plate that fitted the xy-stage of the IR-microscope attached to the synchrotron source.

#### FT-IR spectrometer and synchrotron source

The IR light used in this study was generated by a synchrotron light source (ANKA, Karlsruhe, Germany), a particle accelerator providing a high-brilliance beam of photons covering a broad spectral

range. The synchrotron radiation is emitted when electrons moving at relativistic speed interact with a magnetic field due to quantum mechanical effects. The radiation covers a spectral range from the hard X-ray to the terahertz range. The infrared beamline is set up where one of the magnets interacts with the electrons and the IR light is guided through a diamond window and a dedicated system of filters and mirrors to the IR spectrometer. A conventional Bruker 66v FT-IR spectrometer (Bruker Optik, Germany) was used throughout all of the experiments. The IR beam was coupled to an IR microscope (Bruker IRscope II) using two parabolic mirrors. The scanner of the spectrometer was operated at a HeNe laser modulation frequency of 100 kHz. Fifty spectra were coadded for each spectrum, with a spectral resolution of 8  $\text{cm}^{-1}$ .

Reference spectra of myoglobin were recorded using a diamond ATR (attenuated total reflection) unit from SensIR (Danbury, CT) attached to a Bruker IR-cube spectrometer.

#### IR-chip manifolds

To supply the IR chip for the time-resolved experiments (Fig. 1, design A) with reagent, a precise low flow pump (Novodirect, Kehl, Germany) equipped with three 0.5 ml syringes was used. The capillary electrophoresis system was built in-house, and consisted of a high-voltage power supply (Spellman, New York, USA) and two platinum electrodes inserted into standard FIA fittings. The electrodes were attached to the chip by screwing the corresponding fittings into the support such that the electrodes touched the running buffer.

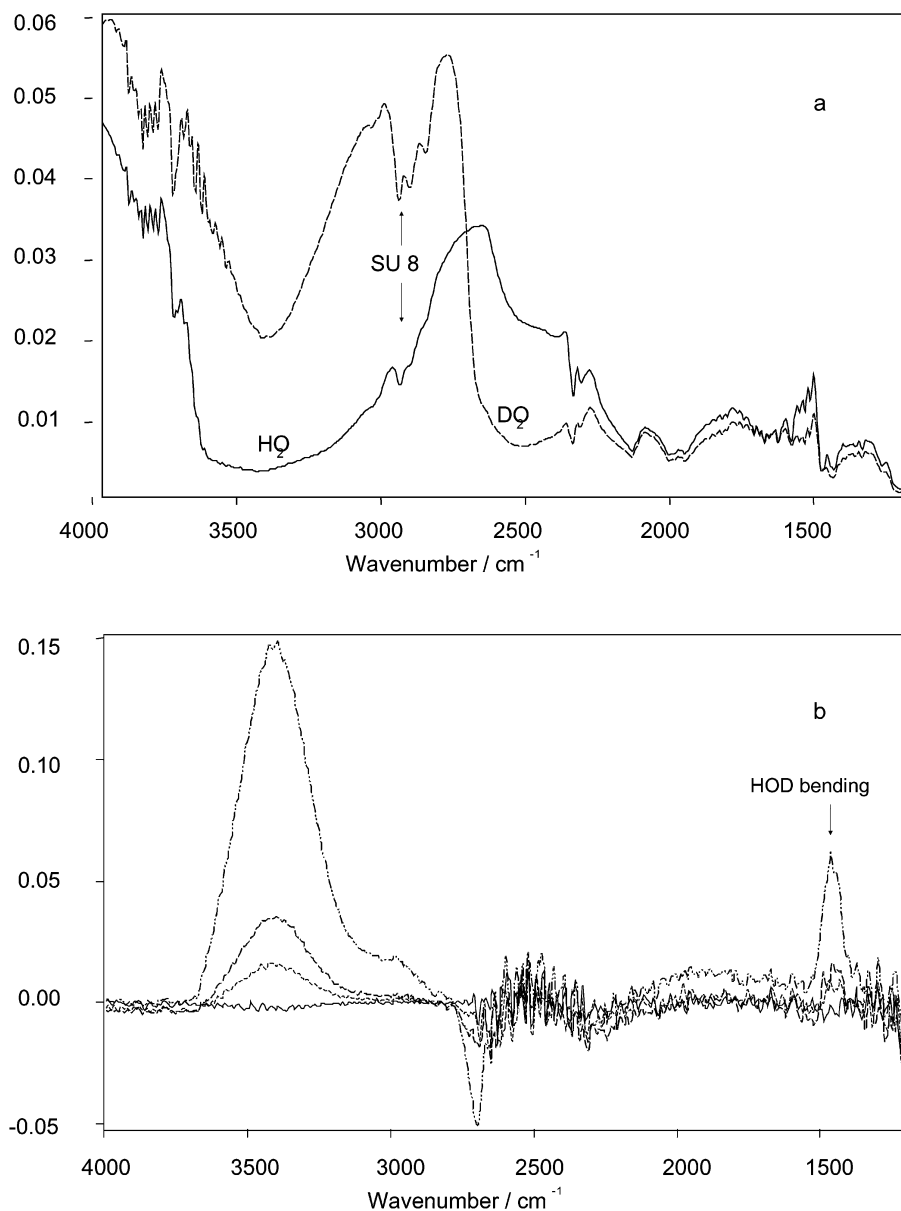
#### Chemicals

HPLC-grade water, heavy water, myoglobin, and borax, all of analytical grade (Fluka, Buchs, Switzerland) were used as received. A 20 mM borax buffer in  $\text{D}_2\text{O}$  (pD=9.2), and a 2 g/L myoglobin standard in this buffer were prepared. Prior to experiments, the solutions were filtered through a 0.2  $\mu\text{m}$  filter to prevent clogging of the microchip channels.

## Results and discussion

At the start of the measurement campaign at ANKA, the microchip designed for time-resolved FTIR spectroscopic investigation was used. The dimensions of the experimental set-up permitted the use of the 15 $\times$  objective at the IR-microscope. With this arrangement, a focus spot of 20  $\mu\text{m}$  can be achieved. Spectra of normal and heavy water with clearly-distinct positions of the corresponding absorption

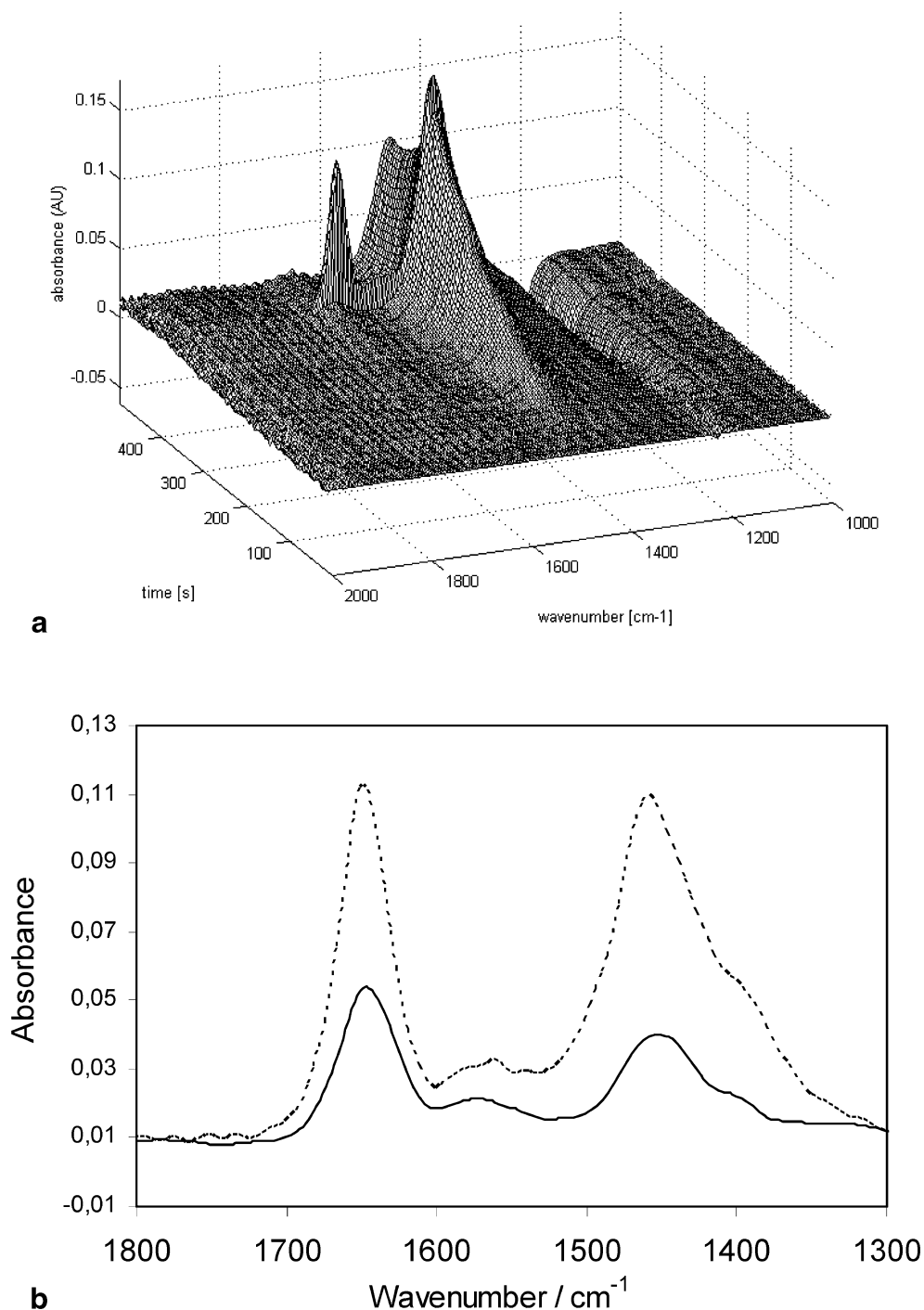
**Fig. 3** **a** Single beam spectra of normal and heavy water as measured in a 15  $\mu\text{m}$ -broad and 10  $\mu\text{m}$ -high channel (sample volume 3 pl). **b** Spectra recorded in the stopped flow mode when feeding the microchip with normal and heavy water. The background was taken at 72 ms reaction time. The spectra display the spectral changes recorded over an 8 min reaction time. The band at 1450  $\text{cm}^{-1}$  indicates the formation of the HOD molecule



bands could be obtained from a volume of 3 pl, as defined by the 15  $\mu\text{m}$ -wide and 10  $\mu\text{m}$ -high fluid channel (Fig. 3a). In an attempt to follow a chemical reaction in these dimensions, heavy water was fed into the microchip via inlets 1 and 3 (see Fig. 1), whereas normal water was introduced via the central channel (inlet 2). The flow rate for each streamline was set to 10  $\mu\text{L}/\text{h}$ . FTIR measurements probing a total volume of approximately 3 pl at a distance of 4 mm after the mixing point were carried out. Taking into account the cross-section of the channel and the flow rates applied, the measured volume corresponded to a reaction time of 0.072 s. Therefore, due to the short diffusion distance between the laminated streamlines (5  $\mu\text{m}$ ) inside the 15  $\mu\text{m}$ -broad channel, and the diffusion coefficients of normal and heavy water ( $\text{H}_2\text{O}$ :  $2.3 \times 10^5 \text{ cm}^2 \text{ s}^{-1}$ ,  $\text{D}_2\text{O}$ :  $1.9 \times 10^5 \text{ cm}^2 \text{ s}^{-1}$  measured at 25  $^\circ\text{C}$  [15]), it may be concluded that complete mixing of the three solutions had

occurred prior reaching the place of measurement. The flow was stopped and subsequent spectra were recorded over the next 8 min and ratioed against the first one. These spectra are given in Fig. 3 and show the formation of HOD molecules (characteristic bending formation at 1450  $\text{cm}^{-1}$ ) from heavy and normal water. In addition to this characteristic spectral feature, an increase in the O–H stretch region (3450  $\text{cm}^{-1}$ ) was recorded too. A full interpretation of the recorded spectral changes must be considered premature at this point, because the spectra of water, despite being a simple molecule, is very complex [16]. This experiment, however, clearly proves the ability of the microchip to follow chemical reactions in aqueous solution within picoliter volumes by FTIR spectroscopy. During measurement, the position of the actual focus spot produced by the optical set-up shifted slightly due to instabilities in the synchrotron source. As a consequence, the full capabilities of

**Fig. 4** **a** 3-D plot of the recording obtained upon loading the CE-IR-chip (design B) with 2g/l myoglobin followed by electrophoretic movement of the analyte through the detection window ( $\sim 450$  s). **b** Comparison of FTIR spectra of the analyte (dashed line), as recorded during the experiment shown in Fig. 4a, with reference spectra (solid line)



the microchip intended for the investigation of chemical reactions could not be fully explored.

In the second study, the microchip designed for electrophoresis and on-chip IR detection was investigated. So far, the use of channels made of SU-8 for electrophoretic separations has not been reported. Before use, the whole chip was flushed with the running buffer. This was accomplished by introducing buffer at the inlets of the separation channel and the sample port by means of a three-channel syringe pump. For sample (myoglobin) loading, the two

exits of the separation channel were blocked and the sample was introduced using the syringe pump. In this way, the sample double tee (Fig. 1) was filled. After loading of the sample, a potential of 3 kV was applied, corresponding to a potential gradient of 680 V/cm. Figure 4a shows a characteristic electropherogram obtained with the passage of the sample through the detection window of the chip. The FTIR spectra corresponding to the peak maximum was extracted from the dataset and is compared with the reference spectra taken of the analyte using an ATR unit. A



characteristic peak at  $1648\text{ cm}^{-1}$ , the C=O stretch vibration of the protein, can be clearly seen in both spectra. In protein analysis this peak is usually called the amide I band, and is the most important peak as it contains direct information about the secondary structure of the protein [8, 17]. Band positions around  $1650\text{ cm}^{-1}$  indicate helical structure, while band positions around  $1630\text{ cm}^{-1}$  are indicative of beta-sheet structure. Band positions in-between show a partial random coil character of the protein. The so-called amide II (out-of-phase N-H bend combined with C-N stretching) can normally be found at  $1550\text{ cm}^{-1}$ , but as  $\text{D}_2\text{O}$  was used in this study a proton exchange can be observed and the amide II' is shifted downwards to  $1450\text{ cm}^{-1}$ . This peak is less important in protein analysis, as it is not influenced directly by the secondary structure. It is mainly used to calculate proton exchange ratios in order to determine the accessibility of the protons to  $\text{D}_2\text{O}$ . The band position of the amide I as recorded on-chip confirms the predominantly helical structure of myoglobin, which is also consistent with X-ray crystallography data. In the spectrum obtained from the electrophoretic run, the amide II band has HDO heavily superimposed on it, which is due to traces of  $\text{H}_2\text{O}$  that have entered the system at the electrolyte reservoir and probably also during sample injection. Even after the analyte has passed the area, the HDO band is still apparent due to the continued presence of this impurity.

## Conclusions

The study detailed in this paper describes, (to the authors' knowledge) the first successful use of micro-chips for reaction and separation monitoring using an IR synchrotron light source. The developed technology for IR-chip fabrication based on the combination of  $\text{CaF}_2$  and SU-8 structuring technology has proven to be a versatile and effective means to produce devices for use with an IR synchrotron radiation source. The results obtained show that a chemical reaction (HD exchange in water) can be monitored in a volume of only 3 pl. Furthermore, using the chip designed for capillary electrophoresis, a protein was successfully injected and recorded as it passed the detector window. From the FTIR spectra recorded, the identity of the analyte could be confirmed by comparison with reference spectra. In addition, the exact position of the amide I band, as recorded on-chip, could be used to determine the secondary structure of the protein.

It is expected that the chip designs developed for separation and reaction monitoring using IR synchrotron detection will be useful for a great many applications, once the stability of the IR focus spot produced by the synchrotron source is improved. In the field of chemical reaction monitoring in particular, including protein folding and bio-ligand interaction studies, the low sample amount required for prolonged experiments is seen as a significant advantage over conventional larger systems. In the case of on-chip electrophoresis, the attractiveness of mid-IR detection is seen in its molecular specific information content and especially in its capability to discern the folding state, as well as the secondary structures of proteins in solution.

**Acknowledgements** Acknowledgement is given to the Austrian Science Fund for support within the project FWF 15531. Furthermore, financial support from the ANKA for carrying out the measurements in Karlsruhe is gratefully acknowledged. J.R.B. also acknowledges support from the Spanish Ministry of Culture, Sport and Science.

## References

1. Limbach P, Meng Z (2002) *Analyst* 127:693–700
2. Jayawickrama DA, Sweedler JV (2003) *J Chromatogr A* 1000(1–2):819–40
3. He L, Natan MJ, Keating CD (2000) *Anal Chem* 72(21):5348–55
4. Hinsmann P, Haberkorn M, Frank J, Svasek P, Harasek M, Lendl B (2001) *Appl Spectrosc* 55:241–251
5. Hinsmann P, Frank J, Svasek P, Harasek M, Lendl B (2001) *Lab Chip* 1:16–21
6. Kauffmann E, Darnton N, Austin R, Batt C, Gerwert K (2001) *P Natl Acad Sci USA* 98:6646–6649
7. Mitchell MC, Spikmans V, Manz A, de Mello AJ (2001) *J Chem Soc Perk T* 1:514–518
8. Fabian H, Mäntele W (2002) In: Chalmers JM, Griffiths P (eds) *Handbook of vibrational spectroscopy*. Wiley, Chichester, UK
9. Koenig JK, Tabb DL (1980) In: Durig JR (ed) *Analytical applications of FT-IR to molecular and biological systems*. D. Reidel, Boston, MA, pp 241–255
10. Arrondo JL, Goni FM (1999) *Prog Biophys Mol Bio* 72(4):367–405
11. Kölhed M, Hinsmann P, Svasek P, Frank J, Karlberg B, Lendl B (2002) *Anal Chem* 74:3843–3848
12. Kölhed M, Hinsmann P, Karlberg B, Lendl B (2003) *Electrophoresis* 24:687–692
13. Mathis YL, Gasharova B, Moss D (2003) *J Biol Phys* 29:313–318
14. Carr GL (1999) *Vib Spectrosc* 19(1):53–60
15. Mills R (1973) *J Phys Chem* 77:685–688
16. Brubach J-B, Mermet A, Filabozzi A, Gerschel A, Lairez D, Krafft MP, Roy P (2001) *J Phys Chem B* 105:430–435
17. Barth A, Zscherp C (2002) *Q Rev Biophys* 35:369–430

## ***Publication III***

N. Kaun, S. Kulka, J.R. Baena, U. Schade, M. Vellekoop, E. De Lorenzi,  
B. Lendl

*„Synchrotron radiation for on-chip detection at the diffraction limit“*  
Proceedings of MicroTAS-2004, Malmö, Sweden, Sept. 2004, proc. vol.  
2, p. 530-532

# SYNCHROTRON RADIATION FOR ON-CHIP MID-IR DETECTION AT THE DIFFRACTION LIMIT

Nina Kaun<sup>1</sup>, Stephan Kulka<sup>1</sup>, Josefa R. Baena<sup>2</sup>, Ulrich Schade<sup>3</sup>, Michiel Vellekoop<sup>4</sup>, Ersilia De Lorenzi<sup>5</sup> and Bernhard Lendl<sup>1</sup>

<sup>1</sup>*Inst. of Chemical Technologies and Analytics, Vienna University of Technology,  
Getreidemarkt 9/164, A-1060 Vienna, Austria*

<sup>2</sup>*Dep. of Anal. Chem., University of Córdoba, Campus de Rabanales, E-14071 Córdoba, Spain*

<sup>3</sup>*Bessy II, Albert-Einstein-Str. 15, D-12489 Berlin, Germany*

<sup>4</sup>*Inst. of Sensor and Actuator Systems, Vienna University of Technology,  
Gusshausstrasse 27-29, A-1040 Vienna, Austria*

<sup>5</sup>*Laboratory of Pharmaceutical Analysis, University of Pavia,  
Via Taramelli 12, I-27100 Pavia, Italy*

## Abstract

Microchips for rapid mixing of two aqueous streams have been produced using CaF<sub>2</sub> wafers and SU-8 microstructuring technology and tested at the IR beamline of Bessy II in Berlin, Germany. Advantage of the synchrotron radiation over thermal globar sources for measuring at sample spots close to the diffraction limit of the employed mid-IR radiation have been documented. The capability of the experimental set-up to initiate and monitor chemical reactions label-free in pL volumina was verified. Simple chemical reactions such as titration of acetic acid and conformational change of the protein  $\beta$ 2-microglobulin have been recorded.

**Keywords:** Mid-IR spectroscopy, synchrotron radiation, micromixing, protein folding

## 1. Introduction

Dedicated chips for (bio)chemical reaction monitoring using mid-infrared synchrotron radiation are introduced. These chips made of calcium fluoride and SU-8 polymer are designed to take advantage of the highly collimated beam of synchrotron radiation, which when coupled to an IR microscope allows high quality measurements even at spot sizes close to the diffraction limit of the light used. In case of mid-IR radiation the smallest sample spots that can be realized are in the order of 5-10 micrometer. In this context it is important to mention that the throughput advantage of an IR synchrotron light source over a conventional thermal (glabar) source is only significant when measurements with spot sizes smaller than 50 micrometers in diameter need to be achieved. To take full advantage of the possible small spot size for a number of different (bio)chemical experiments, dedicated chip based systems are needed. In case of time resolved studies a time resolution of approximately 500 microseconds can be achieved. In case of separation systems like on-chip capillary electrophoresis synchrotron based IR detection would also be of distinct advantage as here a small detection volume is critical to avoid overlapping elution profiles.

Lab-on-a-chip technology in combination with IR synchrotron radiation sources may thus be regarded as an enabling technology for a number of different experiments such as bio-ligand interaction studies or protein folding.

## 2. Design, fabrication and working principles of the applied micro-mixers

A 4  $\mu$ m thick SU-8 layer is deposited on both (bottom- and top-) wafers. After softbake and exposure the wafers are post-exposure baked at 90°C. The 2  $\mu$ m thick metal layer, which forms the separation membrane, is deposited by evaporation on top of the SU-8 layer on the bottom wafer. Silver is used for this layer, because evaporated Ag-layers do not show any internal stress and they can be deposited using relatively low power. The Ag-layer is patterned in a conventional way using

positive photoresist (AZ 1512 HS) and wet etching. The Ag-etchant, which is used, does not attack the SU-8. Subsequently the SU-8 structure (under the Ag-membrane) is developed.

The treatment of the top-wafer is different and depends on the used bonding method. In case of a simple method the SU-8 structure is developed and the holes for inlets and outlet are drilled. Subsequently the two wafers (top- and bottom-wafer) are bonded in an evacuated chamber upon application of pressure (2000N) and temperature (ramp of 3 °C / min. to 150 °C followed by one hour at this temperature).

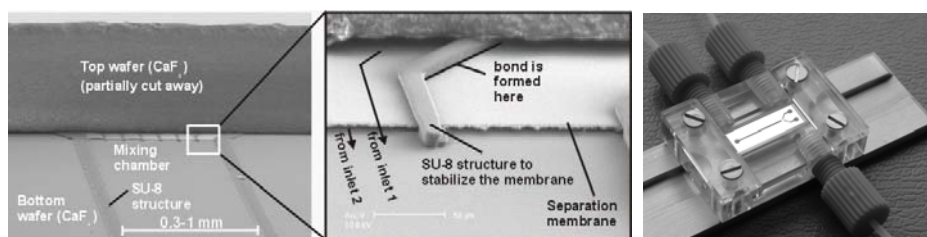


**Figure 1.** Left and middle: SEM images of the produced chips. Right: Picture of the microchip mounted in the dedicated support for placement under an FTIR microscope.

### 3. Spectral baseline noise achievable when using a MIR synchrotron source vs. a global

The dependence of the achievable spectral baseline noise as a function of the probed sample area has been investigated in a systematic study. For this purpose a microchip with a channel cross section of  $10 \times 300 \mu\text{m}$  and filled with water has been used. The aperture of the microscope was set from 10 to  $70 \mu\text{m}$  in increments of 5-10  $\mu\text{m}$ . In case of synchrotron radiation the baseline noise decreased when increasing the sampling spot from 10-20  $\mu\text{m}$ . However, a further increase of the sampling area did not result in an improved spectral baseline. On the contrary when using a global source a continued improvement in baseline noise was achieved upon increasing the sampling area. At a spot size of 20  $\mu\text{m}$  the baselines noise was approximately 10 times lower using a synchrotron as compared to using a global source. However, at spot sizes of 50  $\mu\text{m}$  no significant differences in the baseline noise have been observed. These results clearly show that synchrotron radiation is of significant advantage only when measurements at small sample spots need to be carried out. This is the case in chemical reaction monitoring using the continuous flow approach or in separation systems where band broadening in the detection area needs to be avoided.

### 3. Chemical reaction monitoring in micro-chips by mid-IR synchrotron radiation

The proper functioning of the device was tested using the titration of acetic acid as a simple model system. In figure 2 the spectra are shown which have been recorded at distinct positions along the outlet channel of the mixer. In doing so spectra before and after reaction could be recorded. In a similar way spectra of  $\beta 2$ -microglobulin, a single chain polypeptide (99 residues Mw: 11800), at two different pH values have been recorded.  $\beta 2$ -microglobulin is of relevance in dialysis-related amyloidosis, a protein conformational disease. There is now broad consensus that partial unfolding of  $\beta 2$ -m is required for formation of fibrils. As FTIR spectroscopy is sensitive to the secondary structure of proteins it may be expected that pH induced protein folding may be followed in solution and in-situ by time resolved FTIR studies.

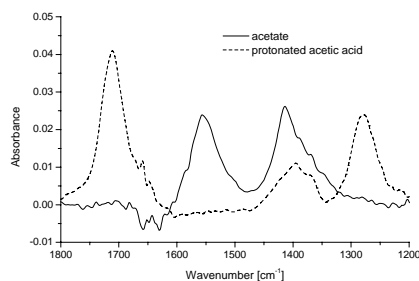


**Figure 2.** Mid-IR spectra recorded from a sample volume of 9 pL (30\*30\*10 $\mu$ m). One clearly can see the differences in the mid-IR spectra of acetic acid and acetate.

The spectra of acetic acid and acetate have been recorded in aqueous solution directly. For the study of protein conformation as in case of  $\beta$ 2-microglobulin heavy water and deuterated reagents (DCI) had to be chosen. This is because the information rich amid I band of proteins, from which their secondary structure may be told, overlap with the bending vibration of normal water. In the studies performed with the micromixers so far  $\beta$ 2-microglobulin solutions of 1g/L have been used. The spectra at two distinct pH values, which have been recorded from a spot volume of 20\*40\*10  $\mu$ m are given in Figure 3a. Despite the fact that these spectra are noisy the expected shift of the amid I band to higher wavenumbers upon decreasing pH may be discerned. The observed band-shift reflects the folding (increase in  $\alpha$ -helical structure) of the protein. Reference spectra recorded from larger volumes using the attenuated total reflection technique (figure 3b) confirm this observation.

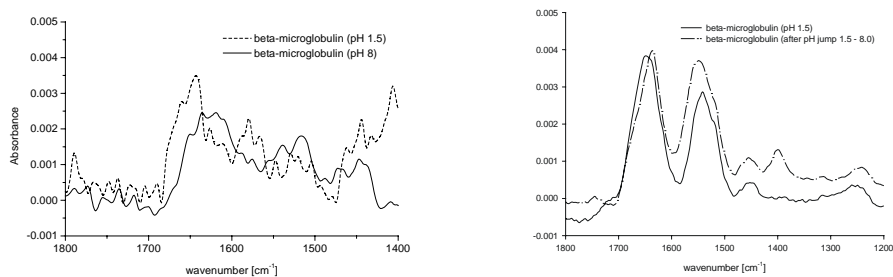


**Figure 3.** a) Mid-IR spectra recorded from 8 pg (conc.: 1g/L, 20\*40\*10  $\mu$ m) of  $\beta$ 2-microglobulin at different pH values in the micro-chip using a synchrotron radiation source. b) Reference spectra

#### 4. Conclusions

The successful coupling of MIR synchrotron radiation with micro-chip technology has been shown by recording MIR spectra from a few pL in aqueous solutions only. However, to take full advantage of the sampling capability of synchrotron MIR microscopy the spectral noise needs to be reduced. Efforts are under way which indicate that this will be possible in the near future.

#### Acknowledgements

N.K., S.K., J.R.B. and B.L. are grateful for financial support received from the Austrian Science Foundation (FWF 15531) and from BESSY.

## ***Publication IV***

N. Kaun, M. J. Vellekoop, E. Pachalis and B. Lendl

*„Time Resolved Fourier Transform Infrared Spectroscopy of Chemical Reactions in Solution using a Focal Plane array (FPA) detector”*  
submitted publication

# Time Resolved Fourier Transform Infrared Spectroscopy of Chemical Reactions in Solution using a Focal Plane array (FPA) detector

*N. Kaun, M. J. Vellekoop, and B. Lendl\**

Institute of Chemical Technologies and Analytics, Vienna University of Technology, Getreidemarkt 9-164, 1060 Vienna, Austria (N. K., and B.L.); Institute of Sensor and Actuator Systems, Vienna University of Technology, 1040 Vienna, Austria (M.J.V.);

\*bernhard.lendl@tuwien.ac.at

## **Abstract**

An FTIR microscope equipped with a single as well as a 64\*64 element focal plane array MCT detector was used to measure chemical reaction taking place in a microstructured flow cell designed for time resolved FTIR spectroscopy. The flow cell allows transmission measurements through aqueous solutions and incorporates a microstructured mixing unit. This unit achieves lamination of the two input streams with cross section of 300\*5  $\mu\text{m}$  each resulting in fast diffusion controlled mixing of the two input streams. Microscopic measurement at defined positions along the outlet channel allows obtaining time resolved information of the reaction taking place in the flow cell. In this paper we show experimental results on the model reaction between formaldehyde and sulfite. Using the single point MCT detector high quality FTIR spectra could be obtained from a spot size of 80\*80  $\mu\text{m}$  whereas the FPA detector allowed recording light from an area of 260\*260  $\mu\text{m}$  focused on its 64\*64 detector elements. Therefore more closely spaced features could be discerned, on the expense of a significantly lower S/N ratio per spectrum. Multivariate curve resolution alternating least squares was used to extract concentration profiles of the reacting species along the outlet channel axis.

INDEX HEADINGS: Focal plane array detector, time resolved IR spectroscopy, micro-mixer,

## **Introduction**

Time resolved Fourier transform infrared (TR-FTIR) spectroscopy has proven to be a valuable tool for obtaining structural information on the course of dynamic processes. This technique enables insight to reaction kinetics, ligand interactions, protein conformational changes or complex formation among others<sup>(1)</sup>.

For initiation of the event under study mixing solutions containing the reactants poses the most widely applicable approach. There are several prerequisites a mixer has to fulfill. First, the mixing process has to occur fast, in order to get access to the early terms of the dynamic process. Then, working with biochemicals for example, constrains the sample consumption, as these are often limited in availability and high concentrations for IR spectroscopy are required. Moreover, IR spectroscopy in aqueous solutions can only be performed on low sample thickness. Otherwise water would prevent obtaining information from solutes due to its strong absorbing effect around 1640 and 3400  $\text{cm}^{-1}$ . The consequences of latter points is downscaling the mixer and the implementation onto a chip.

Our approach to meet these problems was to set-up a chip based IR transmission cell with an integrated mixer<sup>(2)</sup>. Due to the integration of mixer and transmission cell into one chip, no transfer line, which would effect a dead time between the end of the mixing and the first observation point, is needed. The small dimensions and the low flow rate (due to the aimed low sample consumption) implicate laminar flow, which allows only diffusion based mixing. In order to minimize the mixing time according to the formula  $t_D = L^2/4D$  ( $t_D$  the mixing time,  $L$  the diffusive distance to overcome,  $D$  the diffusion coefficient), it is necessary to reduce the thickness of the liquid layers. Thus, two designs were realized<sup>(3)</sup>, basing on the principle narrowing the fluid streamlines. The first design achieves multi-lamination of alternating streamlines with a width of 20  $\mu\text{m}$  and a height of 20  $\mu\text{m}$  resulting in a mixing time of approximately 200 ms for small molecules. In a further development of the mixing chip two reactant flow sheets with a height of 10  $\mu\text{m}$  each are superimposed. It revealed that this design allows mixing in the half of the time and it turns out to be more robust in regard to blocking. Apart from these practically important advantages the latter design also allows for more spectroscopically accurate absorbance measurements<sup>(4)</sup>. This can be exemplified with a simple notional experiment illustrated by Figure 1. It shows two streamlines of the same flow rate, one absorbing the other non-absorbing, fed into the different mixers having an optical path of  $d$ . No reaction between the two streamlines is assumed. At  $d/2$  the absorbing streamline will absorb half of the initial intensity ( $I_0$ ). Therefore, in case of the mixer that



attains superposition of the input streamlines  $I_0/2$  will be recorded before and after the mixing event because the product between concentration and effective optical path remains constant for each point within the cross section of the IR beam. However, in the case of the mixer geometry that achieves multi-lamination the intensity recorded before mixing has been achieved will be different from the intensity recorded after mixing. Prior to the mixing process the intensity will be the sum of radiation passing the non-absorbing streamline, accounting for  $I_0/2$ , as well as the fraction passing through the section containing the absorbing streamline being equal to  $I_0/8$ .

Based on this simple consideration it is evident that superposition of the streamlines must be aimed at in order to avoiding errors due to changes in absorbance due the mixing process only.

Like in many other works<sup>(5,6,7,8,9)</sup>, these mixers were operated in the stopped-flow mode (Fig. 2). Employing high flow rates ( $100 \mu\text{l min}^{-1}$ ) hardly any mixing is performed in the mixing chip while the flow on. Upon stopping the flow the reactants mix rapidly by diffusion, and the reaction can be monitored from the unmixed status up to the finished reaction by acquiring consecutively IR spectra over one broad sample spot. For gaining a high signal-to-noise-ratio this can be repeated as often as required, and the recorded spectra will be averaged. However, the main drawback of this operating mode is the limitation of the time resolution by the scan speed of the spectrometer. Besides, dealing with a linear flow velocity of  $0.3 \text{ m s}^{-1}$  in such a small sample chamber results in high pressures. Thus stopping the flow in the overall system will not set the fluid speed immediately to zero and a time inaccuracy has to be considered.

Several biochemical reaction steps lie in the millisecond range and access to these is desired. Thus by not stopping the flow and regarding the transfer of the mixing fluids along the channel translates the time axis into the distance axis, which is commonly denoted as continuous flow mode<sup>(10)</sup>. Jensen et al<sup>(11)</sup> used this mode by only varying the flow rate, which gives at one point along the channel different time points after mixing. Our approach recently<sup>(12)</sup> was to move the sample spot along the channel while the flow rate was kept constant. Flow rates were about 100 times lower than in the stopped-flow mixer, in order to give the liquids enough time for mixing. The dimensions of the mixer were changed. A thinner channel is now sufficient and for faster time mixing the flowsheets became 5 instead of  $10 \mu\text{m}$  resulting in an optical path of  $10 \mu\text{m}$ . In this mode only the spacing and size of the measurement spot size on the channel is limiting the time resolution (see scheme Fig. 3). In case of the sample under investigation being a  $10 \mu\text{m}$  thick film of aqueous solutions

sandwiched between two 1 mm CaF<sub>2</sub>-plates the lowest spot-size of an state-of-the-art IR microscope giving reasonable signal to noise ratio is about 50 x 50 μm. Using thermal light sources a decrease in spot size would significantly effect the achievable S/N ratio. In case the thermal light source can be replaced by a synchrotron radiation source an improved S/N ratio measurements at spot sizes of 16x16 μm with satisfying S/N ratio become possible.

An alternative solution for probing small areas poses an IR microscope equipped with a focal plane array (FPA) detector. This detector consists of small detector elements arranged usually in a rectangular grid format, allowing the acquisition of thousands of IR spectra simultaneously as a projected image of the sample. Thus with one scan spectral and spatial information of samples can be mapped.

So far the advantage of FPA detectors is adopted in FTIR imaging benefiting from the high spatial resolution with low time consumption. They found application in studies of samples such as polymer blends<sup>(13)</sup>, quality check of solid pharmaceuticals<sup>(14)</sup> or even single cells<sup>(15)</sup>. Also step scan measurements were demonstrated on selected samples<sup>(16)</sup>. Special application, which are still in development, found the FPA detector in dispersive instruments<sup>(17,18)</sup>.

In this paper we present the first time the use of an FPA equipped microscope for continuous flow operation mode on a mixer chip using the addition of sulfite to formaldehyde as a model reaction. The application to the continuous flow approach is illustrated in Figure 4. At constant flow speed, by combining a line scan along the channel the FPA detector can be employed like a zoom into the areas of interest and advantage can be taken of fast acquisition of a high number of spectra, in order to keep the sample consumption low.

The large amount of data received by one FPA image has been treated chemometrically using multivariate curve resolution alternating least squares (MCR-ALS)<sup>(19)</sup>, a powerful tool for analysis for evolving systems. . The MCR-ALS is a self-modeling curve resolution method, which decomposes the data set into concentration profiles (**C**) and spectra (**S**) for each modeled component while certain mathematical and chemical constraints (e.g., non-negativity of **C**, selectivity information in **C**...) can be applied. Thus it has the ability to reduce the large data matrices, on basis of the changes in spectra with time.

## ***Experimental section***

### **Instrumental**

The design of the mixer chip is explained in detail in <sup>(3)</sup>. In brief two inlet channels are superimposed within a CaF<sub>2</sub> flow cell having an optical path of 10 μm. This is achieved by a micro-structured mixer made of SU-8 polymer and a silver layer placed inside the 10 μm high flow channel. The superimposed streamlines are initially separated by the silver layer to achieve stable flow conditions. At the end of the separating silver layer a 10 mm long (y-axis), 300 μm wide and 10 μm high outlet channel follows. Mixing and reaction starts immediately after the end of the silver layer. Chemical reactions taking place in the outlet channel are probed by transmission measurements using an IR microscope.

Here the experiments were carried out on a Hyperion<sup>TM</sup>3000 IR microscope coupled to an Equinox55 FTIR spectrometer (Bruker, Ettlingen, Germany). The microscope was equipped with a 15x Cassegrain-objective operating in the transmission mode. For data acquisition recorded from  $1350 < \omega < 900 \text{ cm}^{-1}$  either the single point MCT detector or the FPA detector were employed. The latter projects an image of 266 x 266 μm onto 64 x 64 detector elements resulting in the measurement of 4096 spectra simultaneously. The spectra consist of an average of 30 scans. The spectral resolution is set to  $8 \text{ cm}^{-1}$ . The flow speed in the mixer was kept constant with  $0.5 \mu\text{l min}^{-1}$  at each channel inlet.

Solutions 0.1 M in concentration of HCHO and Na<sub>2</sub>SO<sub>3</sub> were prepared from Formaldehyde solution and Sodium sulfite (both Merck, Darmstadt, Germany) solved in HPLC grade water from Fluka (Buchs, Switzerland). The solutions were prepared freshly everyday and filtered through a 2μm pore size filter before use in order to avoid any deposits in the mixer.

### **Data processing**

In order to obtain absorbance spectra a background of the water filled channel was acquired. The recorded data set was processed in OPUS<sup>TM</sup> (Ettlingen, Germany). For our purpose only the direction of the flow is of interest and not the width of the channel. Therefore, in order to achieve a better S/N ratio, the received spectra from the FPA measurements were combined along lines of equal distance from the beginning of the mixing zone according to the scheme presented in Figure 5 as single point spectra showed a too poor S/N ratio. The spectra taken from sampling points close to the edges of the channel were not considered in the combined

spectra as these contain information from fluid elements with significantly slower migration speed due to the strongly of laminar flow profile as compared to those from the central part of the outlet channel. <sup>(12)</sup>.

For MCR-ALS analysis, the freely available program (Matlab code) by A. de Juan and R. Tauler<sup>(19)</sup> was used implemented in Matlab 5.3 (The Math Works Inc., Natick, MA, 1999). Theory and application of curve resolution, and MCR-ALS in special, have been described in detail in elsewhere<sup>(20)</sup>.

## ***Results and Discussion***

The reaction under study is the formation of hydroxymethanesulfonate from formaldehyde and sulfite. This reaction can be readily monitored by IR spectroscopy in the region between 1300 and 900  $\text{cm}^{-1}$ . At one channel inlet the sulfite solution was introduced while at the second channel the formaldehyde was fed in. At a constant flow speed the reaction can take place along the channel. This process is presented in a time resolved fashion in Fig. 6. The y-axis here is denoted as the channel length. Recording spectra beginning at the end of the silver layer separating the superimposed flow sheets ( $y = 0 \mu\text{m}$ ) the two substances are hardly mixing thus giving the combined spectra of both pure substances. Within the first 250  $\mu\text{m}$  the mixing is completed<sup>(12)</sup> and from there on only the reaction takes place. The spectra show that the decrease of the sulfite band at 936  $\text{cm}^{-1}$  starts 3000  $\mu\text{m}$  after the channel inlet accompanied by a split of the band at 1028  $\text{cm}^{-1}$  representing the C-O stretch vibration from formaldehyde interacting with water.. This equals a reaction time of 590 ms ( $\pm 50$  ms) determined by the flow speed and evaluated by computational flow simulations. At a distance of 3500  $\mu\text{m}$  along the outlet channel the band of the asymmetric vibration of the sulfite is appearing at 1180  $\text{cm}^{-1}$  within one spectrum, while the band at 936  $\text{cm}^{-1}$  is still decaying.

The FPA detector poses now the possibility to zoom into the part of reaction where the band transition is not well resolved by 100  $\mu\text{m}$  steps of the single point microscope. Fig. 7 presents 62 spectra obtained within one FPA scan measurement of the channel in the region of 3500  $\mu\text{m}$  on the channel axis. The spectra derive from averaging for each channel position in flow direction 54 spectra into one spectrum according to Fig. 5. While the spectral region below 1000  $\text{cm}^{-1}$  is very noisy when using the FPA, the augmenting band at 1180  $\text{cm}^{-1}$  can be well discerned in the spectra.

For better visualisation the data shown in Fig. 6 and 7 were subjected to MCR-ALS. The MCR-ALS procedure reduces the data further to concentration profiles of species involved. In this case this refers to the mixture of the educts and the product and their according spectra. Applying the constraints “non-negativity in concentration” and “unimodality in concentration” the best fit for the data could be yielded for the data recorded by the single point detector. In Fig. 8 the profiles of the two species that contain 99.2 % of the information from Fig. 6 are drawn. It clearly presents the decrease of the first component (C1) represented by the spectrum of a mixture of sulfite and formaldehyde and on the opposite the gain of intensity for the reaction product (C2), presented by the spectrum S2, moving downstream the channel (y-axis). Note that the concentration and the absorbance values are arbitrary units that are not equivalent to the measured values. In Fig. 9 the MCR-ALS result of the FPA measurement, understood as a zoom into the region of the line scan accordant to position 3500 – 3760  $\mu\text{m}$  in Fig. 6 is shown. In case of the FPA measurement a further constraint, “selectivity in concentration” for the concentration profile was implemented. Although the spectra and also the concentration profile contain much more noise, the increase of the second component (C2) presented by the spectrum of the reaction product is well resolved, while the first component (C1) only contains noise arising in FPA measurements.

Depicting 266 x 266  $\mu\text{m}^2$  onto 64 x 64 detector elements gives a calculated pixel size of 4.2  $\mu\text{m}$ . The single spectra obtained from each pixel of the detector are rather noisy though averaging of 30 scans was performed see Fig. 10. However, by binning 55 detector elements located in rows normal to y-axis of the outlet channel spectra were obtained corresponding to lines spaced at 4.2  $\mu\text{m}$  along the outlet channel with reasonable S/N ratio. These binned spectra allowing probing the quasi stationary reaction in the outlet channel. In comparison to the single point MCT measurements, the cut off in frequency of the FPA detector is steeper and leads to a loss of one third of intensity probing through the chip ( $\text{CaF}_2$ ) at 1000  $\text{cm}^{-1}$ . Therefore the FPA spectra have been cut at 1000  $\text{cm}^{-1}$ . As a consequence only the rising band at 1180  $\text{cm}^{-1}$  from the reaction product but not the decreasing band at 936  $\text{cm}^{-1}$  were used in data evaluation by MCR-ALS.

In the flow direction, where no binning was applied, only the first and the last spectrum of 64 deriving from the border of the array had to be left out due to high noise. The actual spatial and hence temporary spacing between the adjacent spectra is difficult to judge. In this work IR wavelengths between 6.6 and 10  $\mu\text{m}$  were employed. Considering the composition of the probed part of the mixer chip, being two times 1 mm  $\text{CaF}_2$  with 10  $\mu\text{m}$  of water in between,

the spatial resolution should be beyond 4.2  $\mu\text{m}$ . Estimated by Rayleigh's criterion for resolution, which is given by  $z = 0,61\lambda/NA$  (with  $z$  distance where 26.4 % contrast is achieved,  $\lambda$  wavelength,  $NA$  numerical aperture of the objective) a spatial resolution between 9 to 14  $\mu\text{m}$  is to be expected. By mapping the channel onto the array of pixels equivalent to 4.2  $\mu\text{m}$  in size information of the imaged fluid elements is overlapping on each pixel. For exact calculations of the overlap point spread functions could be operated revealing the energy distribution from a point in an optical set up to an image. However, a more detailed analysis would also require considering ray propagation across media of different optical densities. As this would go beyond the purpose of this paper the actual spatial resolution achieved can only be estimated.

Concerning the achievable time resolution of the presented experimental set-up additional considerations are necessary. Due to the laminar flow profile in microfluidic systems a delay for the distance – time conversion of about 3 % for 0.5  $\mu\text{l}/\text{min}$  flow speed (derived from computational simulations) has to be taken into account. Furthermore, it has to be considered that diffusion and reaction overlap, thus further blurring the time resolution. However, once the mixing process has been accomplished, time resolution will be determined by spacing of adjacent measurement points and the applied flow rate<sup>(12)</sup>. Considering the experimental set-up under study and the applied flow rate a time resolution down to 0.8 ms can be given.

In comparison to the synchrotron measurements performed on this mixer<sup>(12)</sup> with a single point detector and a measurement spot of 16  $\mu\text{m}$ , the FPA set-up achieves better time resolution with comparable S/N ratio for the studied spectral region. An important advantage of the FPA approach, however, is the fast recording of multiple data points. While the recording of 62 spectra along the channel takes about one hour at the synchrotron facility, the same amount of data could be recorded within 12 minutes on the FPA set-up.

After binning the according spectra MCR-ALS enables further reduction of the data. Commonly, classical principal component analysis (PCA) is used for extracting the main components of the data received by IR imaging<sup>(14)</sup>. The MCR-ALS method, which also uses PCA in its procedure, presents a more powerful tool as it considers the evolving system. It extracts the factors that explain most of the data matrix and represent changes in the components as a function of perturbation as well<sup>(21)</sup>. The data of the FPA measurement could therewith reduced to two spectra and corresponding concentration profiles summarizing 90 %

of the information initially contained in the 62x214 data matrix obtained after binning. The remaining 10 % represent mainly noise and thus could not be assigned to a third component

## **Conclusion**

Within this work a new approach for TR-FTIR is demonstrated using an FPA detector in IR microscopy on for imaging of reacting microfluidics. Following diffusion based mixing and using a flow rate of 0.5  $\mu\text{l}/\text{min}$  a time resolution in the sub-ms region could be achieved and a simple chemical reaction monitored. So far the S/N ratio achieved by FPA measurement of the microfluidics hinders application of the FPA detector to the investigation of spectroscopically more demanding systems. However, as this work shows, it already can provide supplementary information to measurements carried out with a single point detector if strong spectral features are to be observed.. The advantage of the FPA detection system is the simultaneous acquisition of spectra from multiple fluid elements. This property together with the mixer being incorporated in the flow cell allows reduction of the sample consumption to a maximum. With flow rates in the sub- $\mu\text{L}/\text{min}$  range a few tens of microliter of a given sample would be sufficient for a time resolved experiment covering the millisecond – second time regime. Finally, it needs to be iterated again, that conversion of the measurement position to the time axis needs to consider the mixing time and the laminar flow condition as well as the actual imaging capabilities of the FPA microscope. For a theoretical treatment of the latter aspect e.g. calculating point spread functions, detailed information on the actual optical set-up of the used FPA microscope would be needed.

## **Acknowledgment**

The authors are grateful for the discussion with Dr. Ulrich Schade (BESSY Berlin, Germany) on focal plane array optics. The disposal of measurement time on the Hyperion Microscope by Dr. E. Paschalis and Dr. K. Klaushofer (Ludwig-Boltzmann-Institute of Osteology, Hanusch-Hospital, 1140 Vienna, Austria) is gratefully acknowledged. Financial support by the Austrian Science Fund within the project FWF 15531 is gratefully acknowledged. B. L. and M. V. acknowledge support received from TU Vienna within the "Innovative Project 2003".

## Reference List

1. C. Kottling and K. Gerwert, *Chemphyschem* **6**, 881 (2005).
2. P. Hinsmann, M. Haberkorn, J. Frank, P. Svasek, M. Harasek, and B. Lendl, *Applied Spectroscopy* **55**, 241 (2001).
3. P. Hinsmann, J. Frank, P. Svasek, M. Harasek, and B. Lendl, *Lab on a Chip* **21**, 16 (2001).
4. D. A. Moss, (2005).
5. H. Fabian and D. Nauman, *Methods* **34**, 28 (2004).
6. R. Masuch and D. A. Moss, *Applied Spectroscopy* **57**, 1407 (2003).
7. A. J. White, K. Drabble, and C. W. Wharton, *Biochemistry Journal* **306**, 843 (1995).
8. A. Troullier, D. Reinstädler, Y. Dupont, and J. Naumann, *Nat.Struct.Biol.* **7**, 78 (2000).
9. B. C. Dunn and E. M. Eyring, *Applied Spectroscopy* **53**, 292 (1999).
10. E. Kauffmann, N. C. Darnton, R. H. Austin, C. Batt, and K. Gerwert, *Proceedings of the National Academy of Sciences of the United States of America* **98**, 6646 (2001).
11. T. M. Floyd, M. A. Schmidt, and Jensen Klavs F., *Ind.Eng.Chem.Res.* **44**, 2351 (2005).
12. N. Kaun, S. Kulka, J. Frank, U. Schade, M. J. Vellekoop, M. Harasek, and B. Lendl, *Analyst* **131**, 1 (2006).
13. A. Gupper, P. Wilhelm, M. Schmied, S. G. Kazarian, K. L. A. Chan, and J. Reußner, *Applied Spectroscopy* **56**, 1515 (2002).
14. Y. Roggo, A. Edmond, P. Chalus, and M. Ulmschneider, *Analytica Chimica Acta* **535**, 79 (2005).
15. P. Lasch, M. Boese, A. Pacifico, and M. Diem, *Vibrational Spectroscopy* **28**, 147 (2002).
16. R. Bhargava and I. W. Levin, *Applied Spectroscopy* **57**, 357 (2003).
17. I. Pelletier, C. Pellerin, D. B. Chase, and J. F. Rabolt, *Applied Spectroscopy* **59**, 156 (2005).
18. A. J. Sommer, (2006).
19. R. Tauler, <http://www.ub.es/gesq/mcr/mcr.htm> (1999).
20. F. Despagne, R. Tauler, D.-L. Massart, and O. E. de Noord, *Analytical Chemistry* **69**, 3391 (1997).
21. J. R. Schoonover, R. Marx, and S. L. Zhang, *Applied Spectroscopy* **57**, 154A (2003).



## Figures

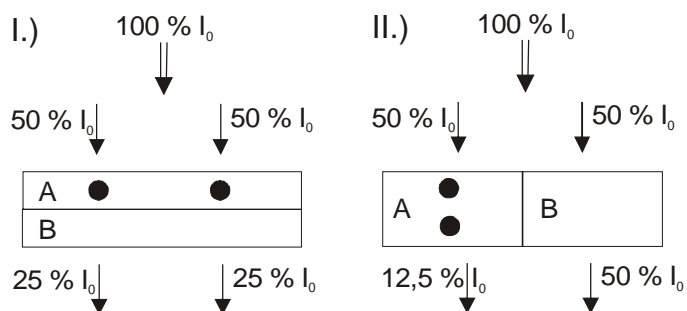


Figure 1. Comparison of intensities reaching the detector for flow superposition (I.) and flow lamination (II.). It is assumed that A is absorbing 50 % at half of the optical path whereas B is non-absorbing.

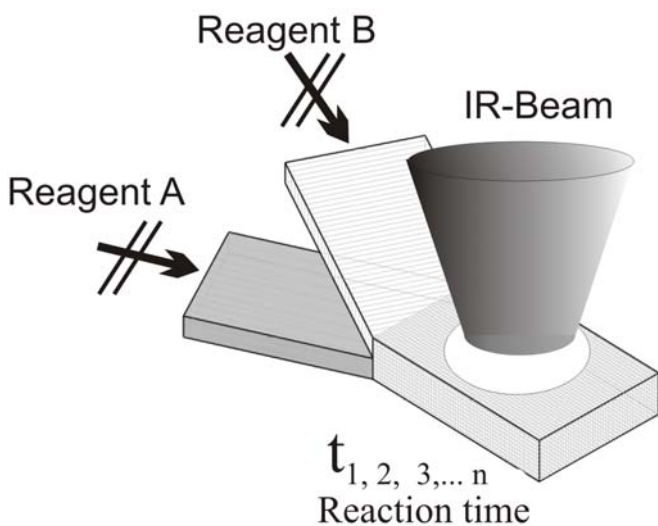


Figure 2. Scheme of the stopped-flow mixer using a beam-condenser for the IR beam

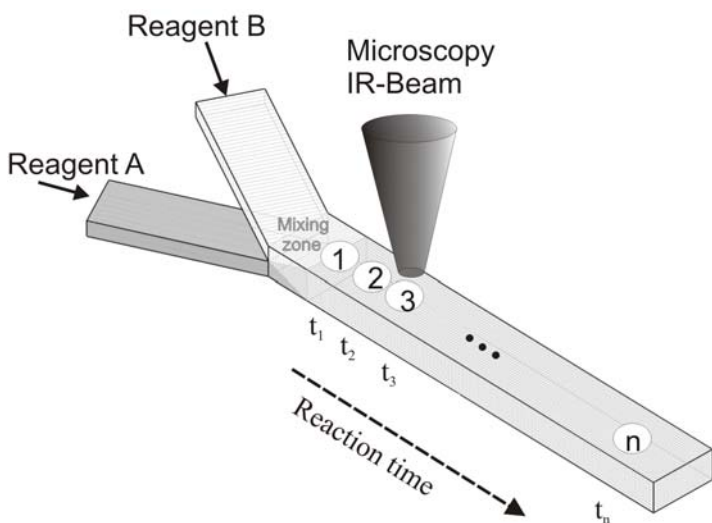


Figure 3. Scheme of the continuous-flow mixer using an IR microscope with a single point detector

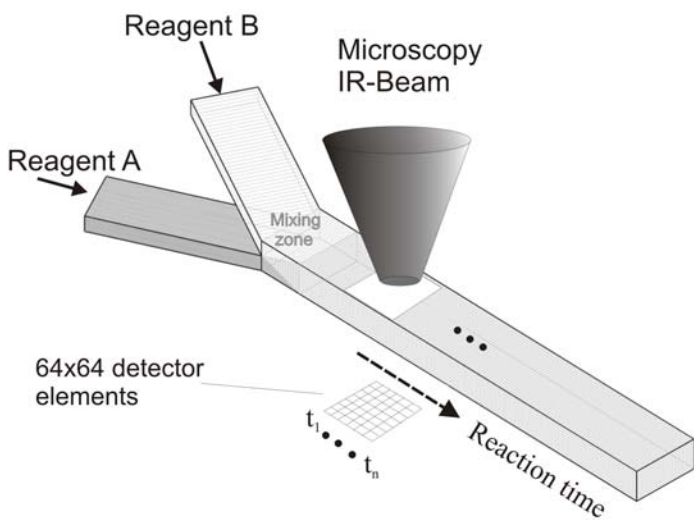


Figure 4. Scheme of the continuous-flow mixer using an IR microscope with an FPA detector

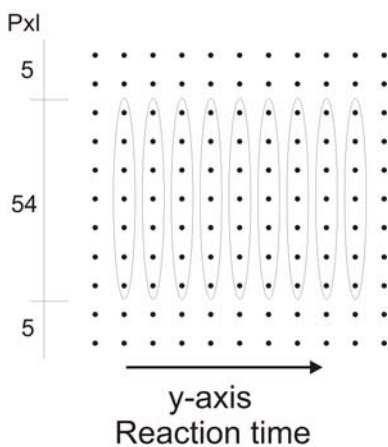


Figure 5. The data consisting of the 4096 spectra is processed by binning columnwise. Each spectrum is considered as Pixel (Pxl).

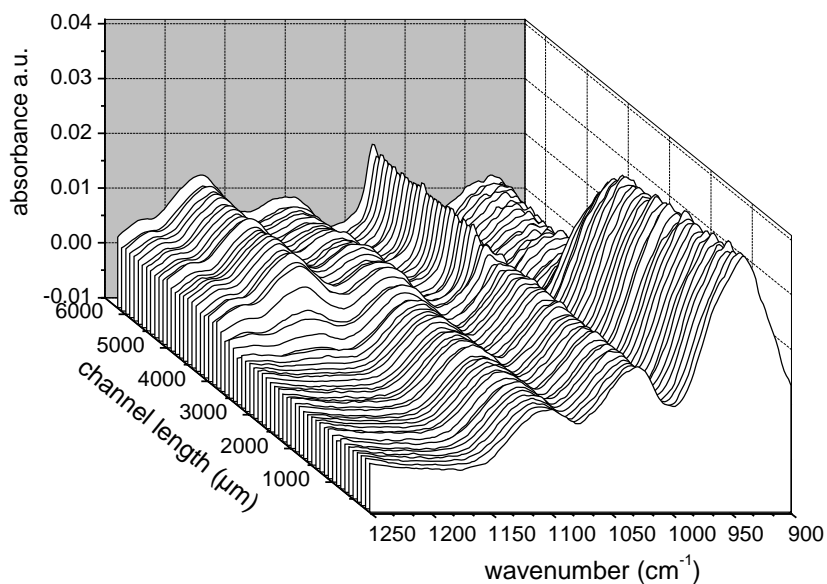


Figure 6. Single point detector measurement on the microchip: The spectra are acquired over 7 mm along the channel in 100 μm steps corresponding to a time axis of 18 ms time resolution presenting the reaction of sulfite and formaldehyde time resolved.

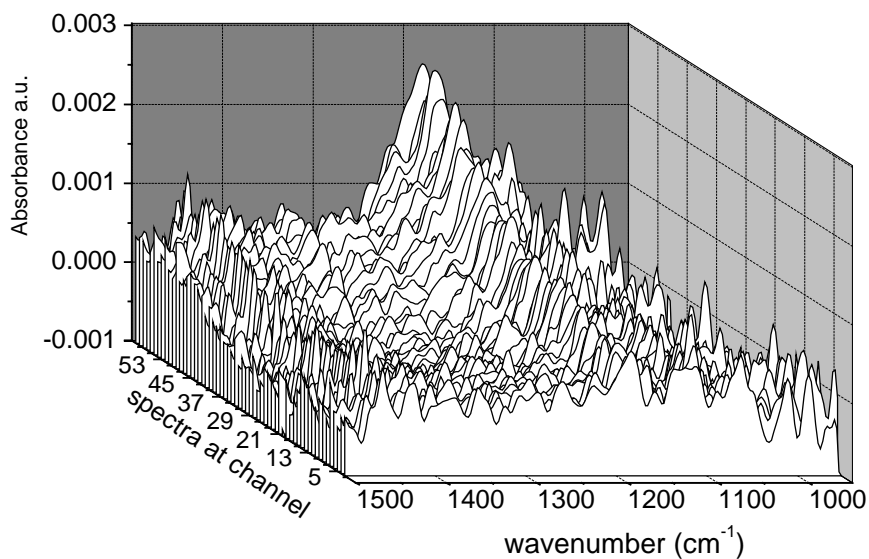


Figure 7. FPA map as zoom in the region at 3000  $\mu\text{m}$  of Fig. 6. The spectra are corresponding to a time axis of 0.8 ms.

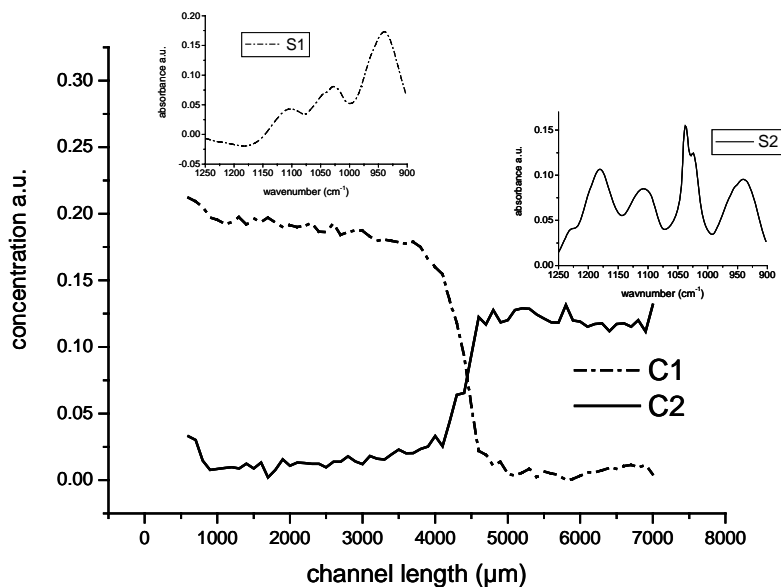


Figure 8. Results from the MCR-ALS procedure on the line scan measurement (Fig. 6) with C1 and C2 being the concentration profile of the educts and the product, respectively. S1 and S2 are the according spectra. Absorbance units are at random scale.

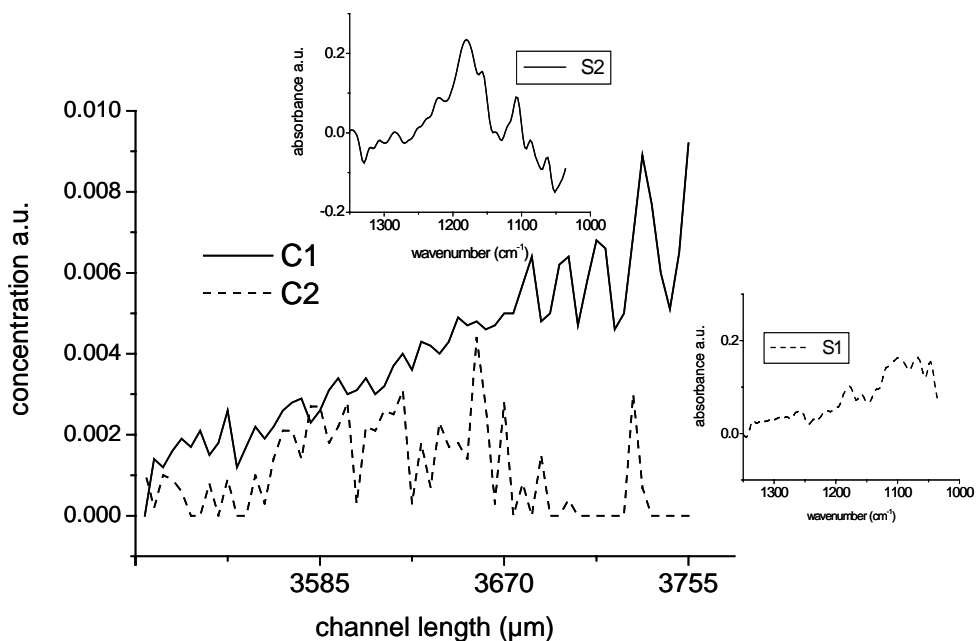


Figure 9. Results from the MCR-ALS procedure on the FPA measurement (Fig.7) with C1 and C2 being the concentration profile and S1 and S2 the according spectra, respectively. Absorbance units are at random scale.

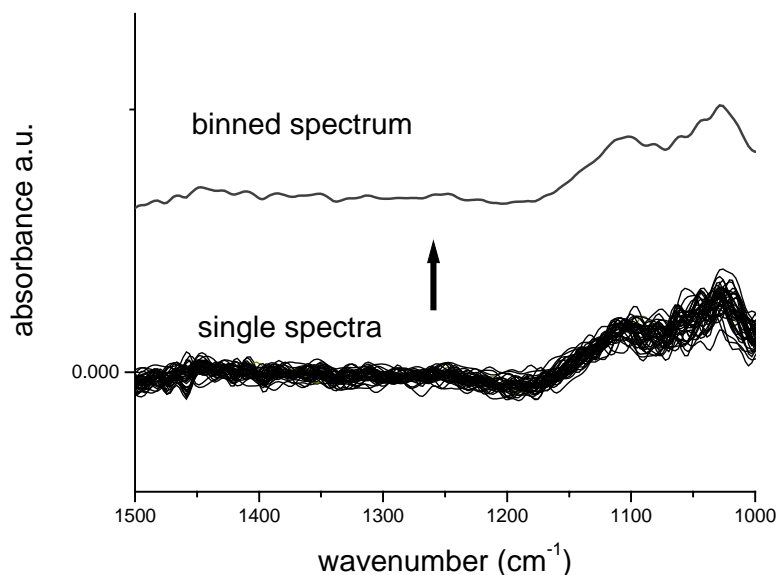


Figure 10. The single spectra come from one row of the FPA detector field recorded through the microchip filled with the unreacted educts. The averaged (binned) spectrum is shifted by an offset of 0.03 AU.

## ***Publication V***

N. Kaun, J.R. Baena, D.Newnham, B. Lendl

*„THz-Spectroscopy as a new tool for measuring the structuring effect of solutes on water”*

Appl. Spectrosc. 59 4 (2005) 505-510

# Terahertz Pulsed Spectroscopy as a New Tool for Measuring the Structuring Effect of Solutes on Water

N. KAUN, J. R. BAENA, D. NEWNHAM, and B. LENDL\*

*Institute of Chemical Technologies and Analytics, Vienna University of Technology, Getreidemarkt 9-164, 1060 Vienna, Austria (N.K., J.R.B., B.L.); and TeraView Limited, Platinum Building, St John's Innovation Park, Cambridge CB4 0WS, UK (D.N.)*

Absorption spectra of aqueous solution of "chaotropes" (structure maker) and "kosmotropes" (structure breaker) have been recorded in the mid-infrared (MIR) and terahertz (THz) spectral region. A different impact of the two groups of solutes on the absorption spectrum of water was found in the recorded THz spectra. A concentration-dependent increased absorption across the investigated THz spectral region (0.04–2 THz, 1.3–66 cm<sup>-1</sup>, respectively) has been recorded for all studied chaotropic solutions, whereas the opposite has been obtained for kosmotrope containing solutions. In the case of ionic solutes a further increase in absorption towards higher frequencies was measured. The distinction between chaotrope and kosmotrope solutes was, as expected, also possible in the MIR spectral region. Depending on the structure-forming effect of the solute the OH stretch vibration of the water (around 3400 cm<sup>-1</sup>) was slightly shifted. A red shift has been observed for solution of kosmotropes, whereas a blue shift was observed in the case of solutions containing chaotropes. Compared to the MIR spectral region the structure influencing effect of solutes can be more efficiently studied in the THz spectral region, which provides information from interactions between neighboring water molecules.

Index Headings: Terahertz pulsed spectroscopy; Aqueous solution; Water structure.

## INTRODUCTION

Significant instrumental developments over the last decades have established spectroscopic techniques from the ultraviolet regions down to the far-infrared spectral region as powerful, often indispensable tools in modern chemical research. In the near (NIR) and mid-infrared (MIR) spectral region a range of experiments in water and aqueous solution are possible today that were considered impossible only some years ago. Two selected examples underpin this statement: determination of secondary structures of proteins in aqueous solution<sup>1</sup> and following the action of single amino acids with nanosecond time resolution in protein reactions.<sup>2</sup> These experiments are now possible using commercially available bench top instruments that can be found in many research and routine laboratories. Significantly less use is made of the far-infrared spectral region due to reduced instrument performance when thermal light sources and photon detectors are employed as in their popular counterparts for the NIR and MIR spectral regions. When moving to the even longer wavelengths of the terahertz (THz) spectral region, few reports on the use of a broadband spectrometer can be found in the literature. This is explained by the poor brightness of thermal light sources and by additional experimental difficulties as this spectral region

covers frequencies too high to be accessible by electronics and too low for photonic devices.<sup>3</sup> However, this situation is about to change as new instrumentation becomes available to the interested chemists who want to explore this still unused spectral region. Among these new possibilities, THz measurement capabilities at synchrotron beamlines across the world<sup>4,5</sup> must be mentioned along with a recently available dedicated portable terahertz pulsed spectrometer that covers a frequency from 0.04 to 4 THz, which corresponds to the spectral region from 1.3–133 cm<sup>-1</sup> or 8 mm to 75 μm wavelength. A terahertz pulsed spectrometer uses low power, ultra-short pulses of broadband electromagnetic radiation at lower frequencies than traditional infrared techniques.<sup>6</sup> The technology uses fs-pulse lasers, which are focused onto a semiconductor, resulting in the emission of a pulse of coherent terahertz radiation. The radiation is detected using a solid-state room-temperature receiver.<sup>7</sup> Very high signal-to-noise ratios (>10<sup>5</sup>) can be achieved using optical gating. As the technique is coherent both electric-field amplitude and phase information can be measured at the same time, from which the spectral absorption coefficients,  $\alpha(\omega)$ , and the refractive indices,  $n(\omega)$ , of the material can be directly extracted.

Terahertz spectroscopy has already found application in imaging instruments, which have been set up recently with great success providing pictures of biological samples with complex structure such as tissue and dry biological cells.<sup>8,9</sup> Furthermore, using sophisticated time domain experiments, physicists have used THz spectroscopy to gain information on fast dynamic systems to extract, for example, the dielectric constants of water as a function of temperature.<sup>10</sup>

To explore this spectral region for (bio)chemical research, fundamental investigation on the spectral properties of aqueous solution are needed. In this contribution we report on THz spectra of selected solutes at different concentrations. The data obtained strongly suggest that THz spectroscopy provides a direct means to observe structure-forming effects of the solutes on water. For water, two distinct bands are found in the THz region: the nominal 60 and 180 cm<sup>-1</sup> intermolecular vibrations.<sup>11</sup> In general intermolecular interactions from the hydrogen-bonded network of water are to be expected down to two wavenumbers.<sup>12</sup>

The structure of water is a very complicated topic and descriptions have been attempted through many different models. Stanley and Teixeira<sup>13</sup> have put these models into two categories: mixture/interstitial models and distorted hydrogen bond models (continuum models). In the mixture/interstitial model, properties of water can be de-

Received 10 August 2004; accepted 30 November 2004.

\* Author to whom correspondence should be sent. E-mail: Bernhard.lendl@tuwien.ac.at.

scribed by a mixture of distinct species of water molecules in certain equilibrium. These species can be identified by a defined number of hydrogen bonds that are interacting.<sup>14</sup> In the continuum model, water is assumed to form a network that is more or less completely hydrogen bonded. Their effort to combine these models has led to the “percolation model”.<sup>13</sup> To understand the influence of a dissolving substance on the structure of liquid water other models more focused on this topic are preferred. In general, solutes can be classified in to two groups: the “kosmotropes” (order makers) and the “chaotropes” (disorder makers).<sup>15</sup> This effect can now be described by, e.g., the increase or decrease of viscosity due to the addition of a solute, which is done well as a basis for simulation in Hribar et al.<sup>16</sup> In a similar way, the influence on the water structure is given by the entropy of water near monovalent ions ( $\Delta S_{II}$ ) as calculated from the entropy of hydration of the ion.<sup>17</sup> The  $\Delta S_{II}$  serves as a measure for the tightness of the bonding of the dissolved ions and water. The solute either strengthens or weakens the water–water interactions and therefore water becomes more or less mobile. In other work,<sup>18,19</sup> the structure of water is given by a root mean square (rms) of the bimodal H-bond angle distribution, made up of nearly linear bonds and stronger bent O···O–H bonds. Adding a solute can increase or decrease the rms value, indicating either more or less distorted water bonds. Rønne and Keiding<sup>14</sup> propose equilibrium between a low-density liquid (LDL) with high local tetrahedral ordering similar to ice and a high-density liquid with less connected water molecules.

Mid-infrared spectroscopy is sensitive to changes in hydrogen bonding. These changes are generally reflected in a decrease in frequency of the respective vibrations. Therefore, a shift in the position of the  $\nu$ -OH of the water molecule may be expected, if the extent and modes of hydrogen bonding in water are affected by the presence of kosmotropes or chaotropes. This has been observed and exploited already by various groups,<sup>18,19,21</sup> who described the  $\nu$ -OH band at  $3400\text{ cm}^{-1}$  as a convolution of several OH stretch vibrations corresponding to water species interacting with each other via hydrogen bonding to a varying extent. For simplicity, two extreme cases, “ice-like”, characterized by a high degree of hydrogen bonding and a  $\nu$ -OH at wavenumbers lower than  $3400\text{ cm}^{-1}$ , and “free” water that is more similar to water in the vapor phase with minimum hydrogen bonding and a corresponding  $\nu$ -OH peak maximum at wavenumbers higher than  $3400\text{ cm}^{-1}$ , have been defined.<sup>21</sup> For discussing the water spectra in the THz spectral region, where we expect to see intermolecular interactions, we will use this simplistic view of the water structure, sticking to the terms “ice-like” and “free” water.

Adding a kosmotrope (an order maker) shifts the equilibrium to the “ice-like” side, which means that the order is increasing. Vice versa, adding chaotropes increases the amount of “free” water. Typical kosmotropes are small or multiple charged ions (e.g.,  $\text{SO}_4^{2-}$ ,  $\text{Li}^+$ ,  $\text{Na}^+$ ) as well as non-ionic kosmotropes like trehalose or sucrose. In general, these ions/molecules are highly hydrated and therefore affect the dynamics of water molecules in their neighborhood by the presence of hydration layers, hindering mobility. Representative chaotropes are large single charged ions with low charge density (e.g.,  $\text{Gdm}^+$ ,

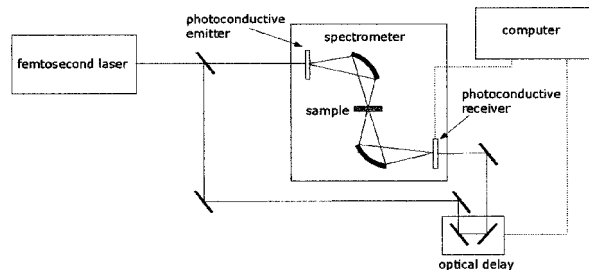


FIG. 1. Schematic showing the configuration of the TPI<sup>®</sup> spectra 1000 (TeraView Limited).

$\text{SCN}^-$ ,  $\text{Cl}^-$ ). Their tendency to bind to water is weaker than the tendency of water to bind to itself. As a consequence, the water adjacent to the ion/molecule becomes more mobile than bulk water (i.e., weakly held). It is very important to consider that the strength of both effects is dependent on the concentration of the solute. Furthermore, ionic kosmotropes should be treated differently from non-ionic kosmotropes. The hydration shell of ionic kosmotropes is characterized by a directed and polarized arrangement of the surrounding water molecules.

## EXPERIMENTAL

For this study, HPLC grade water from Sigma-Aldrich was used. Trehalose, potassium thiocyanate, magnesium sulfate, and guanidium chloride ( $\text{GdmCl}$ ) were purchased from Fluka, and ammonium nitrate and sodium chloride were purchased from Merck. Solutions in concentrations ranging from 0.01 M to 1 M were prepared.

Spectra of water in the MIR spectral region were recorded on capillary films between two  $\text{CaF}_2$  windows on a Bruker Equinox 55 at  $22\text{ }^\circ\text{C}$  equipped with a Globar source and a liquid nitrogen cooled mercury cadmium telluride (MCT) detector. The spectral resolution was set to  $4\text{ cm}^{-1}$ . All measurements and calculations were checked for reproducibility.

The terahertz measurements were made in transmission using a TPI<sup>®</sup> spectra 1000 spectrometer (TeraView Limited, Cambridge, UK). Spectra were the average of 1800 scans (approximately 1 min measuring time). Data were acquired using OPUS<sup>®</sup> software (Bruker Optics, Germany). A schematic diagram of the experimental setup for a terahertz pulsed spectrometer system is shown in Fig. 1. Terahertz pulses are generated when ultra-short laser pulses, from a 75 fs bandwidth-limited titanium–sapphire laser (Vitesse, Coherent, US) operating at 800 nm with a repetition rate of 80 MHz, are focused onto a gallium arsenide (GaAs) photoconductive switch, the terahertz emitter. When the ultra-short laser pulse is present photocarriers are generated in the switch; a transient current flows across a dipole antenna giving rise to a short burst of broadband terahertz radiation. A hemispherical silicon lens couples the radiation out of the GaAs substrate into free-space. Parabolic mirrors focus the terahertz radiation onto the sample. Detection of the terahertz radiation is achieved using an optically gated semiconductor receiver antenna similar to the emitter. The femtosecond near-infrared laser pulses optically gate the switch. The time delay between the terahertz and optical pulses is varied to measure a representation of the terahertz



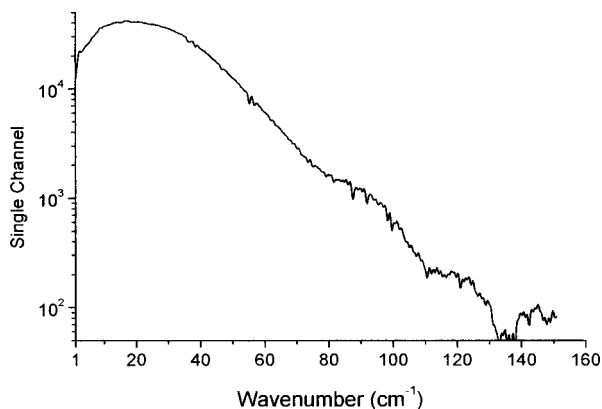


FIG. 2. Single beam spectrum of the empty cell compartment.

hertz field. Fourier-transforming the resultant time-domain waveform provides the frequency information.

For terahertz measurements a standard flow cell, as used for MIR spectroscopy, was equipped with two polyethylene (PE) windows of 4 mm thickness and a 50  $\mu\text{m}$  spacer and installed in the  $\text{N}_2$  purged sample compartment. The cell was connected via Teflon tubing to a peristaltic pump, which was operated at a low flow rate of 0.5 mL/min. Spectra were acquired with the flow on. The procedure was to start with the lowest concentration of a solute, then move on to examining the next higher one. A baseline shift, especially towards the end of the scale during a measurement campaign of several hours, has to be considered for the current instrument performance. Therefore, after each series, a water spectrum for a new background was recorded. The instrument allowed us to acquire spectra from 1 to 133  $\text{cm}^{-1}$  employing a spectral resolution of approximately 1  $\text{cm}^{-1}$ . Figure 2 shows a single beam terahertz spectrum with the empty flow cell. It reveals that there is detectible signal from 1  $\text{cm}^{-1}$  until 133  $\text{cm}^{-1}$ . However, in the experiments reported here, the low signal above 60  $\text{cm}^{-1}$  can lead to reproducibility problems. Therefore, we focused on the region from 1 to 60  $\text{cm}^{-1}$  that provided acceptable baseline stability and noise factor (rms error of deviation in absorbance upon repeated measurement) of less than  $10^{-3}$  a.u. in water for 1800 scans.

## RESULTS

**Mid-infrared Spectra of the Prepared Solutions.** Information about the water structure is collected in a common way by recording absorbance spectra from 2950  $\text{cm}^{-1}$  to 3700  $\text{cm}^{-1}$  for the six different water solutions and pure water versus the empty cell; this information is presented in Fig. 3. The spectra have been normalized to the maximum of their  $\nu\text{-OH}$  band absorption. The appearance of the  $\nu\text{-OH}$  band results from a contribution of all water structures existing in the probed liquid. A clear variation in shape of this band and a shift in the position of the peak maximum of the solutions compared to the HPLC grade water can be observed. Taking into account that each different water structure present in the sample contributes to this peak at other frequencies, it becomes clear that we can observe the influence of the various added solutes on water. In the work of Brubach et al.,<sup>21</sup> a decomposition of the feature into three peaks has been

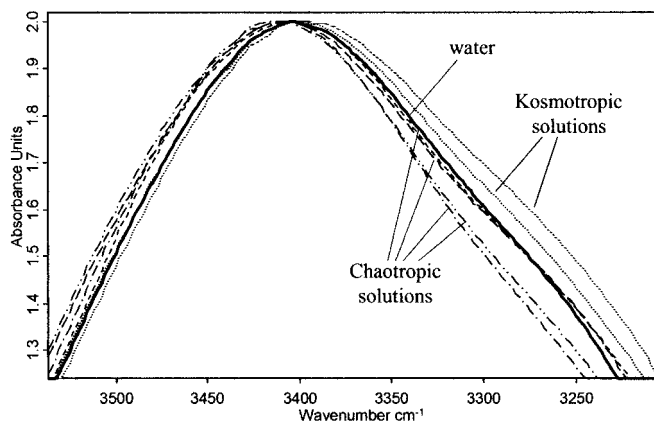


FIG. 3. Spectra of six different solutions. The dotted lines give the kosmotropes trehalose (0.5 M) and  $\text{MgSO}_4$  (1 M). The dashed lines are the KSCN (0.5 M), GdmCl (0.5 M),  $\text{NH}_4\text{NO}_3$  (1 M), and NaCl (1 M). The solid line refers to HPLC grade water.

carried out. The first peak at  $\sim 3310 \text{ cm}^{-1}$  can be assigned to “ice-like” water molecules, the second ( $\sim 3440 \text{ cm}^{-1}$ ) to intermediate water molecules, and the third ( $\sim 3570 \text{ cm}^{-1}$ ) to multimer water molecules, which means going from more “ice-like” structure to “free” water similar to the vapor phase. From our measurements, it can be stated that trehalose and  $\text{MgSO}_4$  solutions have larger contributions from the more “ordered” water than the “free” water. This observation is consistent with the theory that considers them kosmotropes. On the other hand, KSCN, GdmCl,  $\text{NH}_4\text{NO}_3$ , and NaCl show a slightly increased absorbance in the higher wavenumber region and are therefore considered to be chaotropes.

**Recorded Terahertz Spectra.** Figure 4 presents an absorbance spectrum of the dry flow cell with the empty cell compartment as background. A dominant band at 72  $\text{cm}^{-1}$  is assigned to the polyethylene window material used.<sup>22</sup> In Fig. 5 an absorbance spectrum of water with the empty (air filled) flow cell as background is shown. In the THz region generally two vibrational modes for water are found, centered at approximately 60 and 180  $\text{cm}^{-1}$ . The one band at 60  $\text{cm}^{-1}$  accessed by these measurements is weak in absorption spectroscopy (in contrast to Raman spectroscopy) and even diminishes for temperatures higher than 0  $^\circ\text{C}$ .<sup>23</sup> With the current instrument performance the band is hardly discernible from baseline

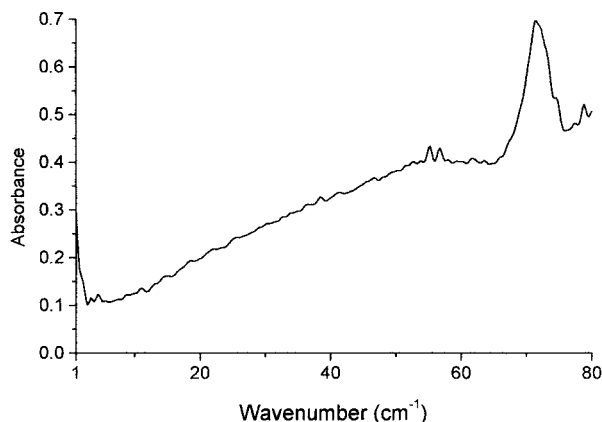


FIG. 4. Absorbance spectrum of the empty flow cell containing PE windows.

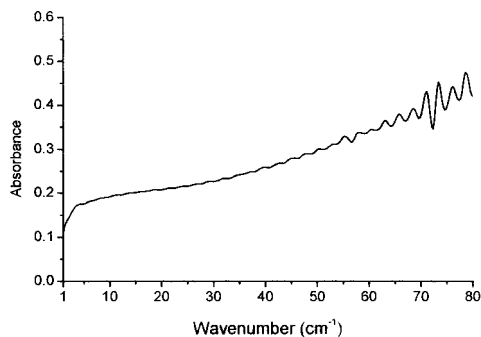


FIG. 5. Spectrum of pure water against the empty cell.

noise. The obtained spectrum, however, is in good agreement with measured literature data.<sup>24</sup>

The influence of various solutes on the absorbance of water in the THz region was studied first by two sets of typical chaotropes in solution and two sets of kosmotropes, each set consisting of various concentrations from 0.01 M up to 1 M. Figure 6 presents the results as absorbance spectra against water. Although no bands of the dissolved solutes could be observed, very interesting changes in the intensity of the water background could be detected.

The ions  $K^+$  and  $SCN^-$ , both large ions, form a typical chaotropic substance.  $SCN^-$  in its linear structure has special hydration properties and is known as an extremely weak hydrated ion.<sup>25</sup> The second tested chaotrope is formed by  $Gdm^+$  and  $Cl^-$ . Guanidinium is known as one of the most weakly hydrated cations.<sup>25</sup> Both sets of solutions give an overall increase in absorption.

The other two dissolved salts are  $MgSO_4$ , which be-

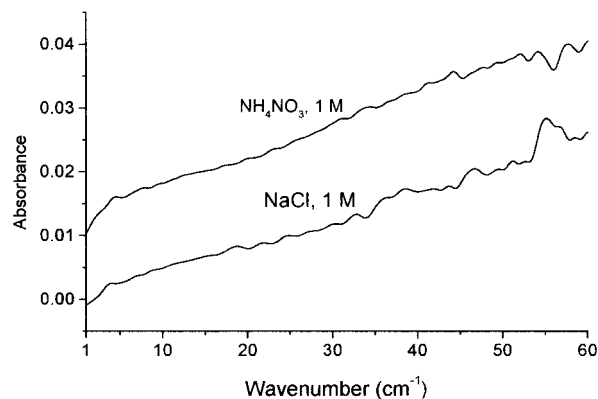
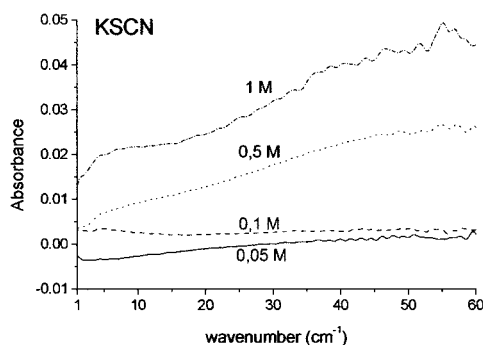


FIG. 7. Absorbance spectra with  $H_2O$  spectra as background of 1 M  $NH_4NO_3$ , which is expected to be a chaotrope, and  $NaCl$  of uncertain character.

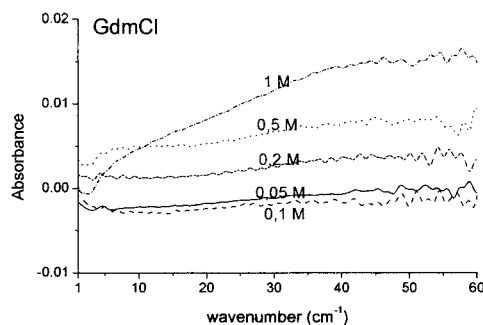
longs to the group of kosmotropes, due to the high charge densities of its ions, and trehalose, a special kosmotrope.<sup>15,26</sup> The spectra in Figs. 6c and 6d show a clear decrease in absorption.

A further substance,  $NH_4NO_3$ , which is categorized as a chaotrope,<sup>15</sup> is measured as 1 M concentrated solution. Indeed, the spectrum also shows increased absorption (Fig. 7). A check for  $NaCl$  was carried out, where the  $Na^+$  ion actually is considered marginally as a kosmotropic ion and  $Cl^-$ , on the other hand, as a weak chaotrope.<sup>17,24</sup> Figure 7 shows that the influence of a 1 M concentrated  $NaCl$  solution on the water leads to an increase in absorbance.

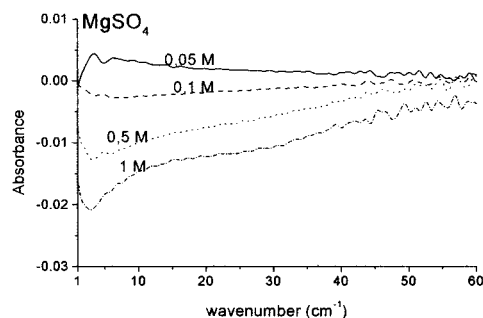
In general, the lowest concentrations (0.05 M and 0.1 M) do not show a distinct change in absorption compared



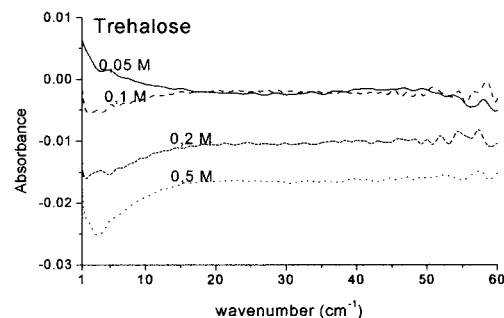
a)



b)



c)



d)

FIG. 6. Absorbance spectra of representative chaotropes (a)  $KSCN$  and (b)  $GdmCl$  and kosmotropes (c)  $MgSO_4$  and (d) trehalose against pure water.

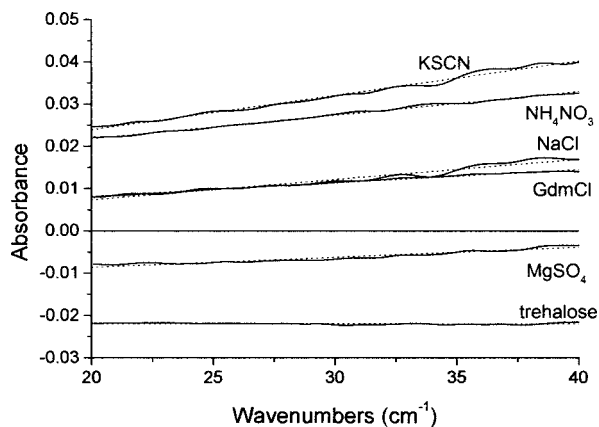


FIG. 8. Recorded absorbance spectra with H<sub>2</sub>O spectra as background and linear fit of the spectra obtained from the highest measured concentration in the region from 20 to 40 cm<sup>-1</sup>. The corresponding equation factors are presented in Table I.

to water. However, the observed shifts upwards or downwards for higher concentrations differ in their behavior from each other and also in absorption intensities. While in most cases a shift in absorbance also results in an ascending slope, the solute trehalose does not show this tendency and also the GdmCl gives a very weakly pronounced slope.

For better comparison, the slopes of the curves of the 1 M concentrated solutions (0.5 M for the trehalose) were calculated according to the formula  $y = m \cdot x + b$  for the region between 20 and 40 cm<sup>-1</sup>, where we observed the best reproducibility, in order to tabulate this observation (Fig. 8). The obtained values for the linear fit are presented in Table I, where the calculated slopes ( $m$ ) and the ordinates ( $b$ ) corresponding to the measured absorbance spectra in the spectral region from 20 to 40 cm<sup>-1</sup> of the solutes 1 M and 0.5 M, respectively, are given.

## DISCUSSION

The chosen solutes, as chaotropes or kosmotropes respectively, yield the expected results in the IR: more “ice-like” water structure for the kosmotropes, more “free water” for the latter. Nevertheless, these variations are marginal and attempts to analyze the difference in a systematic way by peak fitting failed due to ambiguous results. One reason is the influence of drifts in the baseline. As a consequence, the OH band provides a hint, more than an absolute measure, for assigning the influence of a solute in a certain concentration to one or the other effect. This has also been commented on by Brubach et al.<sup>27</sup>

In the studied THz region (1.3 cm<sup>-1</sup> to 60 cm<sup>-1</sup> wavenumber/8 mm to 160 μm wavelength), no peaks of water could be found at room temperature. Also, the solutes did not give any vibrational bands. However, correlating with the results from the MIR, changes in absorption intensities with respect to pure water are observed as an overall increase or decrease in the THz region.

Within this work it was not possible to unravel the exact mechanism causing these shifts, but a direct relation to structural changes of water can be stated. The observed effect of shifting absorbance spectra cannot be explained by varying water concentration due to the presence of

TABLE I. Values for the linear fit of Fig. 8.

	Slope ( $m$ )	Intercept ( $b$ )
MgSO <sub>4</sub>	$2.4 \times 10^{-4}$	$-1.3 \times 10^{-2}$
trehalose	$2.5 \times 10^{-6}$	$-2.1 \times 10^{-2}$
KSCN	$8.2 \times 10^{-4}$	$7.6 \times 10^{-3}$
GdmCl	$3.2 \times 10^{-4}$	$1.9 \times 10^{-3}$
NH <sub>4</sub> NO <sub>3</sub>	$5.6 \times 10^{-4}$	$1.1 \times 10^{-2}$
NaCl	$4.8 \times 10^{-4}$	$-2.3 \times 10^{-3}$

solutes. In order to cause such strong variation by density changes, the concentration of water in solution would have to de- or increase up to 5%, which is not the case.

A more likely explanation for the measured spectra changes is the rotational dynamics due to the alteration of the water structure due to the presence of the solutes.

The measured spectra allow a differentiation between a kosmotropic and a chaotropic behavior of solutes in water, especially when their concentration is high enough, around 0.2 M.

This is given by an overall increase or decrease in absorption with respect to pure water. The value of  $b$  presented in Table I was found to be a discriminator for chaotropic and kosmotropic effects, but due to the instrument instability in the baseline one should still consider this cautiously. NH<sub>4</sub>NO<sub>3</sub>, consisting of two large ions, was in good agreement with theory and its  $b$  value was in the range of the other chaotropes. However, NaCl, stated in literature<sup>17</sup> as more or less neutral to the kosmotropic/chaotropic effect, showed a gain in absorption. NaCl consists of the weak kosmotrope Na<sup>+</sup> and the weak chaotrope Cl<sup>-</sup>. Looking at the value of  $b$ , it is seen that the value is conspicuously lower than from the other chaotropic salts. Probably it is only due to the slope that NaCl shows such a strong shift up. The comparison of the  $m$  values in Table I confirms the following consideration: all ionic substances show a value in the same range, while trehalose, revealing an almost flat line similar to a uniform baseline shift, gives a value two orders of magnitude lower. Furthermore, the slope is increasing with the concentration, independently of whether a movement downwards or upwards is observed. The observed result may be explained by two superposed effects. On one hand there is the overall shift in intensity, which can be directly related to the ability of the solutes to force water into certain structures (kosmotropic/chaotropic behavior). On the other hand, the value of the slope may be used to differentiate ionic from non-ionic solutes. This value is thus most likely correlated to the conductivity of the solutions.

However, at this point we cannot exclude the possibility that there is an influence from the vibrational bands from higher energy on the spectral region below 60 cm<sup>-1</sup>. It can be ruled out from overview spectra that the librational band at 600 cm<sup>-1</sup> does contribute to this region, but an impact from the intermolecular vibration at 180 cm<sup>-1</sup> on the lower wavenumber region may be possible.

## CONCLUSION

The THz spectra of aqueous solution of different solutes can thus be viewed as a combination of two different effects that are reflected in the slope and intercept of the simplified spectrum, respectively. We propose that from

the sign of the intercept (positive or negative) a distinction between chaotrope and kosmotrope can be made. A significant slope is only observed for ionic substances. Salts whose kosmotrope or chaotrope behavior is under discussion in the literature also give rise to unclear results so far. However, these first results using recently available terahertz pulsed spectrometers are highly promising in light of improvements in instrument stability and thus signal-to-noise ratio, which most likely can be expected in the near future, and merit further investigation.

#### ACKNOWLEDGMENT

N.K., J.R.B., and B.L. are grateful for financial support received from the Austrian Science Fund within the project FWF 15531. J.R.B. also acknowledges support from the Consejería de Educación y Ciencia de la Junta de Andalucía.

1. H. Fabian and W. Mäntele, "Infrared Spectroscopy of Proteins", in *Handbook of Vibrational Spectroscopy*, J. M. Chalmers and P. R. Griffiths, Eds. (John Wiley and Sons, Ltd., Chichester, 2002), pp. 3399–3425.
2. K. Gerwert, *Biol. Chem.* **380**, 931 (1999).
3. M. F. Kimmitt, *J. Biol. Phys.* **29**, 77 (2003).
4. L. M. Miller, G. D. Smith, and G. L. Carr, *J. Biol. Phys.* **29**, 219 (2003).
5. M. Abo-Bakr, K. Feikes, K. Hollmack, P. Kuske, W. B. Peatman, U. Schade, G. Wustefeld, and H.-W. Hübers, *Phys. Rev. Lett.* **90**, 094801/1 (2003).
6. P. F. Taday, I. V. Bradley, D. D. Arnone, and M. Pepper, *J. Pharm. Sci.* **92**, 831 (2002).
7. C. Fattinger and D. Grischkowsky, *Appl. Phys. Lett.* **54**, 490 (2002).
8. V. P. Wallace, P. F. Taday, A. J. Fitzgerald, R. M. Woodward, J. Cluff, R. J. Pye, and D. D. Arnone, *Faraday Discuss.* **126**, 255 (2003).
9. U. Schade, K. Hollmack, P. Kuske, G. Wustefeld, and H.-W. Hübers, *Appl. Phys. Lett.* **84**, 1422 (2004).
10. C. Rønne, P. Åstrand, and S. R. Keiding, *Phys. Rev. Lett.* **82**, 2888 (1999).
11. G. E. Walrafen, Y. C. Chu, and G. J. Piermarini, *J. Phys. Chem.* **100**, 10363 (1996).
12. L. Thrane, R. H. Jacobsen, P. U. Jepsen, and S. R. Keiding, *Chem. Phys. Lett.* **240**, 330 (1995).
13. H. E. Stanley and J. Teixeira, *J. Chem. Phys.* **73**, 3404 (1980).
14. C. Rønne and S. R. Keiding, *J. Mol. Liq.* **101**, 199 (2002).
15. <http://www.lsbu.ac.uk/water/kosmos.html>.
16. B. Hribar, N. T. Southall, V. Vlachy, and K. A. Dill, *J. Am. Chem. Soc.* **124**, 12302 (2002).
17. K. D. Collins, *Proc. Natl. Acad. Sci., U.S.A.* **92**, 5553 (1995).
18. K. A. Sharp, B. Madan, E. Manas, and J. M. Vanderkooi, *J. Chem. Phys.* **114**, 1791 (2001).
19. F. Vanzi and B. Madan, and K. J. Sharp, *Am. Chem. Soc.* **120**, 10748 (1998).
20. R. Laenen, C. Rauscher, and A. Laubereau, *J. Phys. Chem. B* **102**, 9304 (1998).
21. J. B. Brubach, A. Mermet, A. Filabozzi, A. Gerschel, D. Lairez, M. P. Krafft, and P. Roy, *J. Phys. Chem. B* **105**, 430 (2001).
22. T. Tanabe, K. Suto, J. Nishizawa, K. Saito, and T. Kimura, *J. Phys. D: Appl. Phys.* **36**, 953 (2003).
23. O. F. Nielsen, *Annu. Rep. Prog. Chem., C: Phys. Chem.* **93**, 57 (1997).
24. E. Zoidis, J. Yarwood, and M. Besnard, *J. Phys. Chem. A* **1003**, 220 (1999).
25. P. E. Mason, G. W. Neilson, C. E. Dempsey, A. C. Barnes, and J. M. Cruickshank, *Proc. Natl. Acad. Sci., U.S.A.* **100**, 4557 (2003).
26. C. Branca, S. Magazu, G. Maisona, S. M. Bennington, and B. Fak, *J. Phys. Chem. B* **107**, 1444 (2002).
27. J. B. Brubach, A. Mermet, G. de Marzi, C. Bourgaux, E. Prouzet, and P. Roy, *J. Phys. Chem. B* **106**, 1032 (2002).

## ***Curriculum Vitae***

NAME

---

Nina Kaun

ADDRESS

---

Preßgasse 9/7  
A-1040 Wien, Austria  
mail: ninakaun@tuwien.ac.at

DATE OF BIRTH

---

04.09.1978, Kirchdorf a.d. Krems, Austria

EDUCATION

---

- |                          |   |
|--------------------------|---|
| Feb. 2003                | Begin of the PhD at the Institute of Chemical Technologies and Analytics (TU Vienna) in the field of Chemical Analysis and Vibrational Spectroscopy |
| Nov. 2002                | Diploma exam (MSc equivalent) passed with distinction   |
| Oct. 1996 –<br>Nov. 2002 | Studies of Technical Chemistry at the Vienna University of Technology<br>Specialisation on Analytical and Physical Chemistry                        |
| 1988 – 1996              | High school ( Stiftsgymnasium Admont)   |
| 1984 – 1988              | Elementary school (Volksschule Windischgarsten)   |

STAYS ABROAD

---

- |                           |   |
|---------------------------|---|
| Feb. 2006 – April<br>2006 | Stay at Bessy, Berlin Germany, on invitation of Dr. Ulrich Schade<br>Financed by the “Mobilitätsstipendium der Akademisch-sozialen Arbeitsgemeinschaft Österreichs“ |
| June 2004 – June<br>2005  | Measurements at the Infrared Synchrotron Beamline at Bessy, Berlin Germany, 5 weeks in total  |
| Oct. 2003                 | Measurements at TeraView (THz light source), CambridgeUK , 4 days   |
| Aug. 2003                 | Measurements at the Infrared Synchrotron Beamline at ANKA, Karlsruhe Germany, 4 days  |

- Feb. 2002 – Sept. 2002 Diploma work at MiTAC Antwerp, Belgium  
 Title: “*Analysis of organic compounds with static secondary ion mass spectrometry (S-SIMS) using monoatomic and polyatomic bombardment*”,  
 7 months
- Aug./Sept. 2000 Employment at Analytical Laboratory of Pharmaceutical Production in Switzerland (Sipharm Sisseln AG), 2 months

## CONFERENCE CONTRIBUTIONS

---

### Oral Presentation

N. Kaun “*Results on (Bio)chemical reaction monitoring using IR Synchrotron Microscopy*”, WIRMS (International Workshop on IR Microscopy and Spectroscopy with Accelerator Based Sources) 2005, Rathen, Germany

### Poster

N. Kaun, S. Kulka, J.R. Baena, U. Schade, M. Vellekoop, E. De Lorenzi B. Lendl  
 “*Lab-on-a-chip devices as enabling technology for novel (bio)chemical studies using mid-IR synchrotron radiation*”

ESF LESC Exploratory Workshop - Recent Progress and Future Perspectives in Infrared Microscopy and Spectroscopy with Advanced Light Sources, October 2004, Trieste, Italy

### Poster

N. Kaun, S. Kulka, J.R. Baena, U. Schade, M. Vellekoop, E. De Lorenzi, B. Lendl  
 “*Synchrotron Radiation for On-Chip Mid-IR Detection at the Diffraction Limit*”  
 MicroTAS-2004, Malmö, Sweden, Sept. 2004

### Poster

N. Kaun, P. Hinsmann, J. Frank, P. Svasek, J.R. Baena, B. Lendl  
 „*Time resolved FTIR Spectroscopy of bioligand interactions using a microfluidic mixing system*“  
 ICAVS-2 in Nottingham, UK (24<sup>th</sup> –29<sup>th</sup> Aug. 2003)

## PUBLICATIONS

---

N. Kaun, S. Kulka, J. Frank, U. Schade, M. J. Vellekoop M. Harasek and B. Lendl  
 “*Towards Biochemical reaction monitoring using FT-IR Synchrotron radiation*”  
 Analyst, 131,( 2006) 489–494

N. Kaun, J.R. Baena, D. Newnham, B. Lendl  
 „*THz-Spectroscopy as a new tool for measuring the structuring effect of solutes on water*”  
 Appl. Spectrosc. 59 4 (2005) 505-510

N. Kaun, S. Kulka, J.R. Baena, U. Schade, M. Vellekoop, E. De Lorenzi, B. Lendl  
 „*Synchrotron radiation for on-chip detection at the diffraction limit*”  
 Proceedings of MicroTAS-2004, Malmö, Sweden, Sept. 2004, proc. vol. 2, p. 530-532

S. Kulka, N. Kaun, J. R. Baena, J. Frank, P. Svasek, D. Moss, M.J. Vellekoop and B. Lendl

*"Mid-IR synchrotron radiation for molecular specific detection in micro-chip based analysis systems"*

Analytical and Bioanalytical Chemistry (2004), 378(7), 1735-1740

#### LANGUAGES

---

German      native language

English     fluently spoken and written

French, Spanish, Dutch      basic knowledge